UiO : Department of Chemistry
University of Oslo

Synthesis and properties of new gold iminocarbene complexes

Master Thesis

Elin Katinka Riiser Dankel

60 credits
May 2014

Preface

The work of this master thesis was done at the Chemistry Department at the University of Oslo in the research group of Mats Tilset. It has been two amazing years and despite being exhausted to the bone at times, I would have happily have done it again. I would first of all like to thank Mats Tilset for being such a caring, enthusiastic and inspiring supervisor encouraging me to try new techniques (fill up my "chemistry tool box") and attempt new reactions.

There are five other people who have been essential in this project and that is experimentalists Marte-Sofie Holmsen and Eirin Langseth, computational chemists Ainara Nova and David Balcells and crystallographer Sigurd Øien. With great patience they have all spent hours on end helping me with my project, and I am extremely grateful. It should also be mentioned that the master theses of Marte and Eirin has been great help when constructing my own thesis, and the Latex preamble from Espen Hagen Blokkdal got me going with the programming. Frode Riise and Dirk Pettersen are maintaining a world class NMR-lab and the possibility of booking a 600 MHz cryoprobe instrument for several days in a row is a privilege I do not expect to have elsewhere. The MS results "magically" appearing have been obtained by Osamu Sekiguchi. A big thank you to all of you!

The rest of the Tilset group, the catalysis group and all the organic chemists in the east wing have also played a big role in my day-to-day life, and a special thanks to office companion Anders L. Sundsdal and fumehood-neighbour Eline Aasen Tråseth for great company.

Over the past six years, the Chemistry Department in Oslo has become somewhat like a second home to me. The community feeling is very reassuring, and academic and social events arranged by Chemistry Society Proton, the Chemistry department (Oslo) and the Norwegian Chemistry Society (NKS) have been some of the highlights.

Despite jokingly dismissing gold complexes as over-prized Lewis acids, my boyfriend Chris Teskey has provided indispensible support and inspiration over the past two years. I would of course also like to thank my family, friends and flat-mates for great support and understanding during these two busy years. Since my plan is to become a balanced, organised and chilled PhD student, I will soon be much more sociable again.

Finally, to quote Mats's group meeting mantra: "Let's move on to the fun stuff: The chemistry!"

Abstract

The prevalence of gold catalysis in the synthetic community has increased dramatically within the last few years, and a wide range of *N*-heterocyclic carbene (NHC) gold(I) and, to a lesser extent, gold(III) complexes have been studied and probed for their catalytic activity in organic transformations. Here, a number of novel iminocarbene gold(I) and gold(III) complexes have been synthesised and characterised by NMR spectroscopy, mass spectrometry and X-ray crystallography. The proposed interaction between the gold(III) metal centre and imine functionality pendant from the NHC ligand has been studied at the DFT level of theory and from an analysis of the electron density and its derivatives it has been shown that there is an attractive non-covalent interaction between these sites. Preliminary results also indicate that a [C,N]-chelating iminocarbene gold(III) complex has been prepared.

Abbreviations

b.p.	boiling point
au	atomic units
br	broad
^{t}Bu	*tert*-butyl
°C	degrees Celsius
cal	calorie(s)
COSY	correlated spectroscopy
d	doublet
D	deviation
DFT	Density Functional Theory
dmso	dimethyl sulfoxide
eq.	equivalents
Et	ethyl
EI	electron ionization
ESI	electrospray ionization
et al.	*et alii*
EXSY	exchange spectroscopy
g	gram(s)
h	hour(s)
HMBC	heteronuclear multiple-bond correlation
HSQC	heteronuclear single-quantum correlation
HR	high resolution
Hz	Hertz
i.e.	id est
IR	Infrared
J	coupling constant
L	ligand
L	litre(s)
µ	micro
M	molar
M	metal
m	milli
m	multiplet
Me	methyl
Mes	mesitylene
min	minutes
MS	Mass Spectrometry
m/z	mass-to-charge ratio

NOE	Nuclear Overhauser Effect
NOESY	Nuclear Overhauser Effect Spectroscopy
NHC	*N*-Heterocyclic Carbene
NMR	Nuclear Magnetic Resonance
ORTEP	Oak Ridge Thermal Ellipsoid Plot
p	*para*
^{i}Pr	*iso*-propyl
Ph	phenyl
ppm	parts per million
ρ	electron density
r.t.	room temperature
RMSD	root-mean-square deviation
s	singlet
s	reduced gradient
t	triplet
T	temperature
Tf	trifluoromethanesulfonyl
THF	tetrahydrofuran
vs.	versus
Å	Ångstrøm(s)

Overview of key compounds

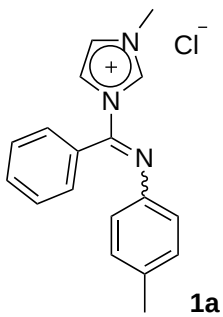

1a

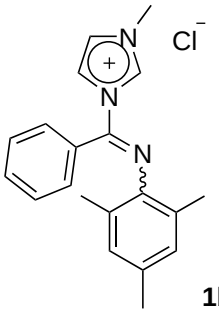

1b

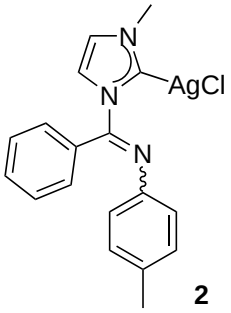

2

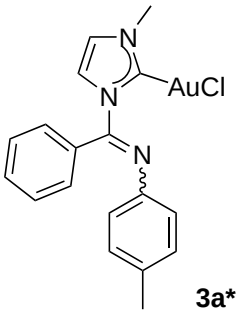

3a*

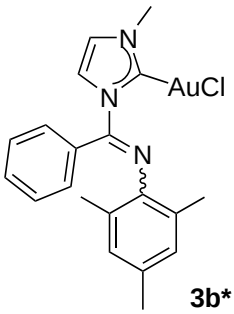

3b*

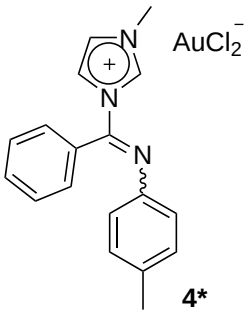

4*

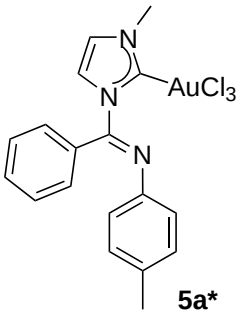

5a*

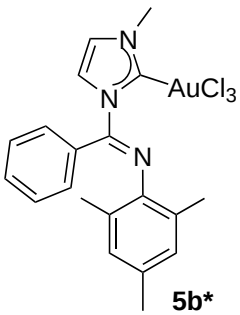

5b*

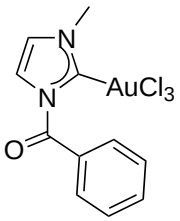

6*

* = new compounds

The aim of the project

Over the last decade, metal complexes bearing chelating N-heterocyclic iminocarbene ligands have been the focus of many projects in the Tilset group. [C,N]-chelating NHC complexes of Pd(II),[1–3] Pt(II),[4] Rh(I)[5,6] and Rh(III)[7] have been prepared. One of the prepared Rh(I) complexes has displayed remarkably high reactivity and cis-diastereoselectivity for catalysing cyclopropanation reactions.[8]

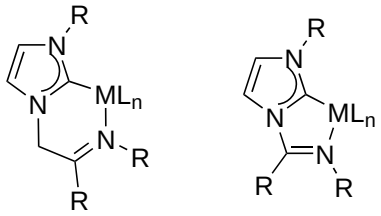

Figure 1: Iminocarbene complexes previsouly studied in the Tilset group

In the last few years, the focus of the Tilset group has shifted towards gold(III) chemistry. Reliable microwave syntheses of cyclometalated gold(III) complexes[9,10] have been the starting point for many novel complexes including the first crystallographically characterised gold(III) alkene complex **7**.[11]

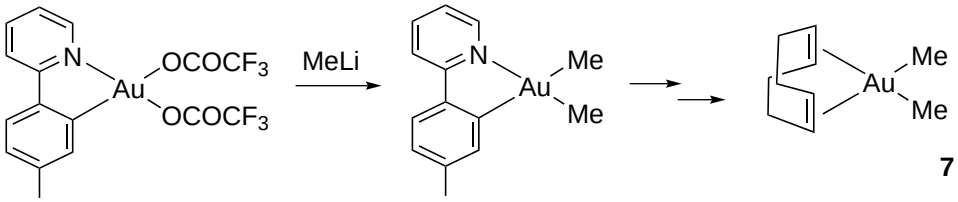

Scheme 1: Gold(III) complexes synthesised in the Tilset group

The project assigned in the autumn of 2012 builds on the interesting work emanating from the Tilset group. The iminocarbene ligands were to be applied in gold chemistry, and target molecules like **3a** and **8** were suggested. An analogue of **3a** had already been synthesised by MSc Eirin Langseth by transmetalation from the homoleptic silver(I) complex. Gold complexes has shown to be effective catalysts for a range of organic transformations,[12,13] and the catalytic acitivity of the new complexes would have be tested if the limited time frame of the project had allowed it.

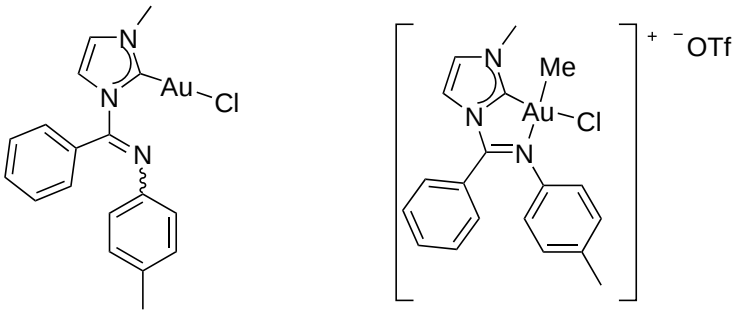

Figure 2: Target molecules

Contents

CHAPTER 1

Introduction

1.1 *N*-heterocyclic carbenes

Carbenes are divalent neutral carbons with six valence electrons, and without α-heteroatom stabilisation they are short-lived electrophilic intermediates. However, when a carbene is incorporated into a nitrogen-containing heterocycle, significant stabilisation results, and the carbene gets a nucleophilic character. A plethora of *N*-heterocyclic carbenes (NHCs) have been reported over the past two decades and examples of the structural diversity of NHCs is presented in Figure 1.1. The imidazol-2-ylidene **9** is of the most commonly encountered NHCs and is the ligand employed in this project.

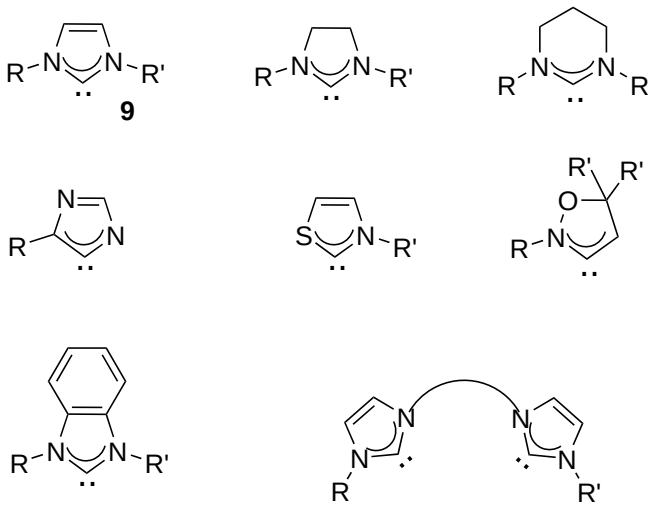

Figure 1.1: Examples of the structural diversity of NHCs

The stability of NHCs is primarily a result of electronic effects. The α-amino substituents donate electron density into the empy p_z-orbital on the carbenic carbon and simultaneously inductively withdraw electron density from the carbene sp^2 orbital containing the lone pair.

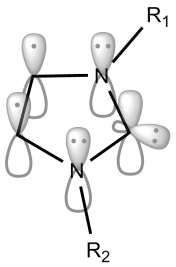

Figure 1.2: Atomic orbitals on a imidazolylidene carbene

The resultant stability from this "push-pull" effect has made it possible to isolate free NHCs, as first done by Arduengo *et al.*.[14] The stability of the carbene is also improved by the use of bulky *N*-substituents (the "wingtip" groups) to sterically shield the carbene. The first isolated NHC (**10**) was stabilised by the highly sterically demanding adamantyl group, however, stable free N-heterocyclic carbenes like **11** with small wingtip groups have later been isolated (Scheme 1.1).

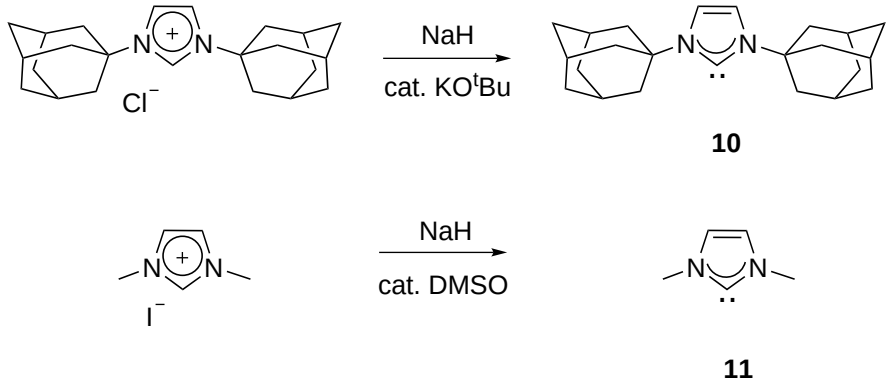

Scheme 1.1: Examples of stable free *N*-heterocyclic carbenes

The two free carbenes in Scheme 1.1 are generated by using a strong base to deprotonate an imidazolium salt. This is the most common way of generating free carbenes. However, far from all NHCs can be prepared as the free carbene.[1,15] This is, for example, the case of NHCs bearing *N*-substituted imino groups which spontaneously rearrange by the migration of the *N*-iminoyl group from the nitrogen to the carbene carbon as shown in Scheme 1.2.[16]

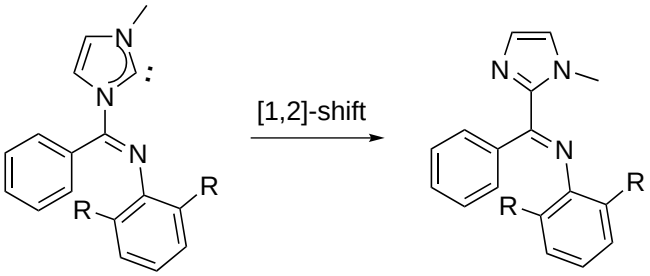

Scheme 1.2: The [1,2]-shift of imino-*N*-heterocyclic carbenes

1.2 *N*-heterocyclic carbenes as metal ligands

In constrast to other carbenes, NHCs are nucleophilic with a high energy lone pair making them exceptionally good σ-donors when coordinated to metals. The σ-donation was long thought to be the only bonding interaction between the NHC ligand and the metal, but studies have since shown that back-donation from a filled metal-based *d*-orbital into the partially filled p_z-orbital of the carbene carbon cannot be neglected.[17] Also, when coordinated to electron-deficient metals in high oxidation states, the NHC-ligand can also act as a π-donor ligand.[18]

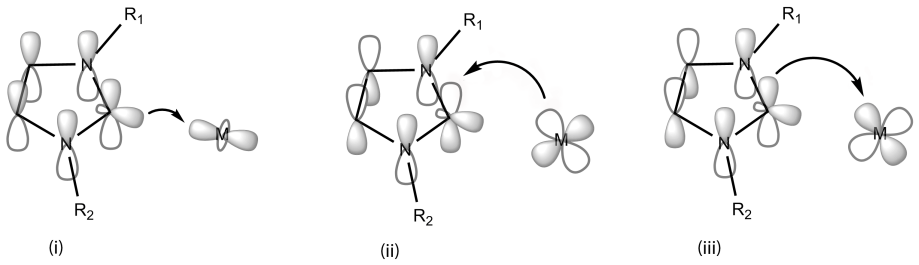

Figure 1.3: Bonding contributions in NHC metal complexes (i) σ-donation from the carbene to the metal, (ii) π*-backdonation from the metal to the carbene and (iii) π-donation from the carbene to the metal

The strong donor ability of the NHC ligands is reflected in the infrared stretching frequencies of CO ligands in $[(NHC)M(CO)_x]$ type complexes. High electron density at the metal centre induced by the NHC ligand increases the back-donation to the CO π*-orbital, weakens the CO double bond and decreases its infrared stretching frequency. The properties of NHC metal complexes are often illustrated by comparisons with tertiary phosphine ligands, and when studying a series of $[(NHC)Ni(CO)_3]$ and $[(PR_3)Ni(CO)_3]$, Dorta *et al.* found the NHC ligands were better electron donors than even the most basic trialkyl phosphines.[19]

Another unique aspect of NHC ligands is their steric demand. The short metal-ligand bond and the way the groups bound to the nitrogens on the NHC ligand are

oriented increase the steric congestion around the metal centre when compared to tertiary phosphines. The substituents on the NHC ligand allow for steric diversity around the metal centre, the inclusion of pendant donor functionalities[20] and chiral enviroment around the metal centre[21] which can be very difficult to introduce to phosphine derived ligands.

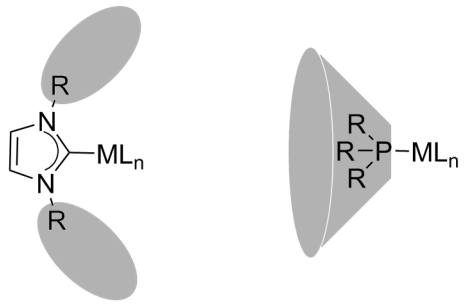

Figure 1.4: The different steric properties of phophine and NHC ligands

In recent years, NHCs have proved to be an important class of ligands in homogeneous catalysis. Perhaps the most well known applications of NHC ligands are in ruthenium catalysed olefin methathesis[22,23] and palladium cross-coupling reactions[24] (Figure 1.5). Gold complexes bearing NHCs have also been applied in a range of catalytic tranformations,[25,26] and the field is dominated by NHC gold(I) complexes.

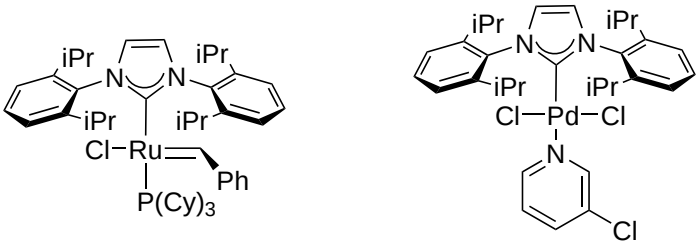

12 Grubbs-II **13 PEPPSI-IPr**

Figure 1.5: NHC metal complexes with excellent catalytic acitvities

1.3 Synthesis of *N*-heterocyclic carbene gold complexes

Gold(I) complexes bearing NHC ligands are accessible by ligand exchange. Gold-containing precursors with labile ligands like dimethyl sulfide and tetrahydrothiophene are commercially available or can be synthesised from metallic gold via chloroauroic acid as shown for the dimethyl sulfide complex in the following redox reactions.

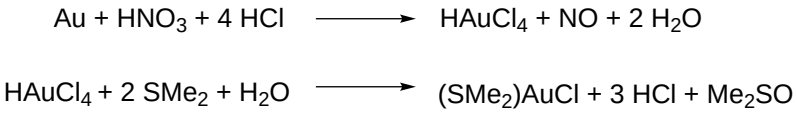

A free NHC can be generated by deprotonation of an imidazolium salt, and the carbene can easily exchange with the labile ligand in a gold-containing precursor and form a much stronger bond to the gold centre. Relatively strong bases (KH and K^{t}BuO) are required and the harsh conditions mean that the functional group tolerance is low. Also, as previously mentioned, not all NHCs are stable as the free carbene, limiting the scope of this synthetic route.

A milder route to gold(I) complex formation was first proposed by Wang and Lin in 1998 and involves transmetalation from a silver(I) complex.[27] The silver complex is first synthesised by using a basic silver salt such as Ag_2O. The base deprotonates the imidazolium halide salt forming an NHC silver(I) halide complex. The NHC is subsequently transmetalated onto gold replacing a labile ligand. The formation of insoluble AgCl is also a driving force in the reaction. In 2010 it was shown Cu_2O could be used in the same fashion generating copper(I) NHC complexes which readily transmetalates the NHC ligand to gold(I) complexes.[28]

The transmetalation reaction has proven to be a very good method to generate a variety of late transition metal NHC complexes, including gold.[29,30] However, the silver species are light sensitive which makes them hard to work with, and one equivalent of metal is wasted during the trasmetalation reactions. It was therefore a great contribution to the field when an optimised weak base route to NHC gold(I) complexes was presented in the literature in the spring of 2013.[31,32] The general procedure is presented in Scheme 1.3 (route **C**) and involves the formation of an imidazolium dichloroaurate(I) salt which is deprotonated by the aid of a weak inexpensive base. NHC gold(I) complexes had previously been prepared by the direct treatment of imidazolium salts with weak bases in the presence of a gold complex, but the new procedures offered by Collado, Nolan and co-workers[31] involves less dangerous solvents, lower reaction temperatures and shorter reaction times than what had previously been reported.

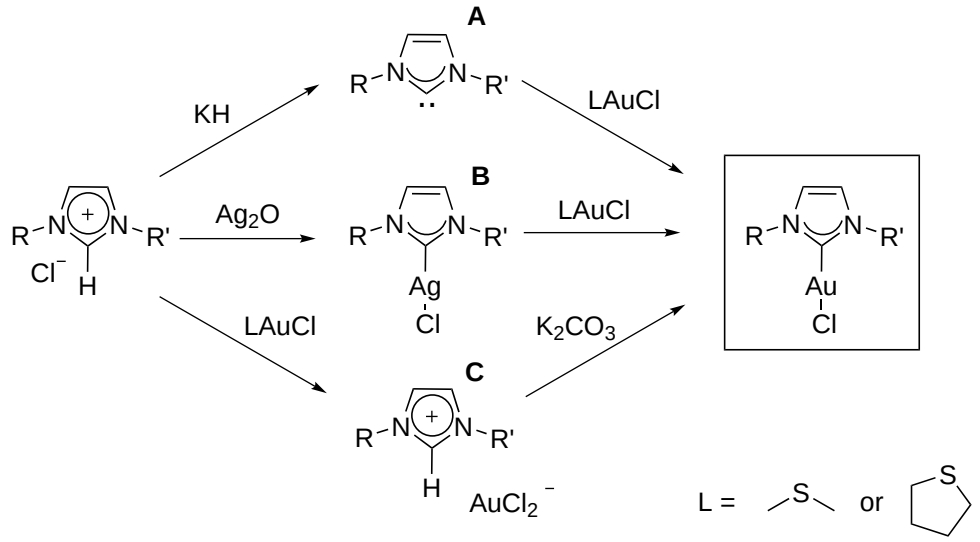

Scheme 1.3: Three synthetic routes to NHC gold(I) complexes starting from an imidazolium salt. **A**: via the free carbene, **B**: by transmetalation from a silver complex and **C**: using a weak base to deprotonate an imidazolium dichloroaurate(I) salt

1.4 Synthesis of gold(III) complexes bearing *N*-heterocyclic carbenes

Gold(III) trihalide complexes bearing *N*-heterocyclic carbenes are accessible by oxidative addition of elemental halogens to the corresponding gold(I) complex.[33–35] The synthesis of NHC gold(III) trichloride by this methods requires low reaction temperatures to avoid significant break down of the gold(I) starting material. At -78 °C chlorine condenses (b.p. -34 °C) and its oxidation ability is diminished. By slowly bringing the reaction mixture to room temperature, clean oxidation of the gold(I) centre may occure. However, even by this method, unwanted side-reactions such as the activation of C-H bonds (Scheme 1.4 (i)) have been reported.[34] Elemental bromine has also caused surprising side reactions like the 1,7-substitution shown in Scheme 1.4 (ii).[36]

A milder route to NHC gold(III) trichloride complexes is by employing the hypervalent iodine oxidant **14**.[37] The reaction has been reported to give selective oxidation and excellent yields,[34,35] and the reaction conditions are more practical and safe compared to using elemental chlorine. The iodobenzene sideproduct is easily removed under vacuum.

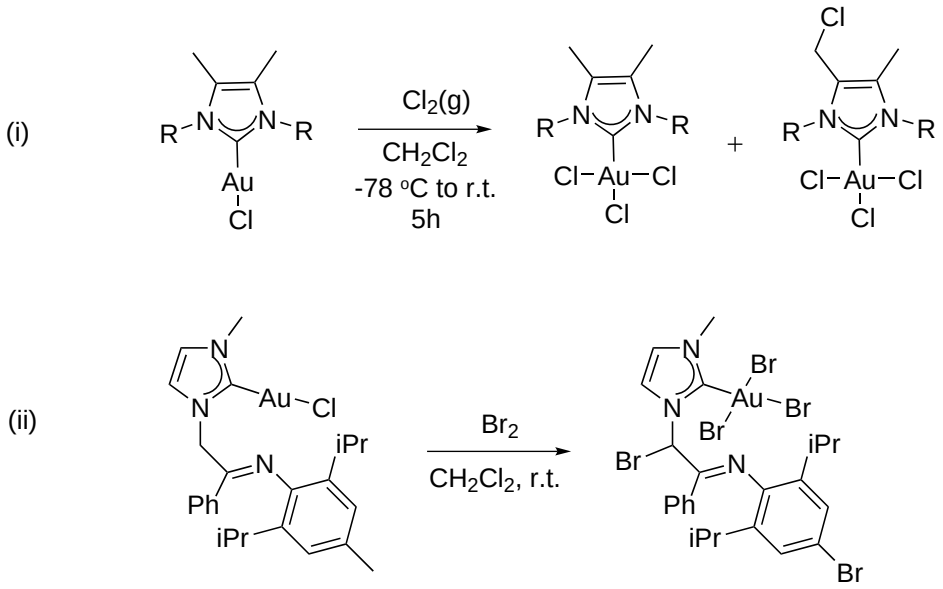

Scheme 1.4: Synthesis of NHC gold(III) trihalide complexes hampered by additional side reactions

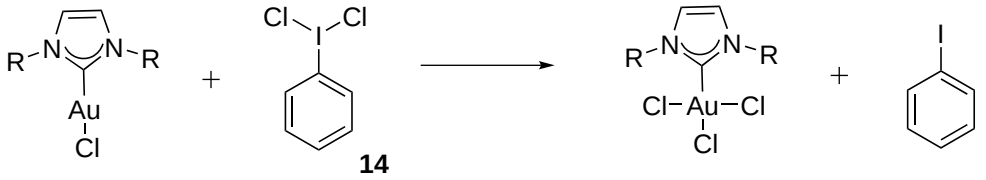

Scheme 1.5: A mild oxidation route to synthesise NHC gold(III) complexes

1.5 Donor functionalised NHC gold(III) complexes

Donor-functionalised NHC have pendant functionalities with anionic or neutral two electron donor atoms which enable them to act as polydentate ligands upon coordination to a metal centre.[20] Imino-functionalised NHCs have been of interest to the Tilset group for over a decade and [C,N]-chelating complexes of Pd(II), Pt(II), Rh(I) and Rh(III) have been prepared.[1–7]

There are a few examples in the literature of cationic gold(III) complexes bearing [C,N]-chelating NHCs (Scheme 1.6).[38,39] Complex **15** is formed by the aid of a silver(I) salt of a poorly coordinating anion. The silver(I) cation acts as a halogen scavenger and forms AgBr and the poorly coordinating BF_4^- becomes the counter anion of the cationic square planar gold(III) complex. Another example of a chelating picolyl-tethered NHC is the zwitterionic compound **16** which in the crystal structure shows a square pyramidal coordination geometry with the gold(III) atom coordinated by the carbene carbon and the halide ligands in the equatorial positions, and an oxygen atom on the sulfonate in the axial position.[39]

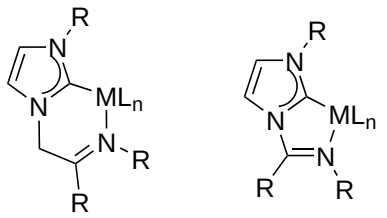

Figure 1.6: Generic iminocarbene complexes previsouly studied in the Tilset group

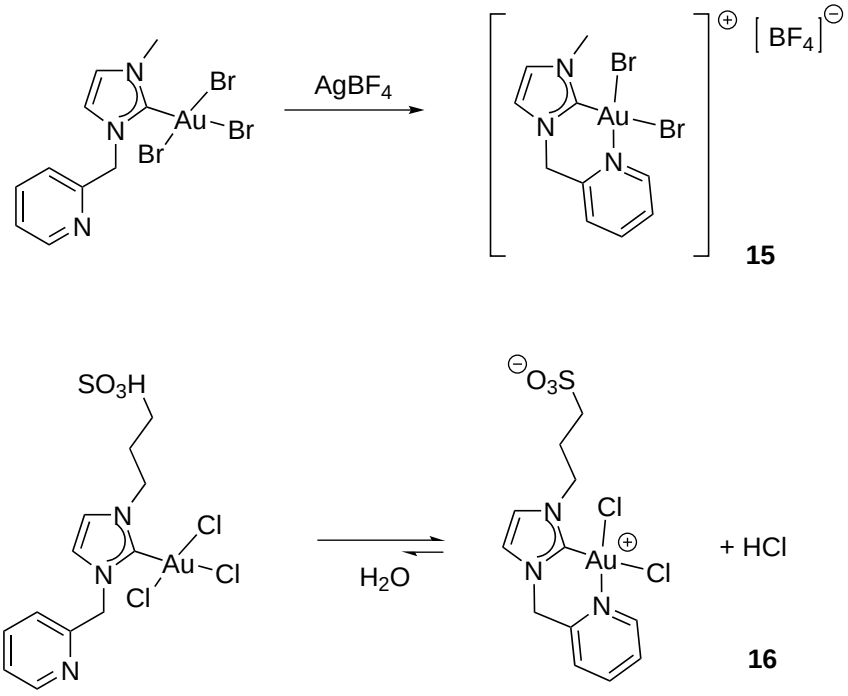

Scheme 1.6: A chelating picoline-NHC gold(III) complex

Non-chelating donor-functionalised neutral NHC complexes of gold(III) have been more frequently reported in the past few years and examples of the donor functionalities include picoline,[38,40,41] dialkylamine,[42,43] pyrazole,[44] imine,[36] alcohol[45] and a 1,10-phenanthroline NHC analogue.[46] The presence of these potentially chelating arms have been observed to induce catalytic ability of NHC gold(III) complexes. In 2012, Muuronen *et al.* reported a study of the catalytic activity of pyridine-tethered NHC gold(III) complexes in benchmark alkyne activation reactions.[40] The complexes that were investigated are presented in Scheme 1.7, and only **17** and **18** showed significant catalytic activity. It was proposed that the active catalysts were the ionpairs **17*** and **18*** which is supported by the observation that the more electron rich pyridine **18*** is the better catalyst.

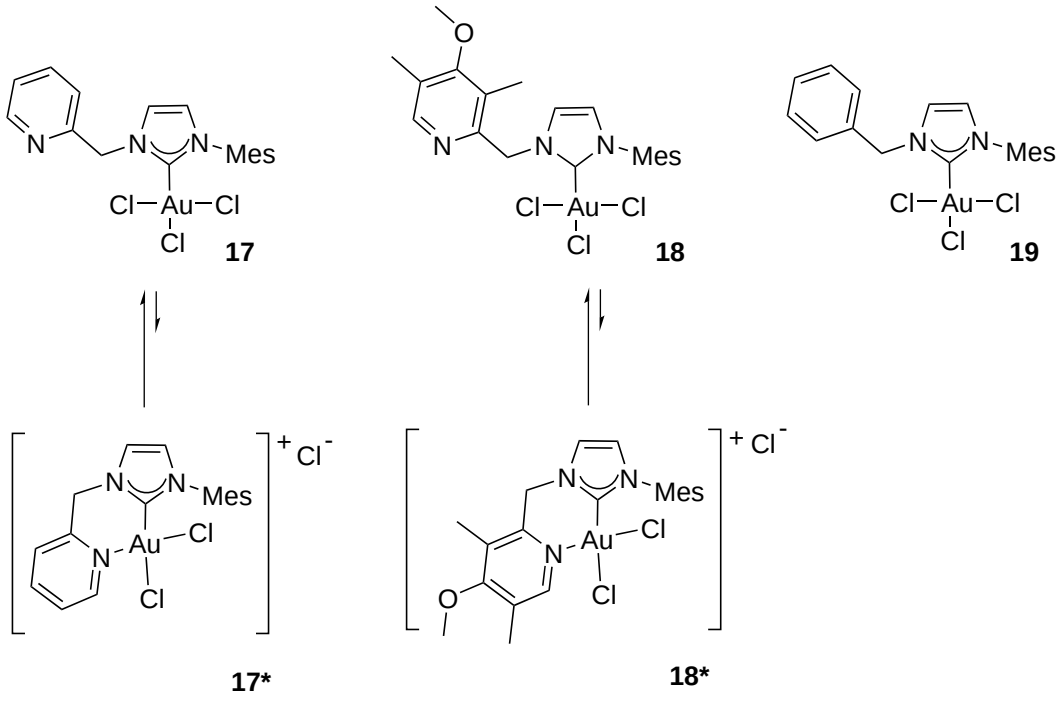

Scheme 1.7: Gold complexes studies in catalytic reaction by Muuronen *et al.*[40]

Evidence for the interaction between a neutral gold(III) centre and a donor-functionality on an NHC side-arm have been reported for complexes in solution[42,43] and in the solid state.[40,42,46] In solution NHC gold(III) halides without donor functionlality usually have characteristic UV-vis signals beween 330 and 400 nm which have been assigned to ligand-to-metal charge transfer (LMCT) states. In acidic solution, these signals are seen for protonated complex **20-H** in Scheme 1.8 whereas in neutal and basic solutions the square pyramidal environment around the gold(III) centre (with the amino nitrogen in the axial position) increases the electron density at gold and shifts the LMCT to a higher energy.[43]

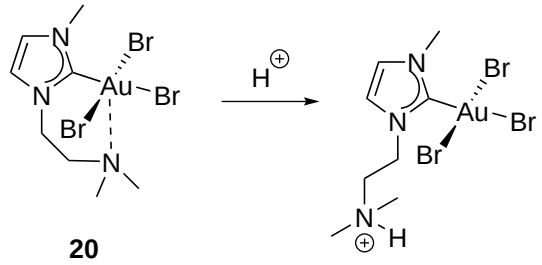

Scheme 1.8: An example of an NHC gold(III) complex with square pyramidal environment around the gold(III) centre in neutral or basic solutuion

Pseudo 5-coordinate gold(III) complexes are well-documented for diimine-type ligands, and 2,2'-bipyridine in its $[(N\cap N)AuCl_3]$ complexes have previously been studied in the Tilset group (Figure 1.7).[9,47] In the solid state the tethered N-N lig-

and is bonded such that the one N occupies a regular position in the square planar coordination plane of the gold(III) atom and the other N occupies a pseudo-axial with elongated Au-N distance. Donor-functionalised NHC gold(III) trihalide complexes have also been found to have pseudo 5- and 6-coordinate geometries in the solid state.[40,42,44,46] As in the 2,2'-bipyridine ligand, the rigid aromatic ligand skeleton of complex **22** somewhat dictates the Au-N distance.[46] However, complex **20** reported by Topf *et al.*[42] has a pseudo square pyramidal coordination geometry around gold and the non-rigid (dialkylamino)ethyl side arm is oriented with the amino nitrogen in the pseudo-axial postition.

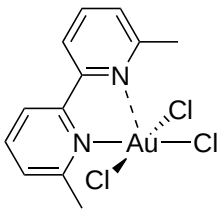

21

Figure 1.7: A pseudo 5-coordinated gold(III) complex previously studied in the Tilset group

The gold-nitrogen interaction in **22** has been studied at the DFT level of theory by Kriechbaum *et al.*.[46] The shared electron numbers calculated for the Au-N pairs was very low (0.01 electrons) which indicated that there was not any covalent character to the interaction. A population analysis resulted in a positive partial charge on gold of 0.83 and a negative partial charge of -0.16 on the pseudo-axial nitrogens, which indicated that there might be a weak intramolecular electrostatic interaction. In the optimised geometry obtained at the DFT level, the Au-N distances was longer than what was observed in the solid state. It was recognised by the authors that DFT calculations cannot reproduce van der Waal type interactions, and another geometry optimisation with an empirical correction for dispersion (D3) was performed. This did not result in any significant structural changes, and it was concluded that weak contacts between gold and nitrogen are primarily stabilised by intramolecular electrostatic interactions.

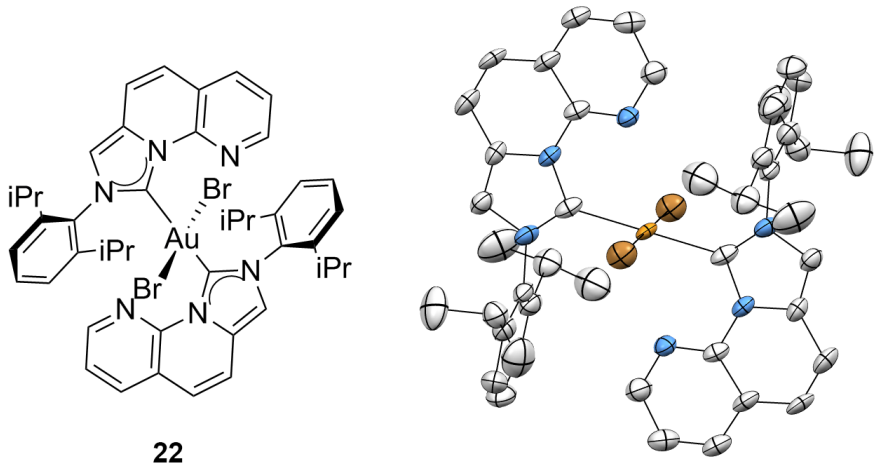

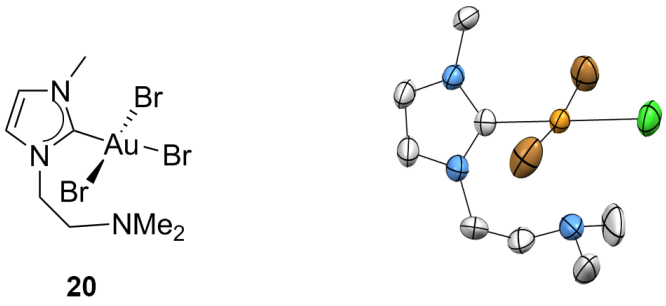

Figure 1.8: Examples of NHC gold(III) complexes with pseudo 5- and 6-coordinate geometries in the solid state.[42,46] ORTEP drawings generated in Mercury[48] from the Crystallographic Information Files published along with the articles

1.6 Non-covalent interaction plots

Non-covalent interactions such as van der Waal interactions, steric clashes and hydrogen bonds are commonly assigned based on comparison of pairwise distances between atoms and the sum of the van der Waals radii.[49] Tables of van der Waals radii are frequently being revised,[50] but the data published by Bondi in 1964[49] are still most commonly encountered in the literature and is thus the reference used in this thesis as well.

More elaborate algorithms to map and analyse non-covalent interactions have been developed based on the fact that critical points of the density ($\bigtriangledown\rho = 0$) arise when atoms interact.[51,52] In 2010 a new approach to analyse and visualise non-covalent interactions was presented in the literature[53] based on a fundamental quantity in Density Functional Theory (DFT), i.e. the reduced density gradient, s.[54,55]

$$s = \frac{1}{2\left(3\pi^2\right)^{1/3}} \frac{|\bigtriangledown\rho|}{\rho^{4/3}}$$

As illustrated in Figure 1.9, when two atomic densities are far apart, the exponential decay of ρ dominates and s diverges. When the atomic densities are brought together, $\bigtriangledown\rho$ dominates and s approaches zero. These regions in space with low values of s and ρ correspond to non-covalent interactions, and the strengths of the interactions are reflected by the electron density values.

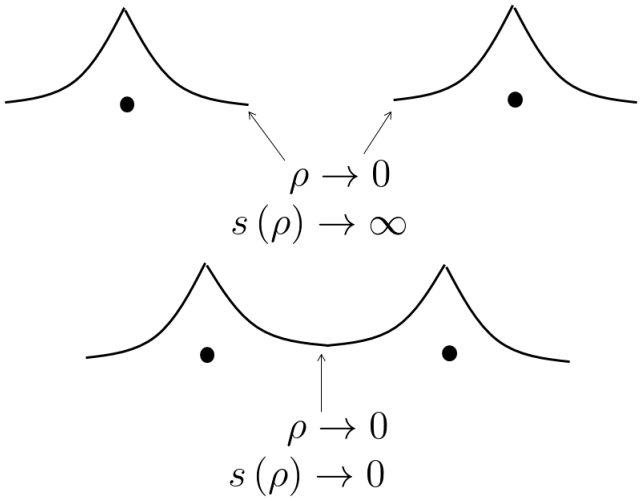

Figure 1.9: When two atomic densities approach eachother a singularity in $s(\rho)$ appears

In order to differentiate between favourable and unfavourable interactions the second derivatives of the electron density are analysed by the aid of the eigenvalues

(λ) of the electron density Hessian matrix. The first eigenvalue reflects the curvature of the electron density along the internuclear axis and is always positive. The sign of the second eigenvalue (λ_2) is diagnostic of the type of interaction. A negative λ_2 is a sign of accumulation of density perpendicular to the bond which indicates an attractive interaction, whilst steric repulsion creates density depletion and λ_2 is positive.

In the NCIPLOT software,[56] isosurfaces of the reduced gradient density are given colour according to the product of the sign of λ_2 and the value of r as shown in Figure 1.10. A blue surface indicates an attractive interaction like the hydrogen bonding in the formic acid dimer. Green surfaces correspond to regions of weak van der Waal interactions such as in the benzene dimer. Red surfaces indicate an unfavorable interaction such as steric repulsion in bicyclooctane.

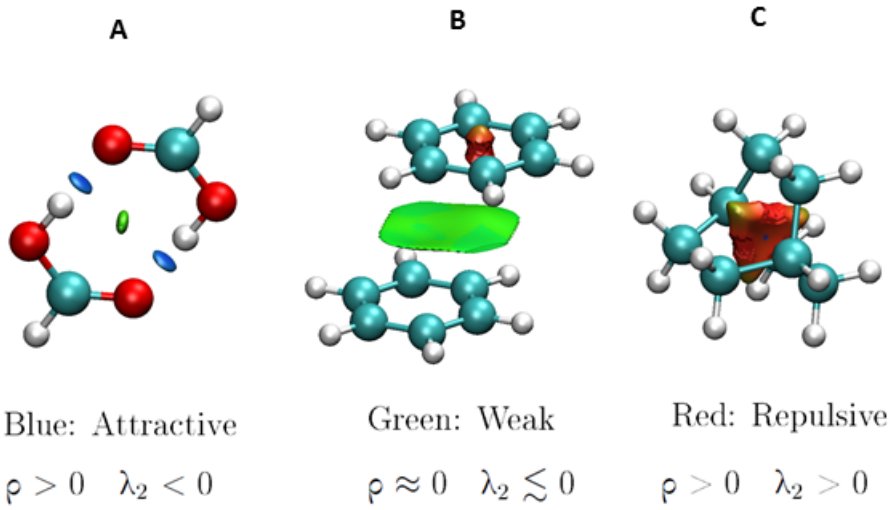

Figure 1.10: Reduced gradient isosurfaces ($s = 0.5$ au) for **A** the formic acid dimer, **B** the benzene dimer, and **C** bicyclooctane. For details about the generation of NCI plots, please see Section 4.1

CHAPTER 2

Synthesis and characterisation of new gold(I/III) iminocarbenes

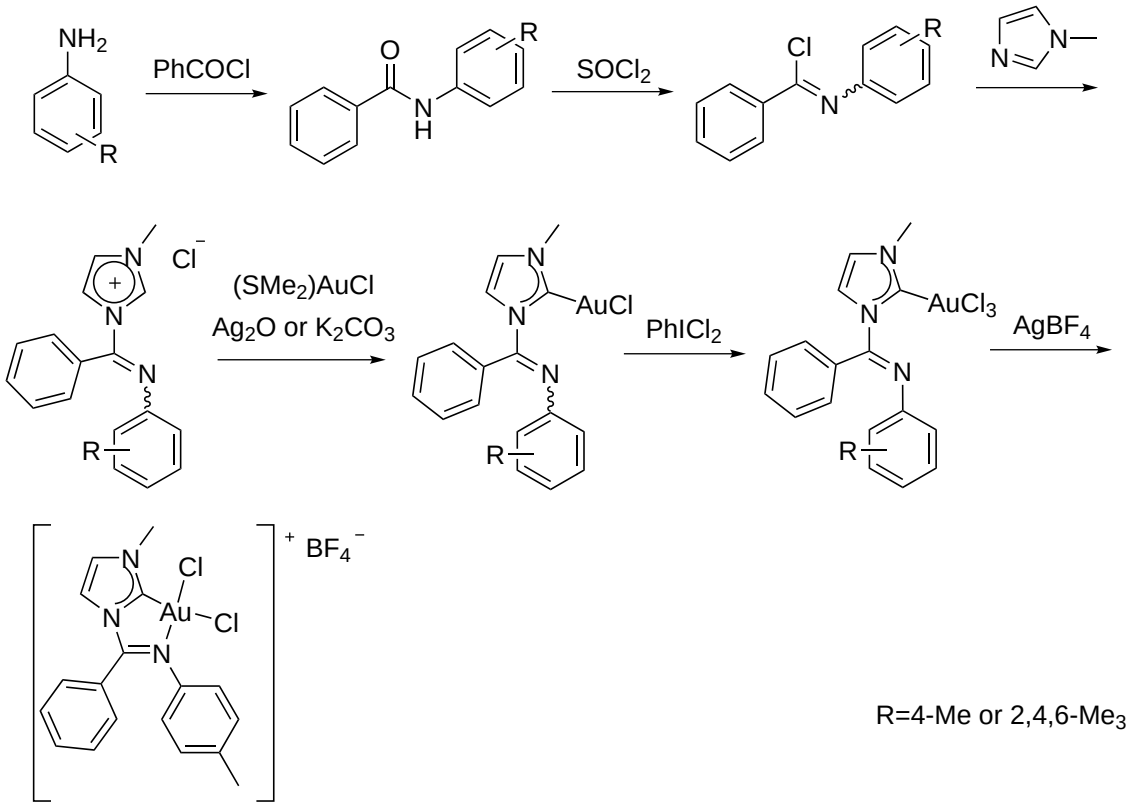

Scheme 2.1: Synthetic route to novel gold(I/III) complexes

A number of novel iminocarbene gold(I) and gold(III) complexes have been synthesised as a part of this project. The synthetic route to these complexes is presented in this chapter and is summarised in Scheme 2.1. Some of the characterisation techniques are described with focus on NMR spectroscopy. The single crystal X-ray analyses of six new compounds are presented in the following chapter.

2.1 Synthesis of iminoimidazolium salt 1a and 1b

The imidazolium salts which were used as carbene precursors have previously been synthesised in the group.[3,7] Starting from methyl substituted anilines, a condensation reaction with benzoyl chloride eliminating HCl afforded *N*-(*p*-tolyl)-benzamide **24a** and *N*-(2,4,6-dimethylphenyl)-benzamide **24b** in good yields. By using $SOCl_2$ as a halogenating agent, the corresponding imidoyl chlorides were synthesised. Extensive drying under vacuum was required to remove excess $SOCl_2$ and the HCl by-product but it could not be guaranteed that these ^{1}H NMR silent compounds were not still present in the product.

By substituting the the Cl in the imidoyl chlorides **25a** and **25b** with 1-methyl-imidazole, the imidazolium salts **1a** and **1b** were synthesised in moderate to good yields. The reported procedure for this reaction is time-consuming (stirring for 48 h). Reducing the reaction time by gently heating the reaction mixture was attempted, but at elevated temperatures, undesired byproducts were formed.

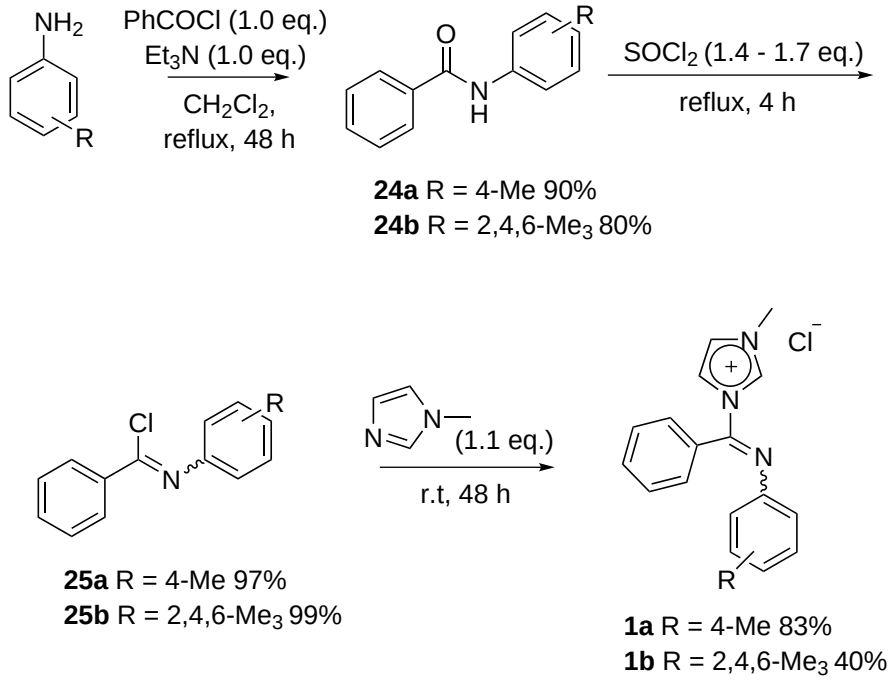

Scheme 2.2: Synthesis of imidazolium salts **1a** and **1b**

2.1.1 The equilibrium of imidazolium salt 1b and its starting materials in solution

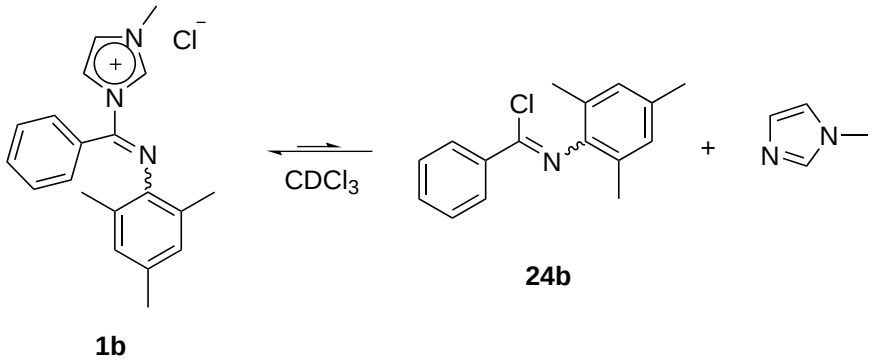

Scheme 2.3: The equilibrium of **1b** in solution

When dissolved in chloroform-*d*, imidazolium salt **1b** was observed to slowly break down to the starting materials. By adding additional 1-methylimidazole to the NMR tube, the equilibrium in Scheme 2.3 is pushed to the left, and any peaks belonging to imidoyl chloride **25b** vanished (Figure 2.1).

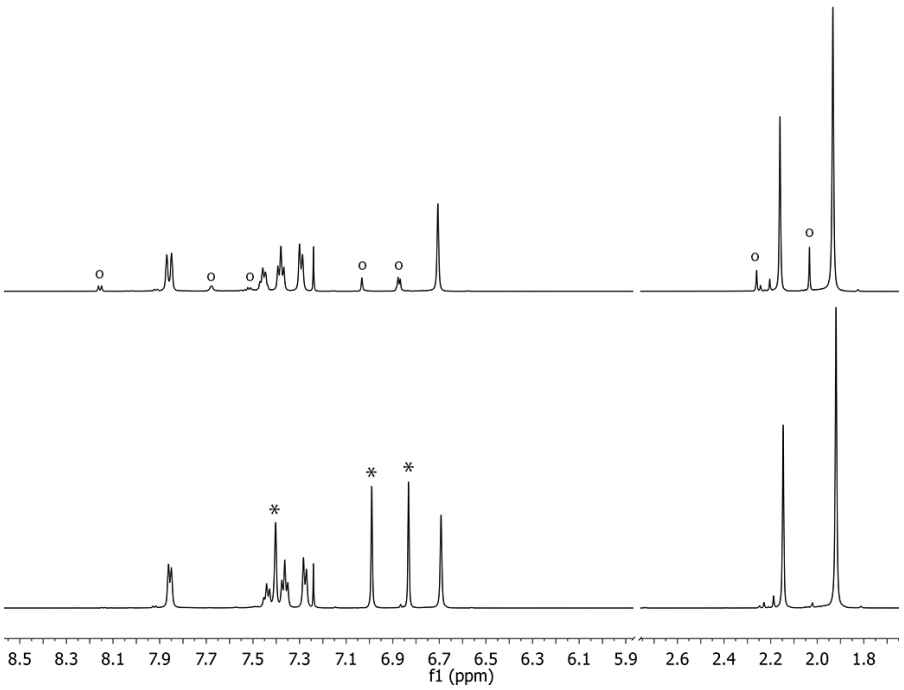

Figure 2.1: Selected sections of the ^{1}H NMR ($CDCl_3$) spectrum of **1b**. Top spectrum: **1b** about 10 min after being dissolved in chloroform-*d* with starting materials marked with circles. Bottom spectrum: A mixture of **1b** and 1-methylimidazole. The peaks belonging to the added 1-methylimidazole marked with *.

2.1.2 The coupling pattern on the imidazolium ring of 1a

The imidazolium salts have been fully characterised by 2D NMR by former group members.[3,7] In the ^{1}H NMR spectrum of **1a** the resonance peaks of the backbone protons, H2 and H3, appear as triplets and have previously only been reported as multiplets without further elaboration.[3] It was therefore of interest to study the origin of these splitting patterns further by COSY NMR and J-resolved decoupling NMR. As illustrated in Figure 2.2 below, H1 has ^4J-coupling with H2, H3 and H4. H2 and H3 share a ^3J coupling.

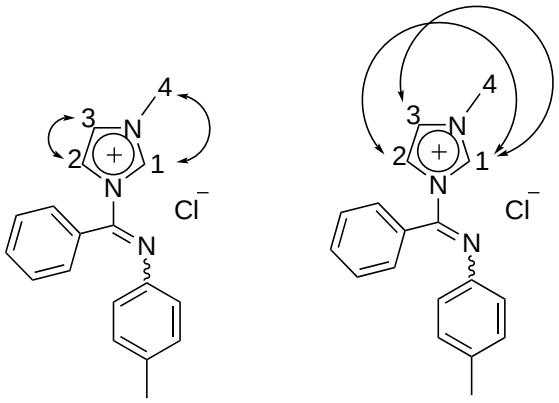

Figure 2.2: Protons correlating in the COSY NMR of **1a**

By saturating the signal from H1 (Figure 2.3), the H2 and H3 signals simplifies to doublets (^3J=2.1 Hz). It is thus shown that the apparant triplets are actually doublets of doublets (dd). By saturating the H4 signal (Figure 2.4), the broad singlet signal from H1 resolves to an apparent triplet (J=1.5 Hz) which is a dd as a result of the coupling to to H2 and H3. Saturating the H2 resonance (Figure 2.5), simplifies the H3 signal to a doublet (^3J=1.3 Hz) and the singlet of H1 becomes less broad.

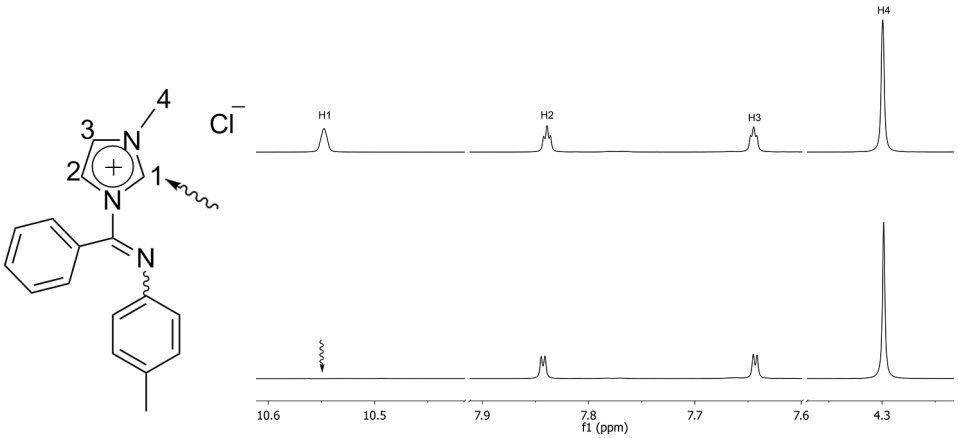

Figure 2.3: Selective decoupling of the resonance of proton H1

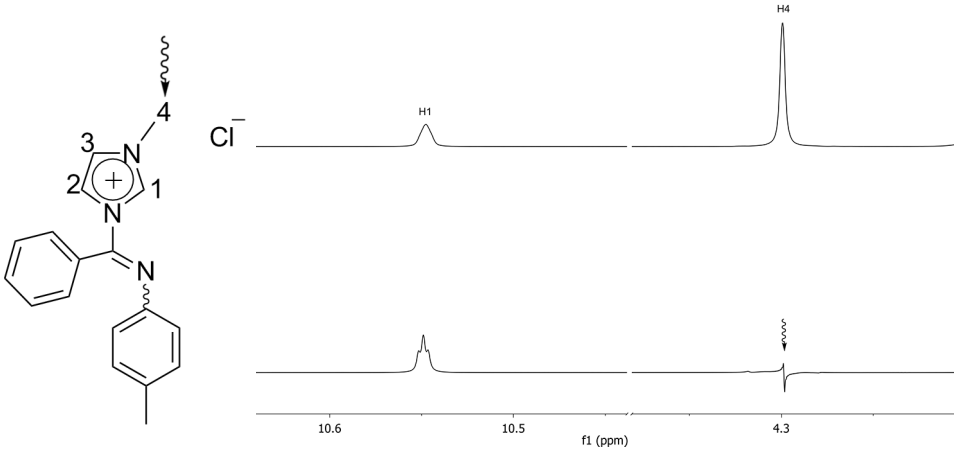

Figure 2.4: Selective decoupling of the resonance of proton H4

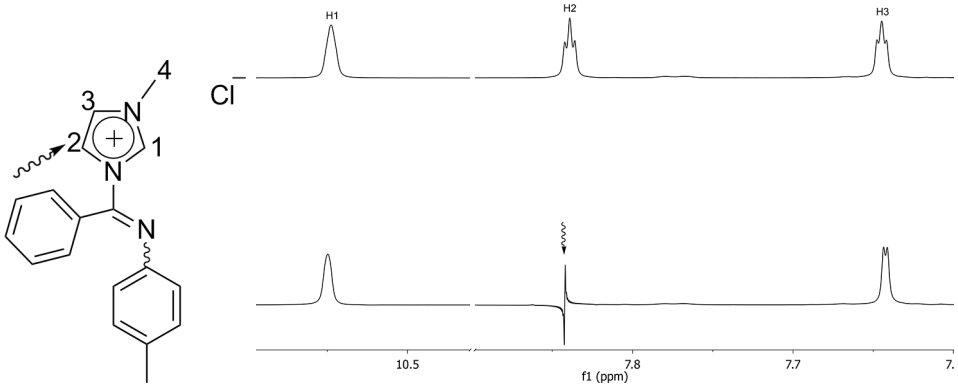

Figure 2.5: Selective decoupling the resonance of proton H2

2.2 Synthesis of iminocarbene gold(I) complexes 3a and 3b

2.2.1 Synthesis of silver(I) complex 2

Silver(I) complex **2** was synthesised according to a procedure previously reported by the group.[3] By using Ag_2O as a mild base, the imidazolium salt was easily deprotonated and the corresponding Ag(I) *N*-heterocyclic carbene complex was formed. Silver salts are hygroscopic and light sensitive and the Ag_2O container might contain decomposition products. Therefore, Ag_2O is commonly used in excess of the 0.5 equivalents required to balance the stoichiometry of the reaction. One of the products of the reaction is water. Molecular sieves were used to remove water from the reaction mixture, driving the reaction towards the product and preventing unwanted side reactions such as hydrolysis of the imine moiety. Silver(I) complex **2** was found to be very moisture and light sensitive, making it complicated to work with. Degraded material was often observed in the ^{1}H NMR spectra and black particles discoloured the light yellow product, both in solution and in the solid phase. However, filtrations and recrystallisation afforded pure material.

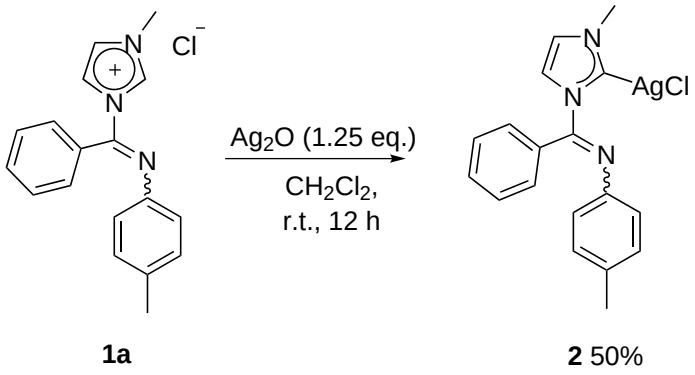

Scheme 2.4: Synthesis of silver(I) complex **2**

2.2.2 Characterisation of silver(I) complex 2

The conversion of the starting material was confirmed by the absence of the downfield ^{1}H NMR signal (10.55 ppm) of the imidazolium salt. Two isomers of **2** were present in solution, and the interconversion between them was slow on the NMR time scale. Two sets of peaks were observed corresponding to the E-isomer and the Z-isomer around the imine double bond, with the major isomer previously reported as the E-isomer.[3] In the ^{13}C NMR spectrum, two downfield signals (181.8

and 184.2 ppm) from the carbenic carbons appeared. The NMR shift values are in accordance with what has been reported previously.[3]

2.2.3 Synthesis of gold(I) complex 3a by transmetalation from the silver(I) carbene 2

Gold complex **3a** was first synthesised by transmetalation from the corresponding silver(I) complex **2** onto gold by the use of $(SMe_2)AuCl$ as a gold-containing precursor.[27] The reaction had previously been performed on a very similar system by fellow group member, MSc. Eirin Langseth, but had not been reported. The labile SMe_2 ligand is easily exchanged for the *N*-heterocyclic carbene, and the precipitation of AgCl drives the reaction forwards. The crude product of the reaction contained byproducts observed by ^1H NMR, but slow recrystallisation from CH_2Cl_2/pentane yielded pure **3a**. However, high purity was not always reproducible using this method.

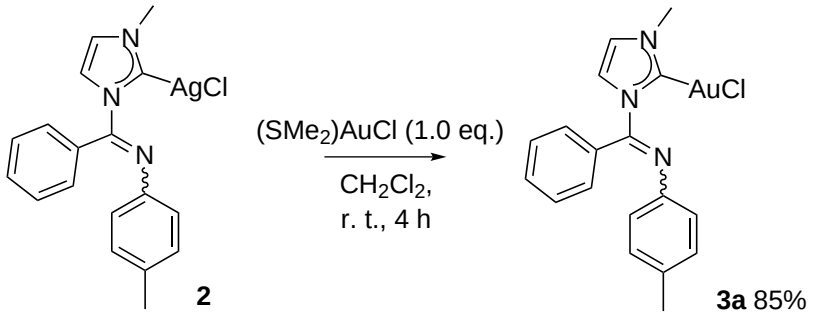

Scheme 2.5: Synthesis of gold(I) complex **3a** by transmetalation from silver

2.2.4 A one-pot synthesis of gold(I) complex 3a using Ag_2O

The poor stability of silver(I) complex **2** inspired the exploration of a one-pot procedure where the silver(I) complex would have to be handled and exposed as little as possible. The reaction conditions gave results similar to the two-step procedure but with a shorter reaction time and with less solvent waste. For most of the duration of this project, this silver one-pot procedure was the method of choice, before a silver-free method was eventually found to be optimal.

2.2.5 Silver-free synthesis of gold(I) complexes using a weak base

The recent publications[31,32] of simple silver-free methods for synthesising *N*-heterocyclic carbenes gold(I) complexes provided a highly efficient synthesis of NHC

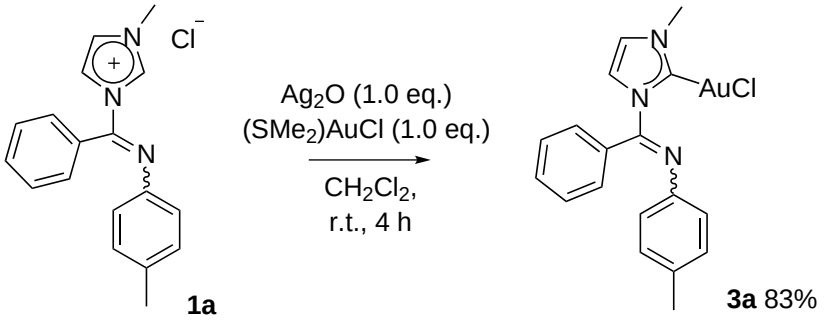

Scheme 2.6: Synthesis of gold(I) complex **3** in a one-pot reaction

gold(I) complexes **3a** and **3b**. The reaction proceeds via imidazolium dichloroaurate(I) salts, one of which was isolated and fully characterised (**4**). Further deprotonation of these salts using a weak base afforded **3a** and **3b** in nearly quantitative yields. The products are pure by ^{1}H NMR and ^{13}C NMR.

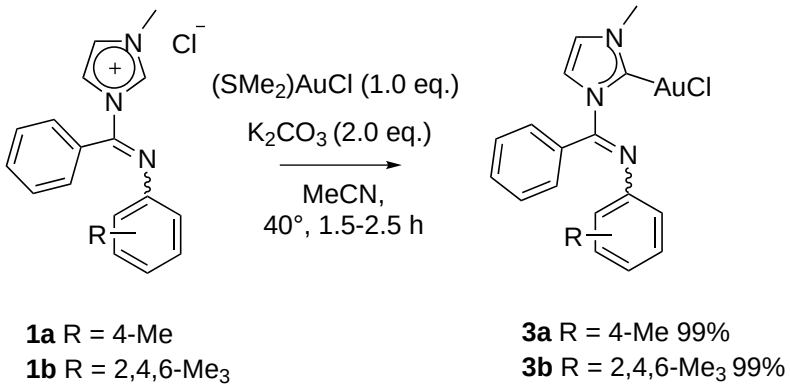

Scheme 2.7: Synthesis of gold(I) complexes using a weak base

For the reactions in Scheme 2.7, the solvents tested were CH_2Cl_2 and MeCN. When using CH_2Cl_2, the solubility of K_2CO_3 is low and Visbal *et al.* reported a procedure using 20 equivalents of the weak base.[32] Despite having ground and dried K_2CO_3 in a vacuum oven prior to use, it was suspected that it still contained some water, and that the minor impurities observed stemmed from hydrolysis of the imine moiety. The optimal reaction conditions reported by Collado and his co-workers in the Nolan group[31] included the use of acetone as a solvent, but good yields had also been obtained using MeCN. The latter was chosen since dry MeCN could easily be obtained from an in-house solvent purifying system.

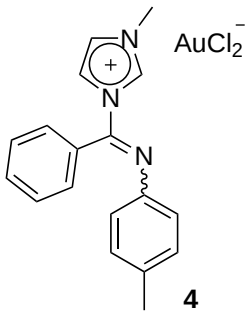

Figure 2.6: Isolated and fully characterised imidazolium dichloroaurate(I) salt **4**

2.2.6 Characterisation of imidazolium dichloroaurate(I) 4

The most salient feature of the ^{1}H NMR spectrum of **4** is the signal corresponding to the H1 proton that appears at 9.28 ppm. This signal is shifted upfield 1.27 ppm relative to that of imidazolium chloride **3a**. The concentration of the salt in chloroform-d has a significant effect on the signal corresponding to the H1 proton, and in weaker solutions, the H1 signal was observed to shift to 9.05 ppm.

The X-ray analysis of **4** can be found in Section 3.2.

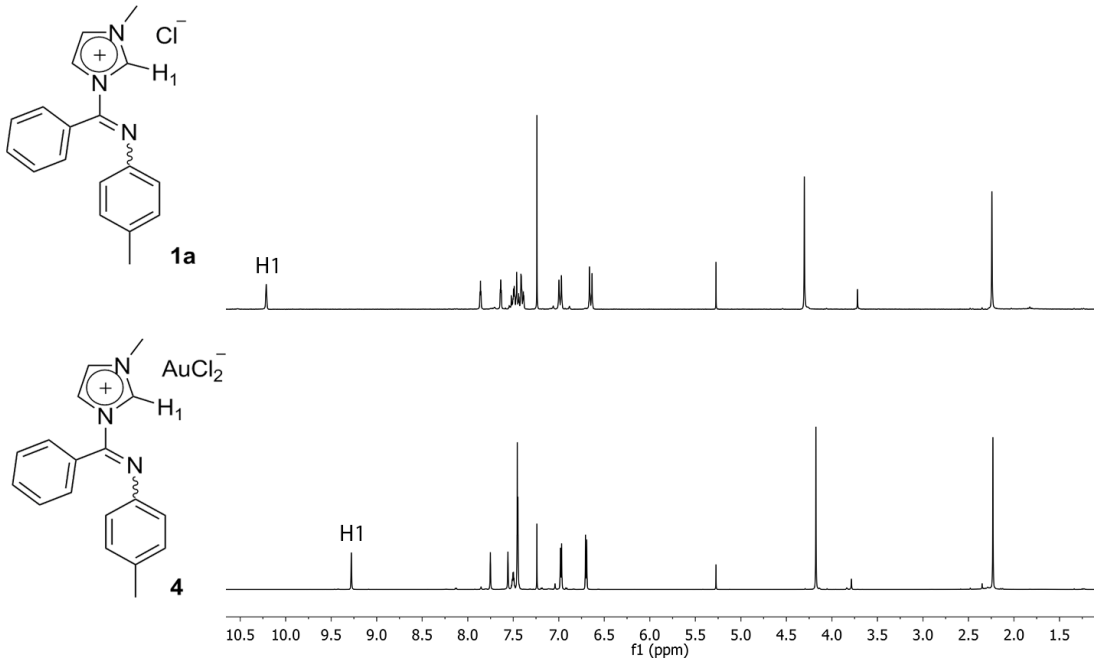

Figure 2.7: Stacked ^{1}H NMR ($CDCl_3$, 600 MHz) of **3a** and **4**

2.2.7 Characterisation of gold(I) complex 3a

The ^{1}H NMR spectrum of **3a** was assigned using standard 2D NMR experiments and the NOESY NMR spectrum is shown in Figure 2.8. The NOESY cross-peaks to the H4 protons on the neighbouring methyl group were used to a distinguish between the two protons on the back-bone of the imidazole, H2 and H3. The signal corrsponding to the H12 proton was assigned on the ground of the NOESY cross-peak with the H14 proton.

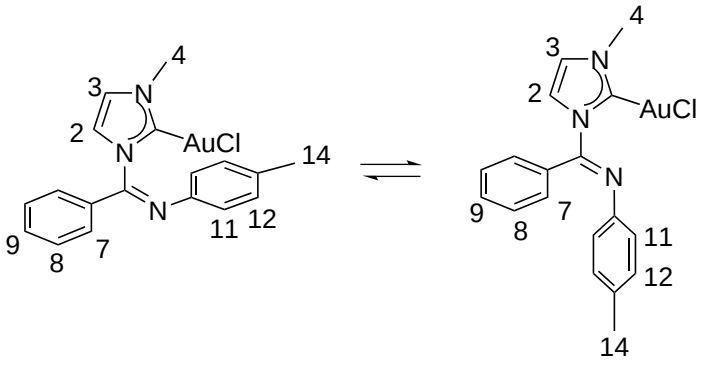

Scheme 2.8: The proposed interconverting isomers of **3a**

In the ^{1}H NMR spectrum of **3a** in $CDCl_3$, the E-isomer and the Z-isomer are observed in nearly equal ratios. Thus, the interconverstion is slow on the NMR time scale, meaning that the difference in the Larmor frequencies of exchanging protons is greater than the rate of the exchange.

The exchange is still happening quite rapidly at room temperature and EXSY cross peaks are observed in the NOESY/EXSY spectrum (Figure 2.9). Both chemical exchange and the Nuclear Overhauser Effect (NOE) transfer longitudinal magnetisation which is why evidence of both processes can be detected with the same 2D experiment. NOESY cross-peaks can be positive in large systems (same sign as the diagonal peaks) or negative in smaller systems, whereas ROESY cross-peaks are always negative. A ROESY spectrum of **3a** can be seen in Figure 7.34 in the Appendix. It confirms that the positive (green) peaks in Figure 2.8 and 2.9 are EXSY cross peaks.

To distinguish between the E-isomer and the Z-isomer of **3a** a series of NOESY NMR experiments were performed with different mixing times in the NOESY pulse sequence. Cross-peaks between the protons on the phenyl ring (H7, H8 and H9) and the H12 protons on the *p*-tolyl ring was expected to be observed for the E-isomer only, whereas cross-peaks between the H2 and H11/H12 protons might have been observed for the Z-isomer. Unfortunately, no such cross-peaks appeared. A second effect of the exchange process is that NOESY cross-peaks between the two

exchanging isomers are observed as seen in Figure 2.9. Even if an appropriate mixing time allowed for the critical cross-peaks to appear, it was assumed that cross-peaks between isomers would have been observed as well.

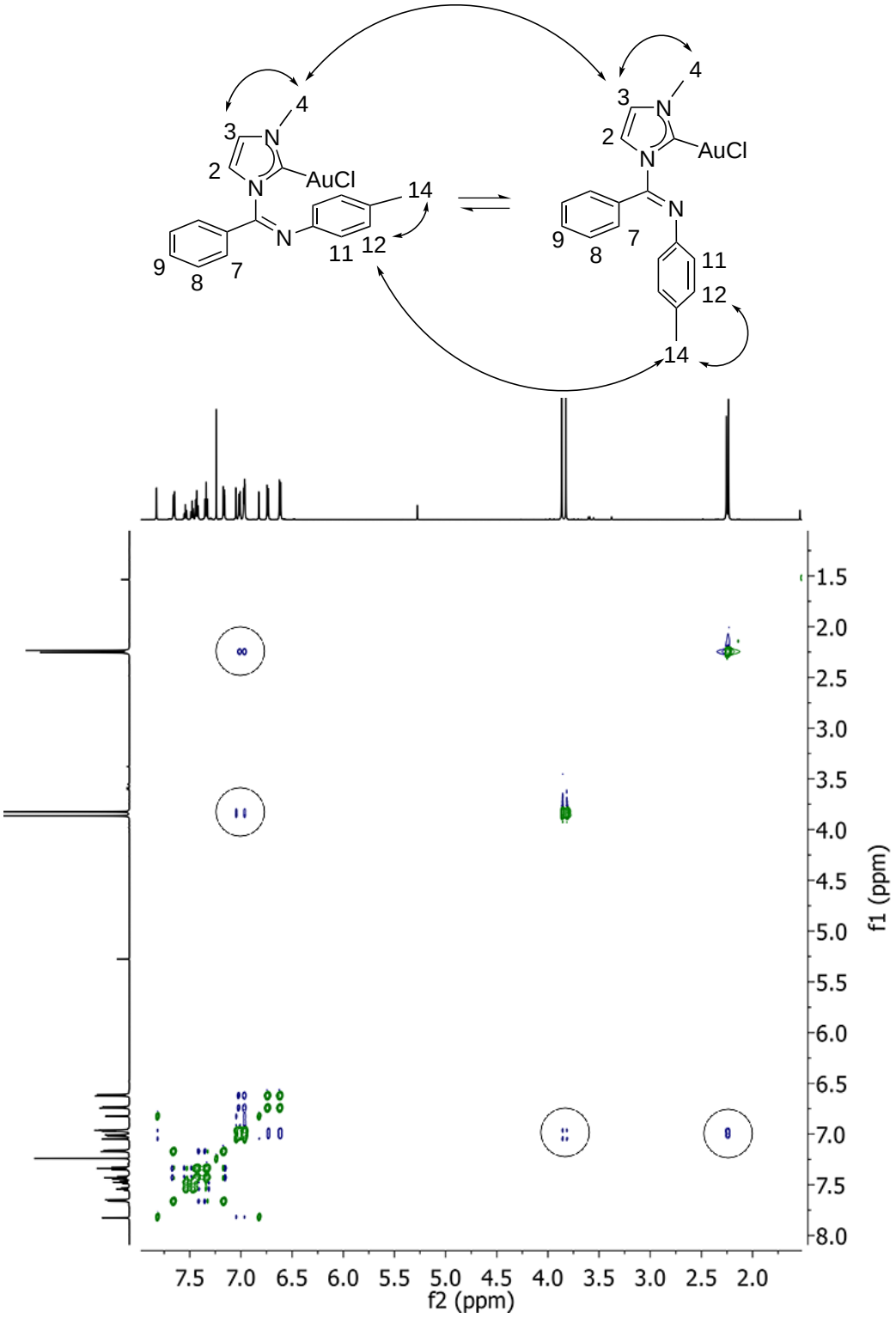

Figure 2.8: NOESY/EXSY NMR of **3a**

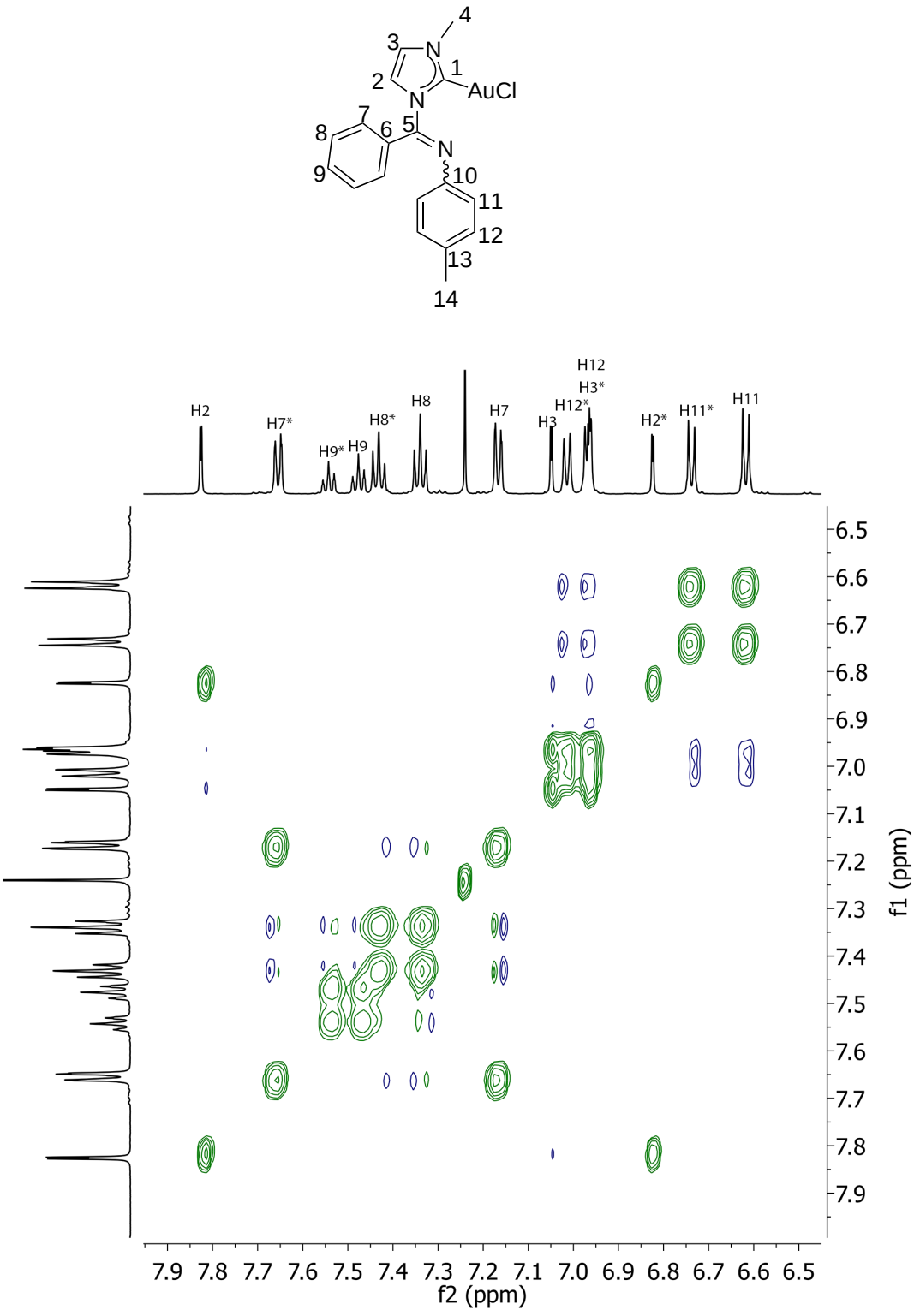

Figure 2.9: NOESY/EXSY NMR of **3a**. * = minor isomer

The NMR signals corresponding to the protons of the two isomers are summarised in Table 2.1. The two protons that have the greatest change in shift value are the H2 proton on the backbone of the imidazole ring and the H7 proton in the *ortho*-position on the phenyl ring. A hypothesis is that the lone pair on the imine nitrogen is deshielding the H2 proton in the E-isomer (assuming rotation occurs) and the H7 proton in the Z-isomer. Hence, the major isomer would be the E-isomer. However, the significant changes in the resonances could also be caused by other effects such as anisotropy of the aromatic rings.

Compound **3a** was further characterised by ^{13}C NMR in which the characteristic downfield shift of the carbenic carbon is found at 174.5 ppm (major isomer) and 172.6 ppm (minor isomer) which is an upfield shift relative to the homoleptic silver(I) complex **2** (184.2/182.1 ppm). Upon investigating **3a** with mass spectrometry the peak of $[(NHC)_2Au_2Cl]^+$ was observed. **3a** was characterised by X-ray diffraction which is presented in Section 3.1.

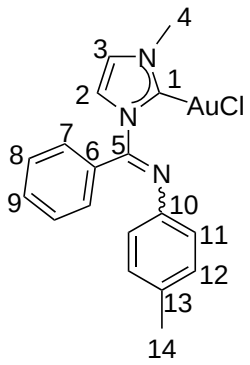

Proton	Major isomer δ (ppm)	Minor isomer δ (ppm)	Difference (ppm)
H2	7.81	6.82	0.99
H3	7.04	6.96	0.08
H4	3.86	3.81	0.05
H7	7.17	7.66	-0.49
H8	7.33	7.34	-0.01
H9	7.47	7.53	-0.06
H11	6.61	6.74	-0.13
H12	6.96	7.01	-0.05
H14	2.23	2.25	-0.02

Table 2.1: ^{1}H NMR chemical shifts of the two isomers of **3a**

2.2.8 Characterisation of gold(I) complex 3b

In solution, two isomers of gold(I) complex **3b** are observed in a 21:79 ratio. The isomers exchange at room temperature as seen for **3a** and the NOESY/EXSY spectrum can be found in Figure 7.46 in the Appendix. The exchange process was also observed when *J*-resolved decoupling NMR was used. As seen in Figure 2.10, selective saturation of the H7 resonance did not only simplify the multiplet of H8 but also diminished the H7* resonance of the minor isomer. Interestingly, the H8* multiplet did not simplify as is expected when the H7* signal is diminished. It may be that longer pre-saturation before acquisition would change this.

The characteristic downfield shift of the carbenic carbon resonance, relative to the imidazolium salt precursor, was observed at 174.4 ppm in the ^{13}C NMR spectrum. Upon investigating **3b** with mass spectrometry in a solution of MeCN with NaCl, the peak of the Na^+ adduct of the complex was observed. **3b** was characterised by X-ray diffraction which is presented in Section 3.1.

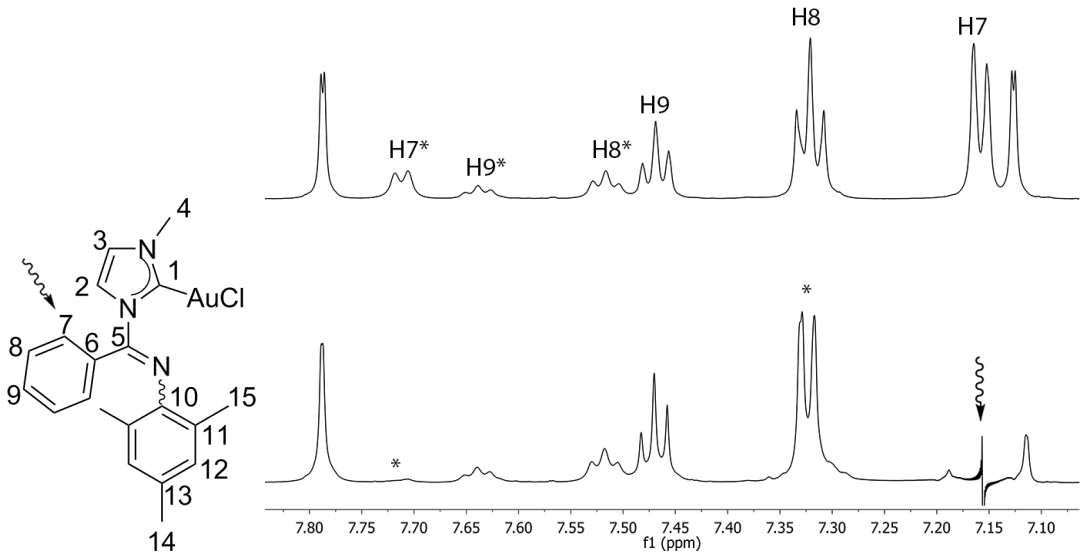

Figure 2.10: * = minor isomer. Selective decoupling of the H7 resonance of the major isomer of **3b** simplifies the apparent triplet of H8 and saturates the H7* resonance belonging to the minor isomer

2.3 Synthesis and characterisation of gold(III) complexes 5a and 5b

The oxidation of **3a** using a hypervalent iodine oxidant[34,37] proceeded cleanly to afford NHC gold(III) trichloride **5a** in quantitative yield. The reaction has been reproduced on several occasions with similar yields and purity. The synthesis of **5b** was only attempted once and gave a mixture of the desired product, decomposition products and unreacted iodobenzene dichloride. The species are moisture sensitive, and water in the reaction mixture was assumed to be the reason for the decomposition. A few crystals were grown from the reaction mixture and the characterisation of **5b** is included for the sake of comparison.

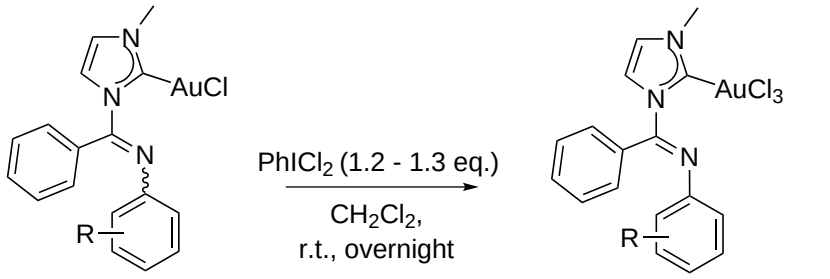

3a R = 4-Me
3b R = 2,4,6-Me_3

5a R = 4-Me 99%
5b R = 2,4,6-Me_3 2%

Scheme 2.9: Synthesis of gold(III) complexes **5a** and **5b**

When gold(I) complex **3a** was oxidised to the corresponding gold(III) complex **5a**, the ^{1}H NMR spectrum simplified and one set of peaks was seen. The single set of signals could be the average of two isomers interconverting fast on the NMR timescale, however, since the less sterically hindered gold(I) isomers interconvert slowly, it is seen as more likely that the signals in the ^{1}H NMR spectrum of **5a** correspond to only one isomer present in solution. From the X-ray analysis presented in Section 3.3, it is determined that **5a** crystallises as the E-isomer. Further, when optimising the geometry of **5a** at the DFT level of theory (Chapter 4), no local minimum on the Potential Energy Surface (PES) was found for the Z-isomer. For these reasons, **5a** is assumed to be present as the E-isomer in solution.

The ^{1}H NMR spectrum of **5b** is of low quality and undefined peaks might be from a minor isomer or impurities. For both **5a** and **5b** the ^{13}C NMR resonances of the carbenic carbons are shifted upfield relative to the gold(I) precursors. This is further discussed in Section 2.5.

Upon investigating **5a** and **5b** with mass spectrometry, the signal corresponding to the molecular ion minus a chloride ligand was observed for both compounds.

5a and **5b** were characterised by X-ray diffraction analyses which are presented in Section 3.3.

2.4 Attemps at coordinating the imine nitrogen to the gold(III) centre

It has been attempted to coordinate the imine nitrogen to the gold(III) centre by using silver(I) salts with poorly coordinating anions, the imine-nitrogen has been attempted coordinated to the gold(III) metal centre. In the initial reactions, AgOTf was used and mixtures of two or three species were repeatedly observed by ^{1}H NMR. One set of signals may have corresponded to unreacted starting material. The species presented in Scheme 2.10 were considered as potential products.

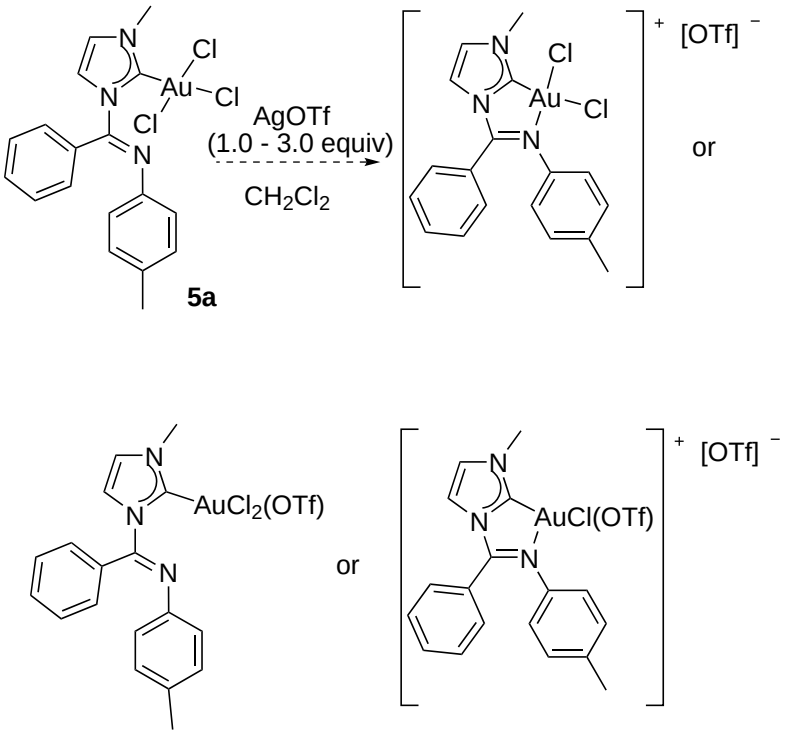

Scheme 2.10: Suggested products in the reaction of **5a** with AgOTf

To gain some insight into what species were present, crystals were grown and characterised by an X-ray analysis. The resultant structure was to our surprise the keto-imidazolylidene gold(III) complex **6** (Scheme 2.11). The discovery confirms that the imine moiety is sensitive and can be hydrolysed. This has long been assumed, but has never been so unambiguously demonstrated. Water may have entered the reaction flask together with the hygroscopic silver salt (which had been stored in a normal refrigerator), with the solvents or as a result of exposure to the atmosphere. An ORTEP-plot of the structure obtained from the X-ray analysis can be found in Section 3.4.

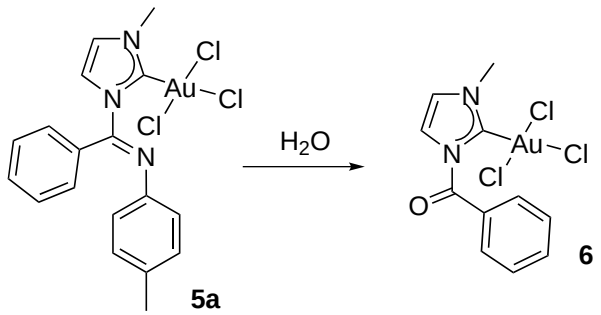

Scheme 2.11: An attempt at coordinating the imine nitrogen resulted in hydrolysis and formation of **6**

Next, a $AgBF_4$ salt stored in a glove-box was used. The reaction of **5a** with $AgBF_4$ gave some very promising results. The ^1H NMR spectra of the starting material **5a** and the new compound which is proposed to be **23** are presented in Figure 2.11. The resonances corresponding to the protons closest to the cationic centre, H4 and H11, are both drastically shifted downfield relative to the starting material. Most other peaks are also shifted downfield as may be expected for a cationic complex.

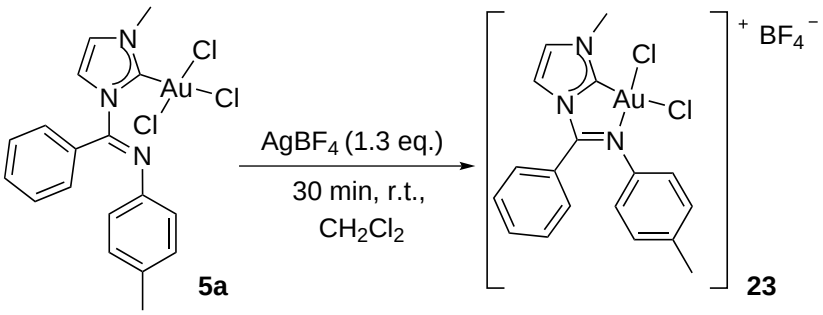

Scheme 2.12: Proposed reaction between **5a** and $AgBF_4$ to form **23**

The imine double bond is expected to weaken upon coordination as an effect of back-donation from the metal to the antibonding π^* of the imine double bond. This would result in a lower IR stretching frequency. An IR spectrum was recorded, but the sample was weak and no clear results could be obtained.

It is highly likely that chelato complex **23** is formed. The reaction was done in a non-coordinating solvent (CH_2Cl_2), and the BF_4^- anion is very poorly coordinating compared to the imine. From a kinetic point of view, chelation is always likely because of the proximity of the donor functionality to the metal centre, and in thermodynamic terms, chelation is favoured for entropic reasons. 5-membered metalacycles of gold(III) are very stable since they allow for a close to square planar coordination geometry around metal centre, and the flat structure has extensive delocation of π-electrons. These preliminary results are very interesting and further work should be done to reproduce the synthesis of **23** and obtain X-ray quality crystals.

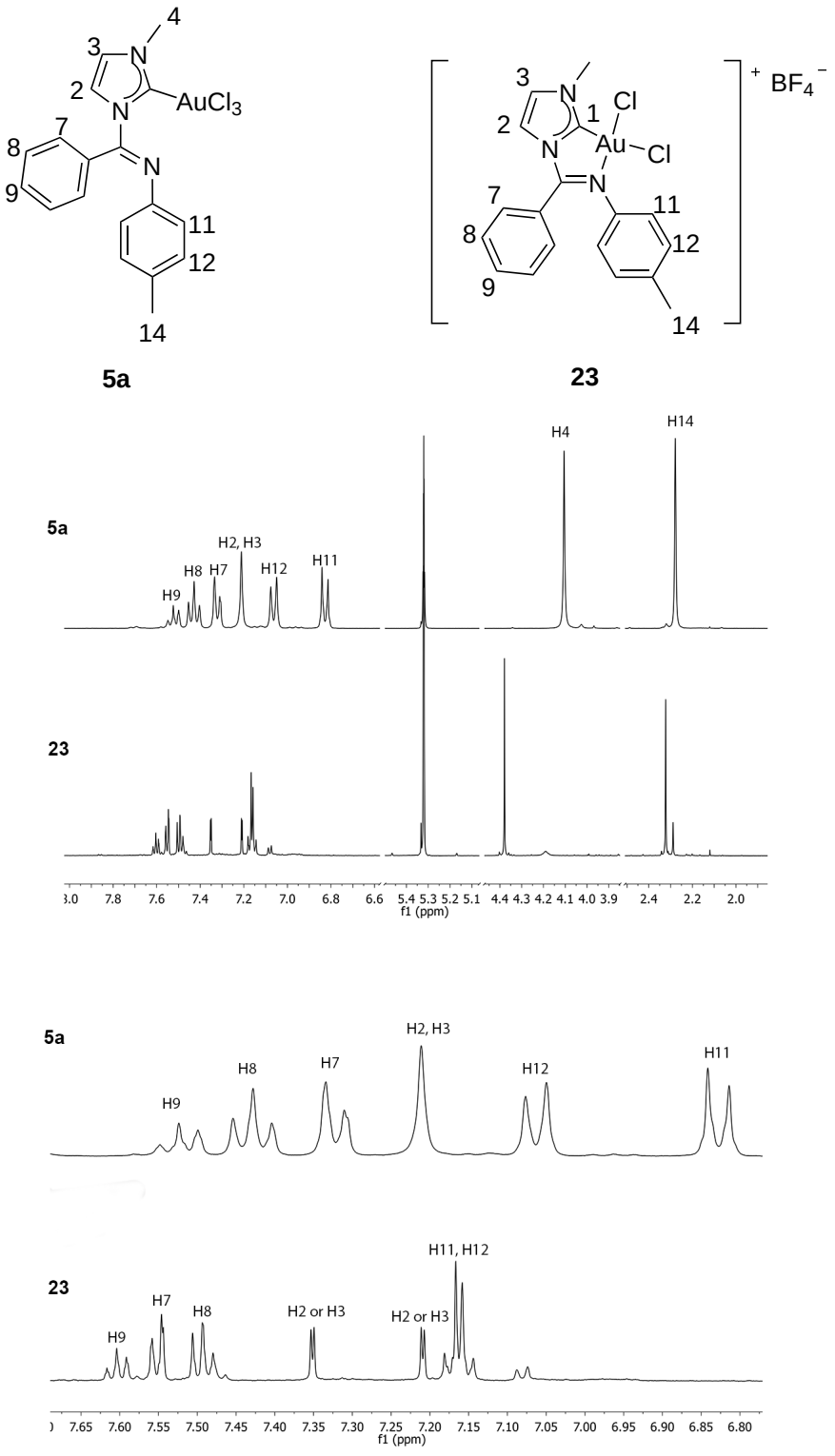

Figure 2.11: ^{1}H NMR spectra of **5a** and a new compound proposed to be **23**

2.5 Diagnostic ^{13}C-NMR chemical shifts of carbenic carbons

When following the reaction going from imidazolium salts to *N*-heterocyclic carbene gold(I/III) complexes, the ^{13}C NMR chemical shift values of the carbenic carbon (C1) are diagnostic. In imidazolium salt **1a** the C1 carbon resonates at 138.0 ppm. When deprotonated and coordinated to gold(I) to give the two isomers of **3a**, the C1 carbon becomes more deshielded and the C1 signal shifts 34.6/36.5 ppm downfield. When oxidised to gold(III) complex **5a**, an upfield shift of 28.6/30.5 ppm compared to **3a** is observed.

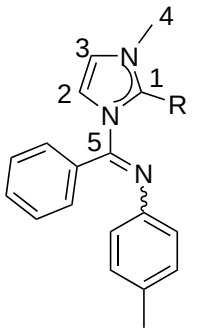

Compound		**C1**	**C2**	**C3**	**C4**	**C5**
4	R=H·[$AuCl_2$]	135.8	120.0	121.6	37.8	147.8
1a	R=H·Cl	138.0	121.6	124.5	37.7	148.6
5a	R=$AuCl_3$	144.0	122.4	124.5	39.0	150.1
3a (minor)	R=AuCl	172.6	121.5	121.4	39.8	152.9
3a (major)	R=AuCl	174.5	120.5	121.7	39.8	147.8
2 (minor)	R=AgCl	181.9	-	-	-	-
2 (major)	R=AgCl	184.2	-	-	-	-

Table 2.2: Selected ^{13}C-NMR ($CDCl_3$) chemical shift values (ppm). Not all compounds were fully characterised in the relevant solvent

Upfield shifts when gold is oxidised is commonly observed.[57,58] It has been postulated that the chemical shift of carbenic carbons can be correlated to the Lewis acidity of the metal to which the *N*-heterocyclic carbon is bound.[59] With two additional electronegative chloride ligands, the gold(III) complex is more Lewis acidic than its gold(I) congener. Electron density is therefore more efficiently donated to the formally empty p_z-orbital on the carbene from the neighbouring nitrogen atoms and the extended conjugated system. The lone-pairs on the Cl_{cis} ligands

might also contribute to shielding the carbenic carbon. The signal of the gold(III) coordinated carbenic carbon is thus shifted upfield relative to its gold(I) congener. The strongest Lewis acid is H^+ with an $AuCl_2^-$ counterantion and the resonance peak of the C1 carbon of **4** is shifted furthest upfield.

With the exception of one entry, the imine-carbon (C5) resonance is shifted slightly downfield when the C1 resonance is shifted upfield. The improved donation of electron density from the α-amino nitrogens to the carbenic carbon could mean that the electron donation to the C5 from the imidazole ring decreases and C5 gets more deshielded. The other NMR resonance of carbon nuclei do not seem to correlate with the C1 shift and only small changes in chemical shifts are observed.

The gold complexes bearing a mesityl group were all characterised in a different solvent than the **1a-5a** series and direct comparison of chemical shifts cannot be made. However, the same trend in relative C1 shift values is observed (Table 2.3). The C5 chemical shifts are following an oposite trend in this series, as it is shifted a downfield by 2-3 ppm in correlation with the much more significant downfield shift of the C1 resonance. It is thus clear than the C5 resonance is not diagnostic of the Lewis acidity of the metal to which the imino-imidazolylidene is coordinated.

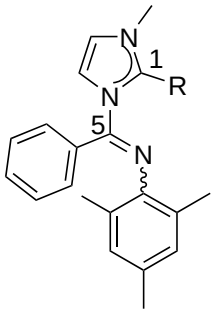

Compound		**C1**	**C5**
1a	R=H·Cl	138.5	147.7
5b	R=$AuCl_3$	143.8	149.8
3b (major)	R=AuCl	174.4	152.7

Table 2.3: Selected ^{13}C-NMR (CD_2Cl_2) chemical shift values (ppm).

CHAPTER 3

Single crystal X-ray diffraction analysis of new gold(I/III) complexes

Six new compounds have been characterised using single crystal X-ray diffraction. X-ray quality crystals were grown at about 4 °C by slow diffusion of pentane onto a nearly saturated CH_2Cl_2 solution of the respective compounds. Data collection and refinement has been done by MSc. Sigurd Øien. All but one of the datasets were obtained using the in-house Bruker D8 Discover instrument with Mo Kradiation. The dataset for **3a** was recorded at the MAX Laboratory in Lund, Sweden, using a Bruker MD2 instrument with the I911-3 Casiopeia beam line.[60] The quality of the datasets are good and all structures are unambiguosly determined. The single-crystal X-ray diffraction was not followed up by powder X-ray diffraction and no comment can be made about the overall compositions of the samples. However, representative crystals were chosen apart from for **5b** and **6** where amorphous phases also were present. The following ORTEP-plots are drawn in Diamond[61] with ellipsoids at the 50% level of probability. Several of the asymmetric units contain two complexes, but for the sake of clarity, only one complex is included in the figures. In the tables of bond distances and angles, Complex 1 and Complex 2 denotes the two complexes which together constitute the asymmetric unit. Crystallographic data can be found in Figures 7.1 - 7.6 in the appendix.

3.1 Crystallographically determined structure of gold(I) complexes 3a and 3b

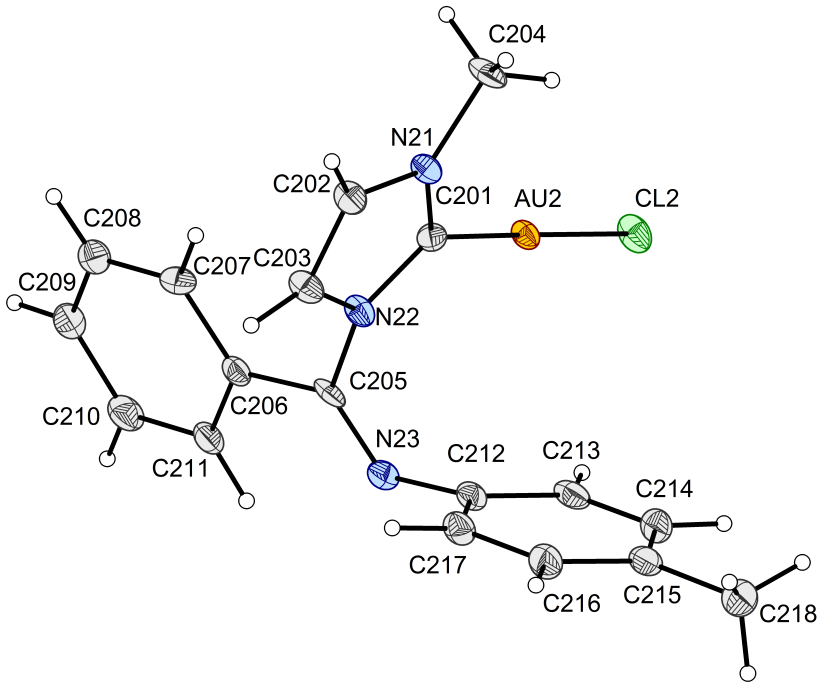

Figure 3.1: ORTEP-drawing of complex **3a**

#	Atoms	Complex 1 Distances (Å)	Complex 2 Distances (Å)
1	Cl2-Au2	2.288(1)	2.293(1)
2	Au2-C201	1.987(5)	1.985(5)
3	C201-N21	1.346(6)	1.344(6)
4	N21-C202	1.382(6)	1.380(6)
5	C202-C203	1.349(6)	1.355(6)
6	C203-N22	1.392(6)	1.398(6)
7	N22-C201	1.352(6)	1.354(6)
8	N22-C205	1.452(5)	1.457(6)
9	C205-C206	1.474(7)	1.473(7)
10	C205-N23	1.265(5)	1.265(5)
11	N23-C212	1.422(6)	1.431(6)

#	Atoms	Complex 1 Angles (°)	Complex 2 Angles (°)
1	Cl2-Au2-C201	178.5(1)	179.3(1)
2	C205-N23-C212	122.5(4)	121.6(4)
1	Cl2-Au2-C201-N22	85(5)	-69(12)
2	Au2-C201-N22-C205	-4.6(6)	-8.7(6)
3	C201-N22-C205-C206	-99.4(5)	-95.7(5)
4	C201-N22-C205-N23	76.4(6)	81.4(6)
5	N22-C205-C206-C211	-168.8(4)	171.6(4)
6	N22-C205-N23-C212	4.6(6)	5.1(6)
7	C205-N23-C212-C213	67.6(6)	75.3(6)

Table 3.1: Selected bond lengths and angles for complex **3a**

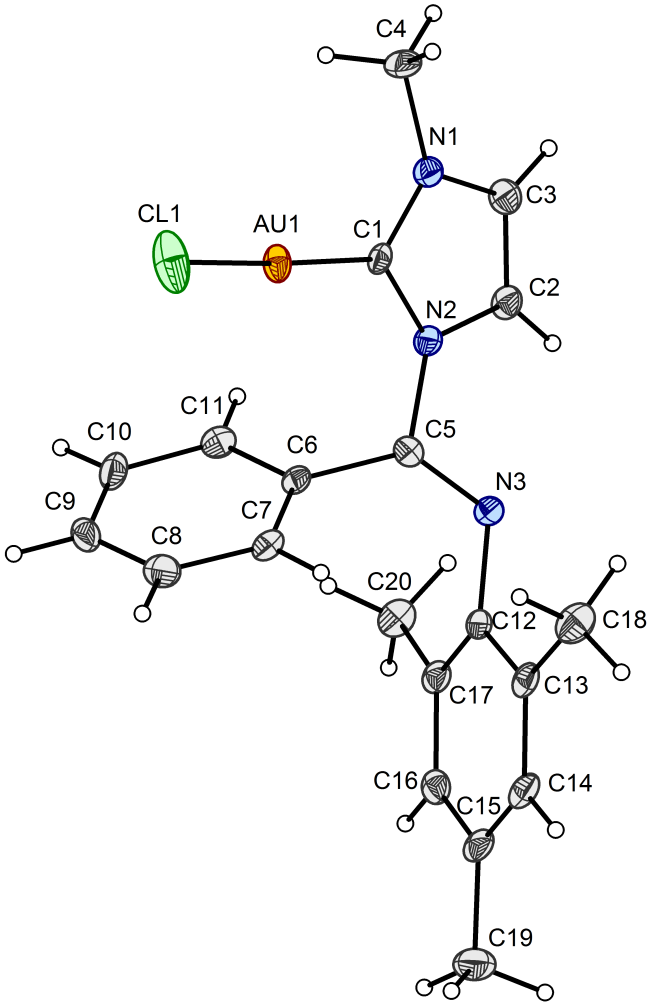

Figure 3.2: ORTEP-drawing of complex **3b**

#	Atoms	Distances (Å)
1	Au1-Cl1	2.2799(9)
2	Au1-C1	1.990(3)
3	N1-C1	1.334(4)
4	N1-C3	1.382(4)
5	C2-C3	1.341(5)
6	N2-C2	1.393(4)
7	C1-N2	1.370(4)
8	N2-C5	1.437(4)
9	C6-C5	1.485(5)
10	N3-C5	1.267(4)
11	N3-C12	1.438(4)

#	Atoms	Angle (°)
1	Cl1-Au1-C1	174.6(1)
2	C5-N3-C12	121.5(3)
1	Cl1-Au1-C1-N2	113(1)
2	Au1-C1-N2-C5	4.0(5)
3	C1-N2-C5-C6	39.4(5)
4	C1-N2-C5-N3	-143.8(3)
5	N2-C5-C6-C7	-132.5(4)
6	C5-N3-C12-C17	72.1(5)

Table 3.2: Selected bond lengths and angles for complex **3a**

In the X-ray analysis of **3a** two molecules comprises the asymmetric unit, whilst **3b** has only one molecule in the asymmetric unit. **3a** and **3b** are two-coordinate gold(I) complexes in near linear environment with $C_{carbene}$-Au-Cl bond angles of 178.5°/179.3° and 174.6° respectively. The Au-$C_{carbene}$ distances are 1.987/1.985 Å and 1.990 Å which is in good agreement with what is commonly observed for NHC gold(I) complexes.[31,57,62] The Au-Cl distances ranges from 2.288-2.293 Å which is slightly longer than what is observed for the $AuCl_2^-$ counteranion of **4** (2.259/2.255 Å). This is a consequence of the trans influence of the strongly σ-donating carbene.

The packing diagrams show pairwise intermolecular gold-gold distances of 4.252 Å for **3a** and 3.984 Å for **3b**. These distances are longer than the sum of the van der Waal radii for two gold atoms (3.6 Å),[49] but in the case of **3b**, a gold-gold attraction might still contribute to the packing of the molecules in the solid state.[62]

As earlier discussed, two isomers are observed in the NMR spectra of **3a** and **3b**. Interestingly, **3a** crystalises as the Z-isomer and **3b** crystalises as the E-isomers. Alas, this does not prove which isomer is the more favourable in solution. In both crystals the imine nitrogen is pointing away from the gold centre.

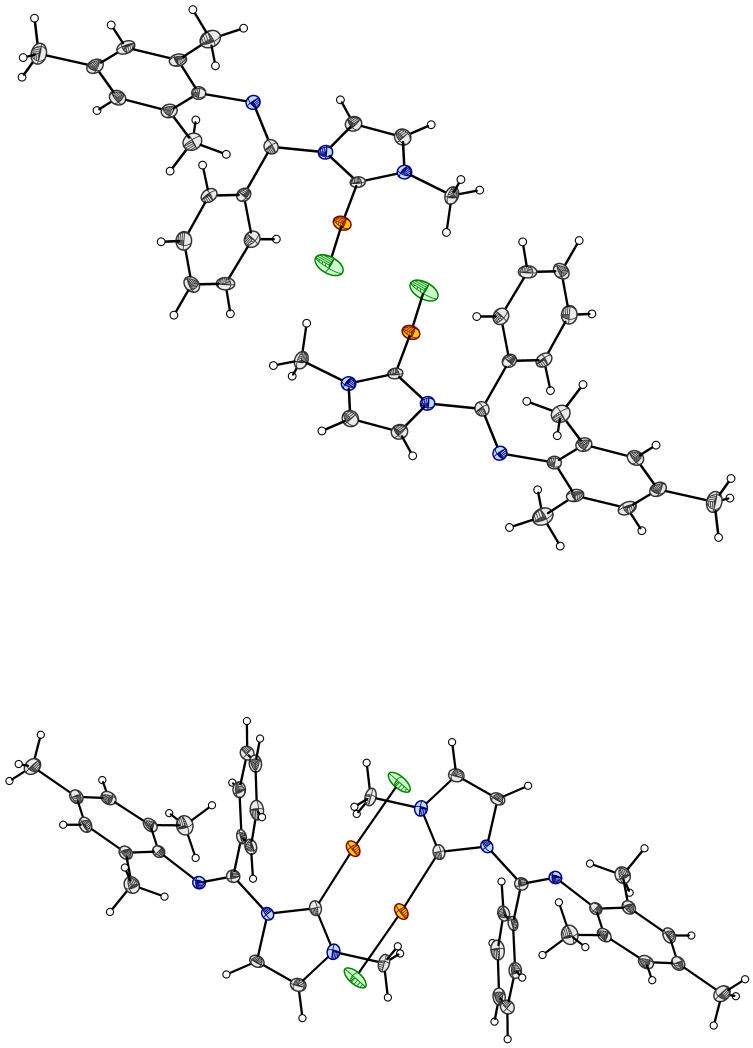

Figure 3.3: Packing feature of **3b** with gold-gold distances of 3.984 Å

3.2 Crystallographically determined structure of 4

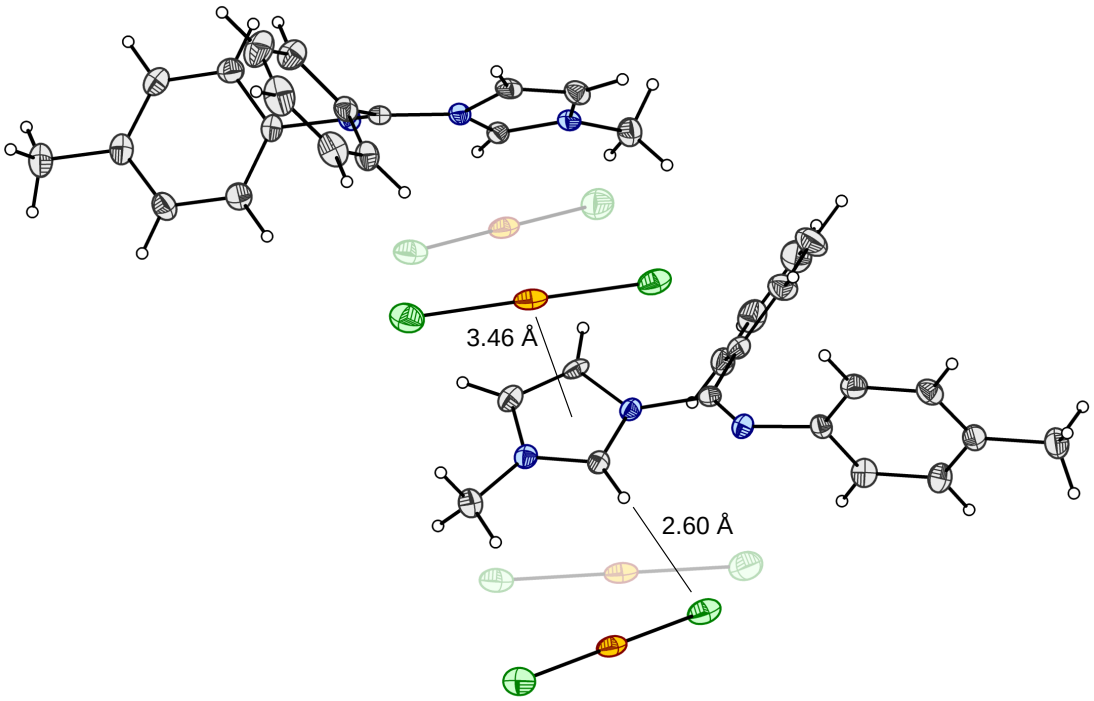

Figure 3.4: Packing features of **4**

In the structure obtained from the X-ray analysis of **4** the dichloroaurate(I) anion is essentially linear with a Cl-Au-Cl angle of 179.6°. The Au-Cl distances of 2.259 and 2.255 Å are similar to the previously published structure of an imidazolium dichlorideaurate(I) salt (2.261 and 2.231Å)[31] and other salts of the same anion.[63] In the packing diagram (Figure 3.4) it is seen that the $AuCl_2^-$ anions pack around the imidazolium ring with the shortes $H_{imidazole}$-Cl_{anion} distance being about 2.6 Å (Note that the hydrogen atoms are inferred from neighbouring sites and constrained in the refinement). Another $AuCl_2^-$ unit lies straight over the centroid of the imidazolium ring with a Au-centroid distance of 3.456 Å.

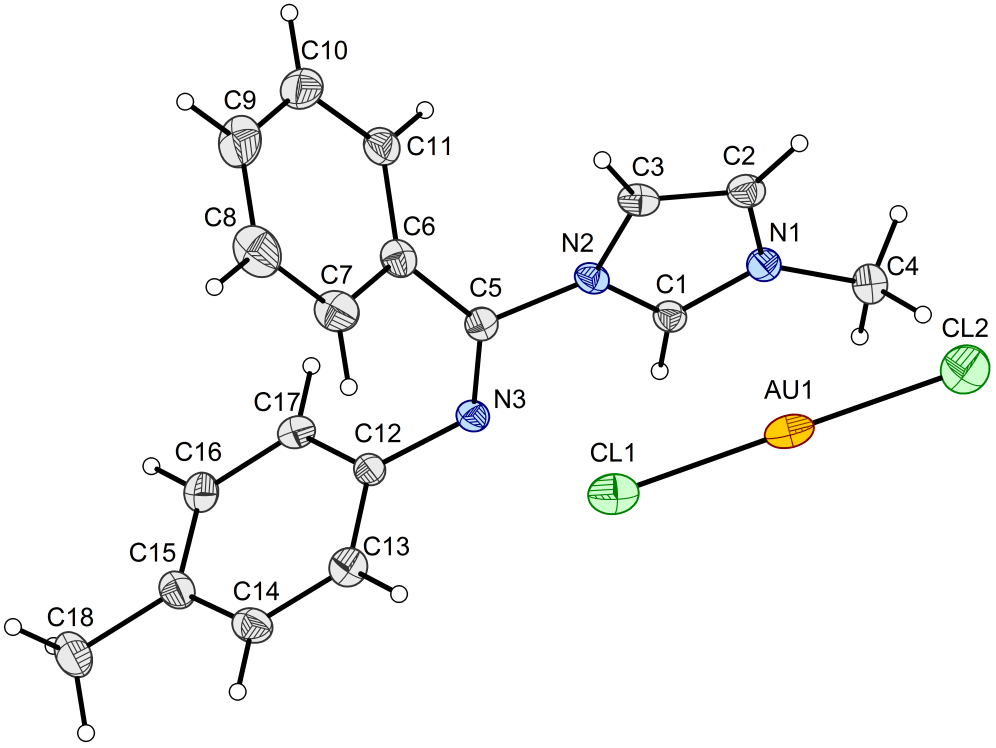

Figure 3.5: ORTEP-drawing of complex **4**

#	**Atoms**	**Distance (Å)**
1	Au1-Cl1	2.2590(8)
2	Au1-Cl2	2.2549(9)
3	Au1-C1	3.735(3)
4	Au1-N1	3.526(2)
5	Au1-N2	3.809(2)
6	Cl1-N2	3.506(2)
7	Cl1-N3	3.460(2)
8	N1-C1	1.326(4)
9	N1-C2	1.384(4)
10	N2-C3	1.381(4)
11	C1-N2	1.341(4)
12	N2-C5	1.446(4)
13	C5-C6	1.482(4)
14	N3-C5	1.258(4)
15	N3-C12	1.421(4)

#	**Atoms**	**Angle (°)**
1	Cl1-Au1-Cl2	179.61(3)
1	C1-N2-C5-C6	-167.3(3)
2	C1-N2-C5-N3	15.2(4)
3	N2-C5-C6-C7	-127.7(3)
4	N2-C5-N3-C12	-173.4(2)
5	C5-N3-C12-C13	-112.8(3)

Table 3.3: Selected bond lengths and angles for complex **4**

3.3 Crystallographically determined structure of 5a and 5b

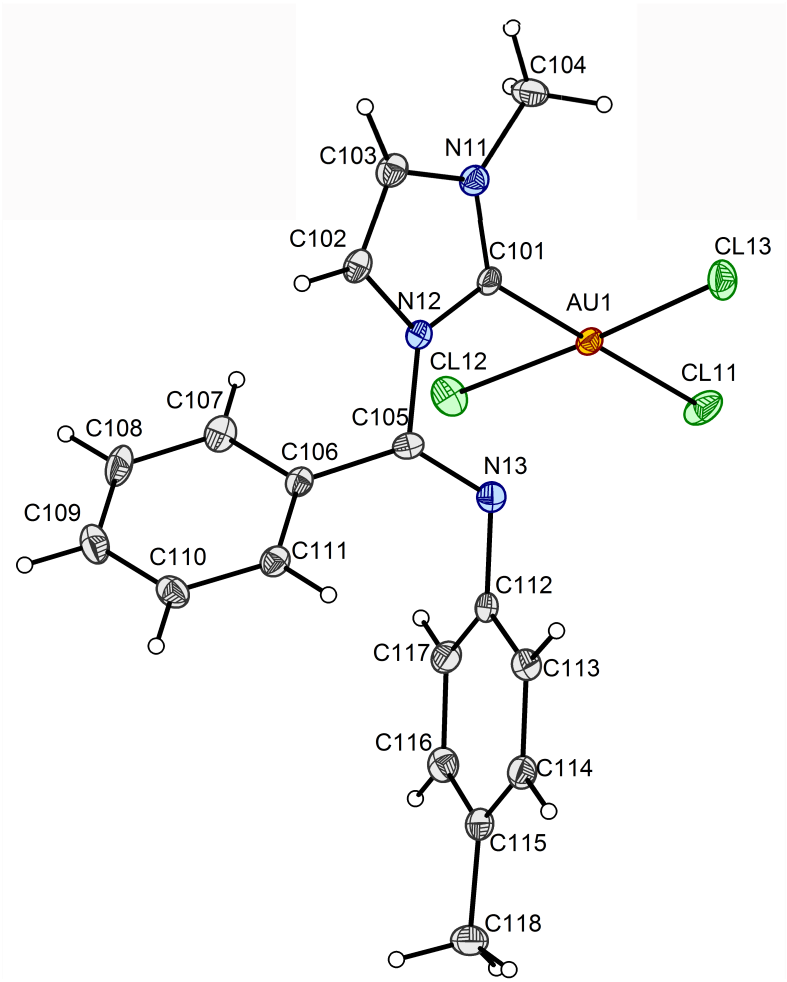

Figure 3.6: ORTEP-drawing of complex **5a**

#	Atoms	Complex 1 Distances (Å)	Complex 2 Distances (Å)
1	Au1-Cl11	2.3152(8)	2.3097(8)
2	Au1-Cl13	2.2882(8)	2.2868(8)
3	Au1-Cl12	2.2816(8)	2.2779(8)
4	Au1-C101	1.992(3)	1.996(3)
5	C101-N11	1.337(4)	1.330(4)
6	N11-C103	1.389(4)	1.389(4)
7	C102-C103	1.340(4)	1.334(5)
8	N12-C102	1.393(4)	1.384(4)
9	C101-N12	1.349(4)	1.349(4)
10	N12-C105	1.442(4)	1.442(4)
11	C105-C106	1.490(4)	1.483(4)
12	N13-C105	1.264(4)	1.269(4)
13	N13-C112	1.430(4)	1.430(4)
14	Au1-N13	3.071(3)	2.970(3)

#	Atoms	Complex 1 Angles (°)	Complex 2 Angles (°)
1	Cl13-Au1-Cl12	176.01(3)	174.58(3)
2	Cl11-Au1-C101	177.77(9)	177.45(9)
3	Cl12-Au1-C101	87.10(9)	87.88(9)
4	Cl13-Au1-C101	88.95(9)	88.38(9)
5	C105-N13-C112	119.4(3)	119.6(3)
1	Cl11-Au1-C101-N12	119(2)	-26(2)
2	Cl12-Au1-C101-N12	-118.8(3)	-111.6(3)
3	Au1-C101-N12-C105	4.5(4)	-0.7(4)
4	C101-N12-C105-C106	-146.4(3)	-150.8(3)
5	C101-N12-C105-N13	34.5(4)	29.2(4)
6	N12-C105-C106-C111	-135.9(3	-132.5(3)
7	N12-C105-N13-C112	-175.5(2)	-172.9(3)
8	C105-N13-C112-C113	-113.1(3)	-111.5(3)
9	Au1-C101-C105-N13	34.4(2)	25.4(2)

Table 3.4: Selected bond lengths and angles for complex **5a**

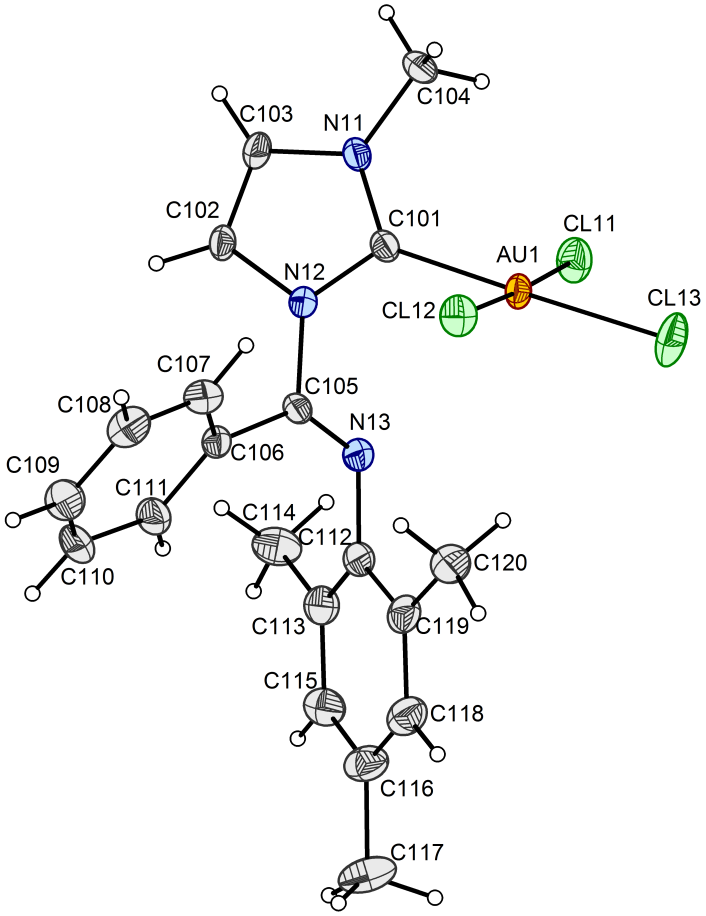

Figure 3.7: ORTEP-drawing of complex **5b**

#	Atoms	Complex 1 Distances (Å)	Complex 2 Distances (Å)
1	Cl13-Au1	2.296(1)	2.314(1)
2	Cl12- Au1	2.274(1)	2.286(1)
3	Cl11- Au1	2.282(2)	2.281(1)
4	Au1 -C101	1.994(4)	2.002(4)
5	C101- N11	1.332(6)	1.323(6)
6	N11 -C103	1.381(5)	1.387(5)
7	C103- C102	1.352(6)	1.337(6)
8	C102- N12	1.386(5)	1.396(5)
9	N12 -C101	1.353(5)	1.357(5)
10	N12- C105	1.451(6)	1.449(5)
11	C105-C106	1.489(6)	1.484(5)
12	C105-N13	1.257(5)	1.257(5)
13	N13-C112	1.426(6)	1.431(6)
14	N13-Au1	3.343(3)	2.938(4)

#	Atoms	Complex 1 Angles (°)	Complex 2 Angles (°)
1	Cl13-Au1-C101	177.7(1)	178.9(1)
2	Cl12-Au1-Cl11	177.32(5)	176.16(5)
3	Cl12-Au1-C101	88.0(1)	88.5(1)
4	Cl11-Au1-C101	90.0(1)	87.9(1)
5	C105-N13-C112	121.7(4)	121.7(4)
1	Cl13-Au1-C101-N12	-110(3)	168(6)
2	Cl12-Au1-C101-N12	-66.4(4)	-103.5(4)
3	Au1-C101-N12-C105	-11.9(6)	1.3(6)
4	C101-N12-C105-C106	-45.5(5)	-112.8(4)
5	C101-N12-C105-N13	-45.7(6)	11.1(6)
6	N12-C105-C106-C111	133.9(4)	-112.8(4)
7	N12-C105-N13-C112	-177.8(4)	-177.8(4)
8	C105-N13-C112-C119	-80.9(6)	-114.5(5)
9	Au1-C101-C105-N13	-50.1(3)	11.1(3)

Table 3.5: Selected bond lengths and angles for complex **5b**

The X-ray analysis of **5a** and **5b** show that both complexes have the expected square planar configuation with near linear $C_{carbene}$-Au-Cl_{trans} and Cl_{cis}-Au-Cl_{cis} angles. The plane defined by the $AuCl_3$ moiety and the plane defined by the imidazole ring are not perpendicular which can be attributed to the unsymmetrical substitution of the imidazole ring or packing effects. Au-$C_{carbene}$ bond lengths range from 1.992-2.002 Å and are within the region of what is commonly observed (1.98-2.13 Å).[34,35] The observed Au-Cl_{trans} distances of 2.296-2.315 Å are slightly longer than the Au-Cl_{cis} distances of 2.274-2.288 Å as an effect of the stronger trans influence of the strongly σ-donating NHC ligand.

The observed $C_{carbene}$-Au–Cl_{cis} angles are slightly smaller than 90° which is commonly observed for NHC gold(III).[35] This could be an effect from repulsion between the lone pairs of the halogen atoms, or it can be due to donation of electron density from a chlorine lone pair into the formally empty orbital on the $C_{carbene}$.

The disance between the metal centre and the imine nitrogen is 3.071/2.970 Å for **5a** and 3.343/2.938 Å for **5b** which is shorter than the sum of the van der Waal radii (r(N)+r(Au)=3.21 Å). An attractive interaction between the nitrogen lone pair and the lewis acidic gold(III) centre might be present and is discussed further at the end of this chapter.

3.4 Crystallographically determined structure of 6

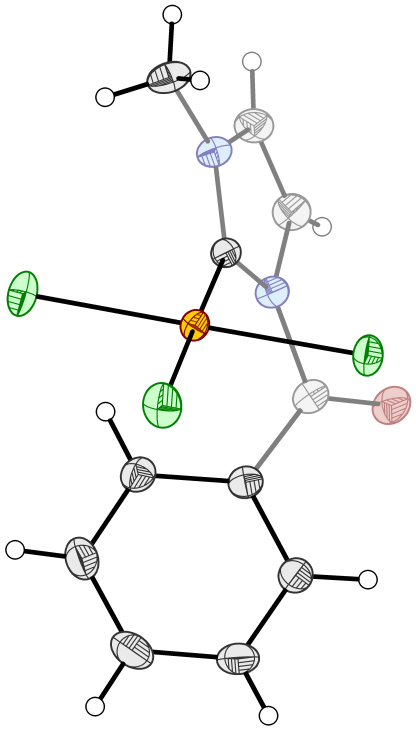

Figure 3.8: ORTEP-drawing of complex **6**

The crystallographically determined structure of **6** has bond lengths and angles around the gold centre similar to those of **5a** and **5b**. The plane of the $AuCl_3$ moiety is oriented so that there might be an interaction between the π-density of the aromatic ring. Aromatic stacking of pairs of phenyl rings is also a feature of the crystal packing.

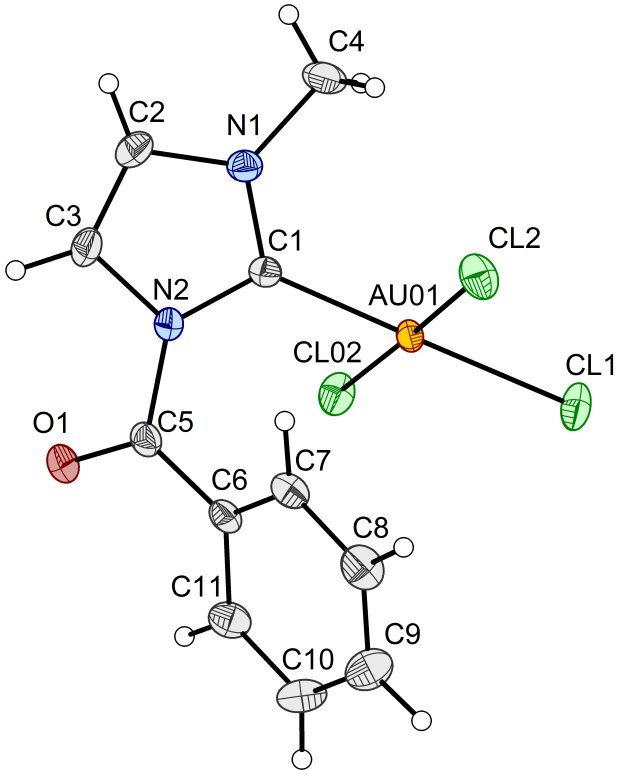

Figure 3.9: ORTEP-drawing of complex **6**

#	**Atoms (Å)**	**Distance**
1	Au01-Cl1	2.2972(5)
2	Au01-Cl2	2.2811(5)
3	Au01-Cl3	2.2829(5)
4	Au01-C1	2.005(2)
5	N1-C1	1.329(3)
6	N1-C2	1.386(3)
7	C2-C3	1.335(3)
8	N2-C3	1.394(3)
9	C1-N2	1.355(3)
10	N2-C5	1.456(3)
11	O1-C5	1.199(3)
12	C5-C6	1.473(3)
13	Au01-C6	3.335(3)
14	Au01-C7	3.210(2)
15	Au01-C11	4.162(3)

#	**Atoms**	**Angle (°)**
1	Cl1-Au01-C1	178.48(7)
2	Cl2-Au01-Cl3	178.58(2)
3	Cl02-Au01-C1	88.72(7)
4	Cl2-Au01-C1	89.88(7)
3	C6-C5-N2	117.0(2)
1	Cl1-Au01-C1-N2	114(3)
2	Cl2-Au01-C1-N2	-119.6(2)
3	Cl3 Au01 C1 N2	60.1(2)
4	Au01-C1-N2-C5	0.2(3)
5	C1-N2-C5-C6	42.0(3)
6	C1-N2-C5-O1	-139.7(2)
7	N2-C5-C6-C7	28.1(3)

Table 3.6: Selected bond lengths and angles for complex **6**

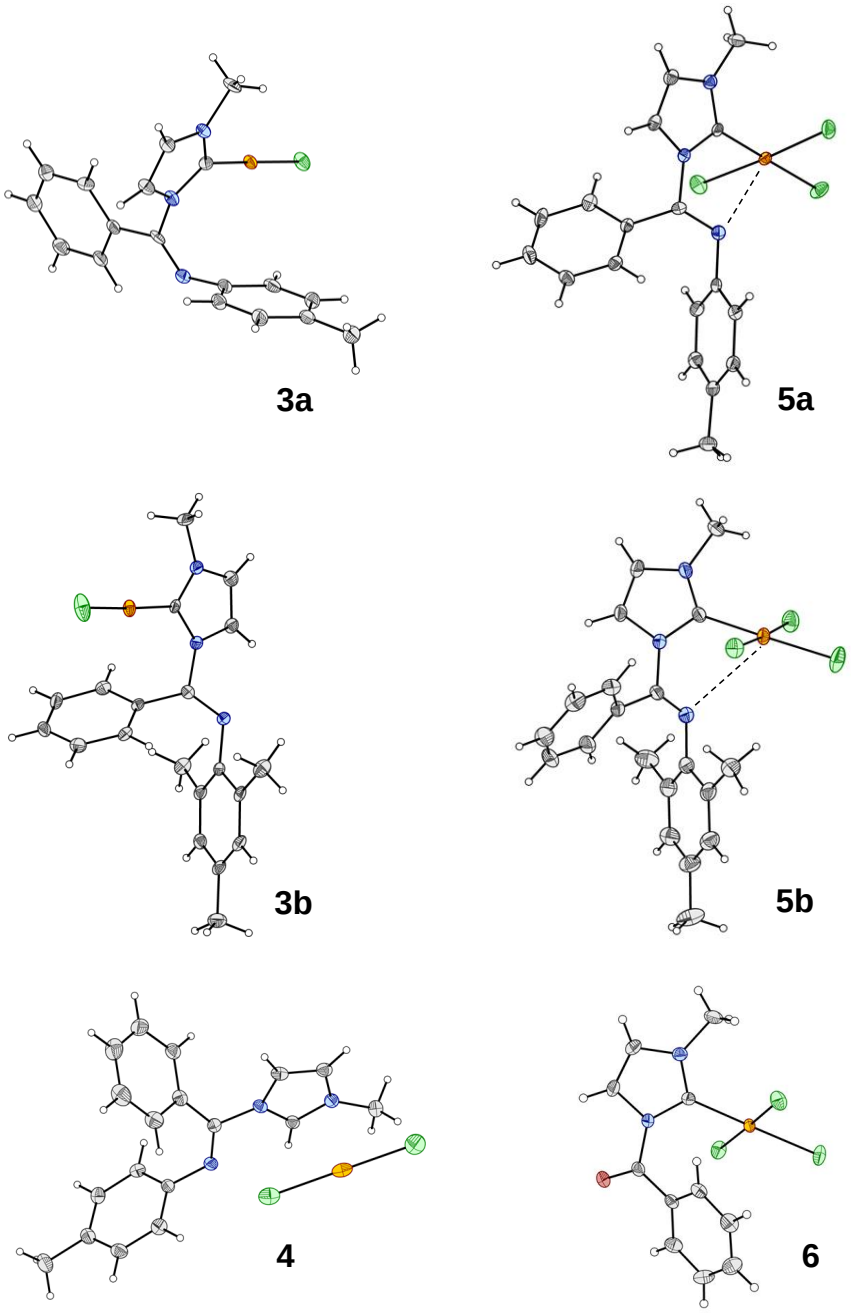

Figure 3.10: Overview of new compounds characterised by X-ray diffraction

When results from X-ray analyses are compared and contrasted, it should be noted that the crystal structure need not be a minimum energy conformation for the isolated molecule. The crystal packing effects are often significant, particularly for bigger molecules. For instance, dihedral angles are often twisted away from an equilibrium value. The increase in potential energy associated with the distortion is often small and can easily be compensated for by improved intermolecular attractive interactions.

When the new crystal structures obtained are compared (Figure 3.10), it can be seen that iminocarbene gold(I) complexes **3a** and **3b** crystalise with the imine nitrogen pointing away from the gold(I) centre, whereas the iminocarbene gold(III) complexes **5a** and **5b** feature short Au-N distances which are lower or similar to the sum of the van der Waal radii (r(N)+r(Au)=3.21 Å).[49] As discussed above, the different conformations observed in the solid state may be due to packing effects. The gold(III) complexes may also pack in a way such that the steric interactions of the chloride ligands and the aromatic rings are reduced. However, even with these precautions made, it is highly likely that there is an attractive interaction between gold and nitrogen which is only significant when gold is in the higher oxidation state. In the crystal packing of both **5a** and **5b**, two complexes comprise the asymmetric unit and the Au-N distances are different in the two complexes (**5a**: 3.071 and 2.970, **5b** 3.343 and 2.938). This indicates that the interaction is weak and the increase in potential energy when increasing the Au-N distance is small enough to be compensated for by more efficient packing.

As described in the introduction, Kriechbaum *et al.* have performed a theoretical study of NHC gold(III) complexes with weak Au-N contacts.[46] The study indicated that the interaction is not significantly orbital based but rather an effect of intramolecular electrostatic interactions. With this in mind, it was surprising to find that ketocarbene gold(III) complex **6** would not have the electronegative oxygen oriented towards the gold(III) centre. It would have been expected that the electrostatic Au-O interaction would have been even stronger compared to Au-N as oxygen is more electronegative. It could well be that such an interaction is overruled by packing effects, or that the adopted conformation accommodates a better delocalization of the π-electrons in the complex. The plane $AuCl_3$ moiety is also oriented with a short distance to the plane of the aromatic ring, and there might be an attractive interaction between the π-electrons in the ring and the gold(III) centre.

If, however, the interaction between gold(III) and a heteroatom can be understood as an electron donor-acceptor interaction, the lone pair of the less electronegative nitrogen is higher in energy and can thus be a better energy match for an empty gold(III) d-orbital or a Au-Cl anti-bonding orbital.

The nature of the gold-heteroatom interaction has caught our attention, and is currently studied by computational methods. Some of the preliminary results are presented in the next chapter.

CHAPTER 4

Computational Studies

4.1 Computational details

All calculations were carried out at the DFT level with Gaussian09[64] on the Abel computing cluster at the University of Oslo.[65] For geometry optimisations , all atoms apart from Au were described with the triple-ζ 6-311+G** basis set[66,67] whereas Au was described with a Stuttgart–Köln basis set including a small-core quasi-relativistic pseudopotential.[68] Geometries were fully optimised without any constraint. Vibrational frequencies were computed to verify that the stationary points found were minima. Several functionals were compared as described in Section 4.2, and PBE0 gave the lowest root-mean-square deviation from selected experimental (X-ray) atomic distances. Further calculations were thus carried out with the PBE0 functional. Solvent effects were simulated as a continuum with the SMD method.[69]

Non-covalent interaction regions were calculated with NCIPLOT[53,56] from electronic densities obtained with the PBE0 functional and the double-ζ 6–31G** basis set[70] on all the atoms except for Au, for which the W06 basis set was used.[71] The non-covalent interaction regions were graphed with VMD.[72]

4.2 A comparison of functionals

In the crystal packing of **5a**, two complexes (**5a-1** and **5a-2**) comprise the asymmetric unit. The two complexes have almost identical bond distances, but the weak Au-N_{imine} contacts differ as a result of crystal packing. In **5a-1** the Au-N_{imine} distance is 3.071 Å and in **5a-2** it is 2.970 Å. The geometry of **5a** has ben optimised using several functionals: BP96,[73] B3LYP,[74] B97D,[75] M06,[76] PBE[77] and PBE0.[78] The optimised geometries are all in good agreement with the X-ray structures (Table 4.1), and for all functionals apart from M06 the gas phase geometries have slightly longer Au-N_{imine} distances than in **5a-1**. In the geometry optimised using the M06 functional the Au-N_{imine} distance is significantly shorter than in the

other geometries and is very close to the experimental distance of **5a-2**. The Au-N_{imine} distance depends on other bond lengths and torsions, and the closer contact beween the two could be a random effect of other properties. However, the M06 functional has been reported to show good performance in modelling non-covalent interactions[76] and the geometry obtained could be the lower energy geometry because of a more accurate modelling of a Au-N_{imine} non-covalent interaction.

The geometry optimised with the PBE0 functional gave the lowest root-mean-square deviations from the experimental X-ray bond distances, and the Au-N_{imine} identical to that of **5a-2** to two significant figures (Table 4.2). The excellent performance of the PBE0 functional in combination with the Stuttgart–Köln basis set and pseudopotential for gold[68] has previously been reported by the group[11] and the combination is used for most calculations done by other members of the Tilset group. For this reason, the PBE0 functional was chosen for further calculations, but for future work, the difference in results from the PBE0 and M06 functionals may be of interest to explore.

Functional	**Au1-C1 distance (Å)** ***D***	**Au1-N3 distance (Å)** ***D***	**Other distances (Å)** ***RMSD***	**Dihedral angles (°)** ***RMSD***
BP86	0.026/0.021	0.062/0.162	0.037/0.038	2.8/6.4
B3LYP	0.036 /0.032	0.072/0.173	0.037/0.038	2.4/6.2
B97D	0.042/0.038	0.120/0.221	0.045/0.046	10.0/13.0
M06	0.033/0.029	-0.100/0.009	0.038/0.039	3.8/6.0
PBE	0.021/0.017	0.044/0.145	0.035/0.036	3.0/6.4
PBE0	0.009/0.005	0.003/0.100	0.020/0.022	2.4/6.0

Table 4.1: Deviations (D)[a] and root-mean square deviations $(RMSD)$[b] from the X-Ray structure of **5a** for a selected DFT functionals.
[a] $D = y - x$
[b] $RMSD = \sqrt{\frac{\sum_{i=1}^{n} (x_i - y_i)^2}{n}}$
x = X-ray parameter, y = optimised geometry parameter

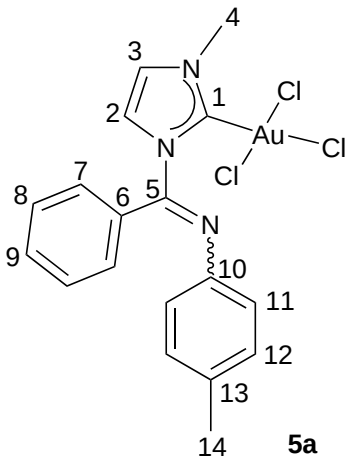

5a

Atoms	**X-ray structure**	**Calculated structure**	
	Distance (Å)	**Distance (Å)**	**Deviation (Å)**
Au-Cl1	2.315	2.308	-0.007
Au-Cl2	2.282	2.316	0.028
Au-Cl3	2.288	2.325	0.043
Au-C1	1.992	2.001	0.009
C1-N2	1.349	1.350	0.001
N2-C5	1.440	1.438	-0.002
C5-C6	1.490	1.481	-0.009
C5-N3	1.264	1.262	-0.002
N3-C10	1.430	1.402	-0.028
Au1-N3	3.071	3.074	0.003
	Valence angle (°)	**Valence angle (°)**	**Deviation (°)**
Cl1-Au1-C1	177.8	179.0	1.2
Cl2-Au1-Cl3	176.0	175.6	-0.4
Cl2-Au1-C1	89.0	89.1	0.1
Cl3-Au1-C1	87.1	87.0	-0.1
	Dihedral angle (°)	**Dihedral angle (°)**	**Deviation (°)**
Cl2-Au1-C1-N2	-118.8	-115.7	3.1
Au1-C1-N2-C5	4.5	6.5	2.0
C1-N2-C5-N3	34.5	36.5	2.0
C1-N2-C5-C6	-146.4	-144.5	2.0
N2-C5-N3-C10	-175.5	-172.0	3.5

Table 4.2: Bond distances and angles of **5a** in the experimental X-Ray structure and the geometry optimised employing the PBE0[78] functional. (The valence angles were not included in the comparison of functionals)

4.3 Non-covalent interaction plots of 5a

Intramolecular non-covalent interactions were mapped for both of the conformations of **5a** found in the X-ray analysis. Isosurfaces of the reduced density ($s = 0.5$ au) in low electron density regions ($\rho < 0.5$ au) reveals an attractive interaction between the imine nitrogen and the gold(III) centre. This interaction observed in the solid state may also be of importance in solution and have an impact on the reactivity of the gold centre in catalytic reactions.

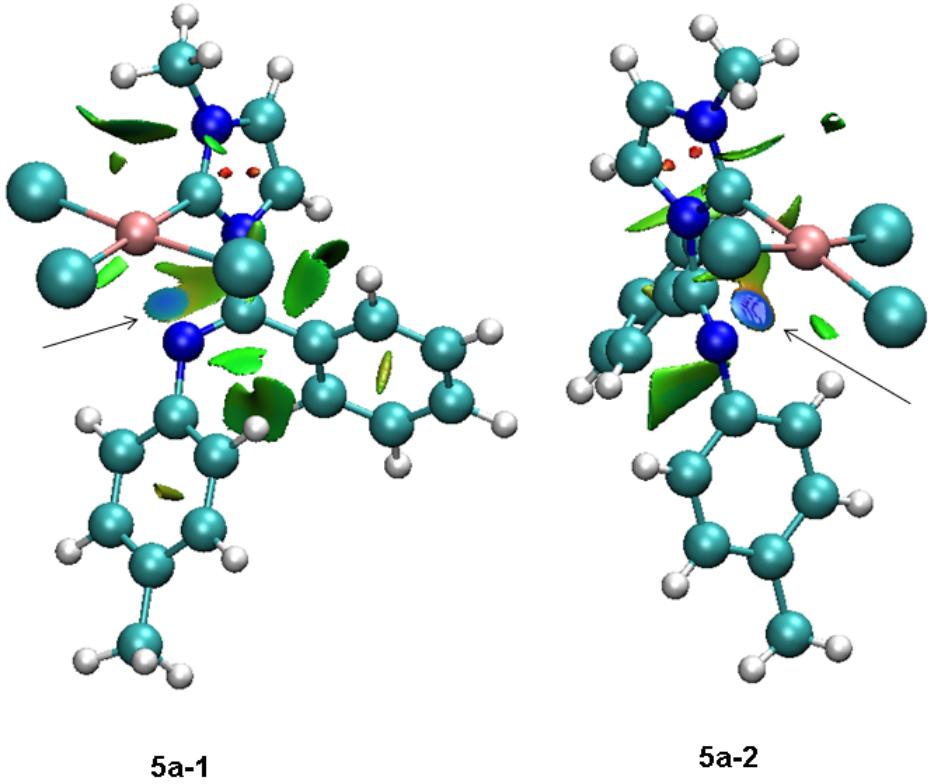

Figure 4.1: NCI plot[56] of the two complexes comprising the asymmetric unit in the crystal packing of **5a**. $s = 0.5$ au, $\rho < 0.5$ au

4.4 Computing the equilibrium between 5a in the neutral state and as an ion pair.

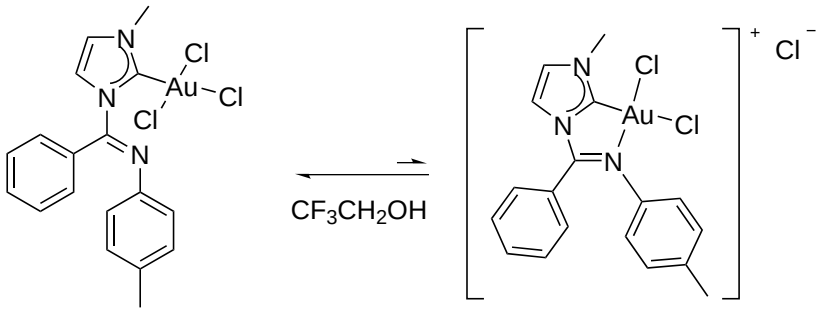

Scheme 4.1: The proposed equilibrium of **5a** in solution

In solution, a small portion of **5a** may exist as an ion pair with [C,N]-chelation of the iminocarbene ligand and Cl^- as a counter anion (Scheme 4.1). The position of the equilibrium would depend greatly on the properties of the solvent. A polar solvent would favour the formation of ions, a protic solvent would stabilise the chloride anion, and a non-nuclephilic solvent would favour the coordination of the imine nitrogen over the coordination of the solvent itself. Trifluoroethanol has these desired properties, since the electronegative fluorine atoms reduce the nucleophilicity of the oxygen atom and the hydroxy proton would allow for solvation of the chloride anion (Figure 4.2).

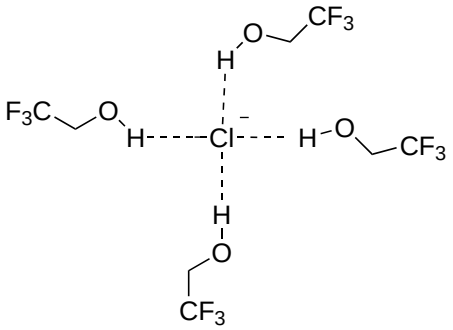

Figure 4.2: Solvation of a chloride anion by trifluoroethanol

The energy difference between the neutral state and the ion pair of **5a** was calculated. The geometries were optimised in trifluoroethanol solvent modelled as a continuum with the SMD method.[69] The ion pair was calculated to be 7.6 kcal/mol higher in energy than the neutral state. The solvent model will not fully account for the solvation of the chloride ion and the calculated energy of the ionpair is likely to be too high. The Gibbs free energy difference between the two states

was calculated to be 6.9 kcal/mol which corresponds to an equilibrium constant of $8.5 \cdot 10^{-6}$. ($K_{eq} = e^{\frac{-\Delta G}{RT}}$, as follows from the Eyring equation)

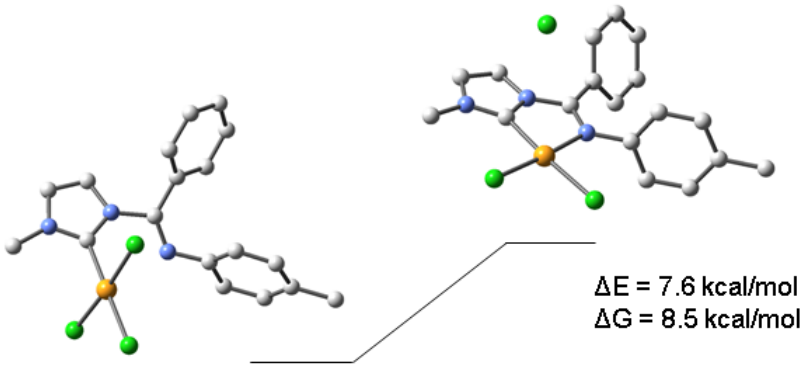

Figure 4.3: The optimised geometries of **5a** in the neutral state and as an ion pair

As described in the introduction, there is precedence in the literature for ion pairs like that of **5a** being an active catalyst.[40] The cationic gold complex may have a much lower activation energy for exchanging the imine ligand with a substrate, compared to exchanging a chloride ligand in the neutral complex. This is illustrated for alkyne coordination in Scheme 4.2 and the rate constant k_{ion} may be much greater than $k_{neutral}$.

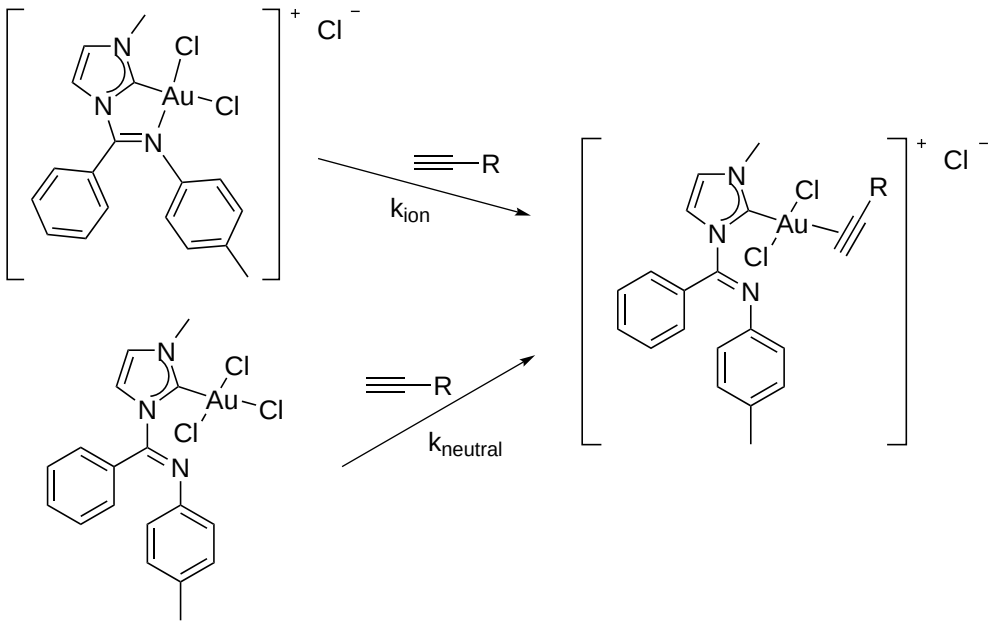

Scheme 4.2: Substrate binding as a first step of a catalytic reaction

Gold(I/III) complexes usually require additives like sodium or silver salts of non-coordinating anions to generate active catalysts. The cation of the salt abstracts a chloride ligand and opens up a coordination site where a substrate may bind and catalysis may occur. The use of additives brings uncertainty to what is actually

the active catalyst, and the role of silver salts has been shown to be more than as a halogen scavenger in many reactions.[79] For this reason this novel concept of additive free catalysis is very interesting and the small population of **5a** in the ion pair state may have a significant impact of the catalytic ability of **5a**.

CHAPTER 5

Conclusion and future work

A number of novel gold(I) and gold(III) complexes have been synthesised and characterised by NMR spectroscopy, mass spectrometry and X-ray crystallography and studied by computational methods. The new complexes have been synthesised by reliable, mild methods in generally excellent yields.

It can be seen from the X-ray analysis of the new iminocarbene gold complexes that a weak Au-N contact is only present when gold is in the higher oxidation state. From an analysis of the electron density and its derivatives it was shown that there is an attractive non-covalent interaction between the gold(III) centre and the imine nitrogen. A computational study supports that iminocarbene gold(III) complex **5a** is in an equilibrium with its ion pair which could be a catalytically active species.

It has been shown that NHC ligands with pendant imine functionalities have the ability to form chelated complexes to other metals[3] and here it is believed that we have shown that for the first time a [C,N]-chelated iminocarbene gold(III) complex (**23**, Figure 5.1) has been synthesised. Further studies including ^{13}C NMR spectroscopy, MS, IR and finally X-ray crystallography will however be necessary to unambiguously characterise the new compound.

A ketocarbene gold(III) complex was obtained by unintended hydrolysis of an iminocarbene complex. The ketoimine crystallises with the oxygen atom oriented away from the gold(III) centre. The nature of the interaction between gold(III) centres and pendant donor functionalities has caught our interest and is currently the focus of a computational study in the group.

For future work, it would be interesting to employ the new complexes in benchmark catalytic reactions. The cycloisomerisation of alkynylfurans to isobenzofuranoles catalysed by gold complexes has been well studied[40,80,81] and could be a good starting point. If catalytic activity of **5a** or **23** is observed, it would be interesting to further derivatise the ligand in order to alter the electronics at the gold centre and see what effect this would have. For instance, the population of the ionpair of **5a** may be increased by including an electron donating group on the aromatic ring in conjugation with the imine (**26**) or by changing the chloride ligands for

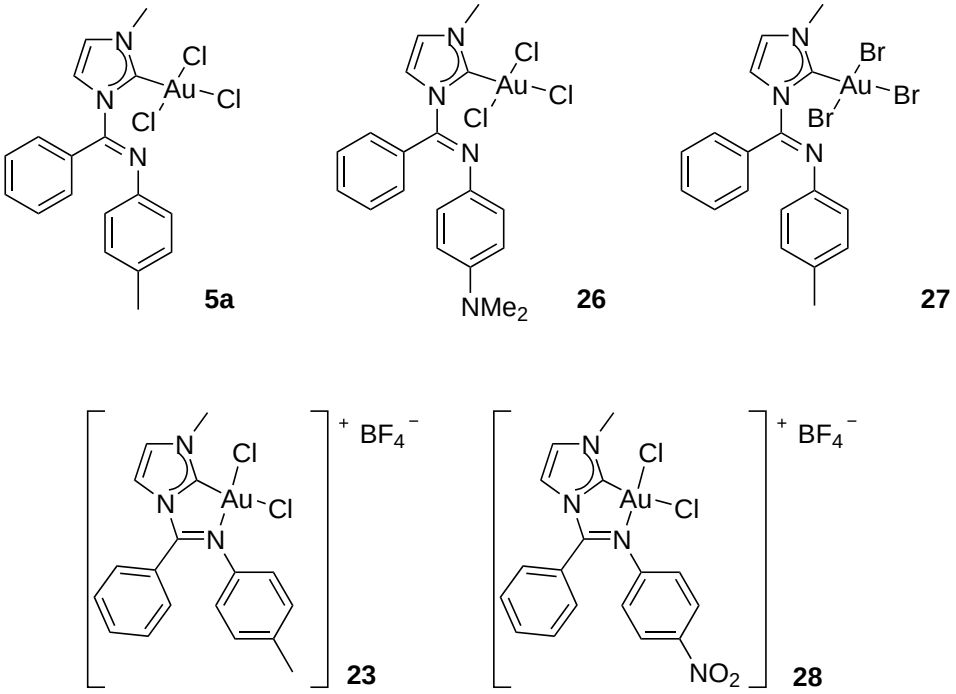

Figure 5.1: Suggested derivatisation of **5a** and **23**

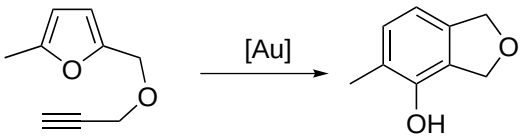

Figure 5.2: The cycloisomerisation of alkynylfurans to isobenzofuranoles catalysed by gold complexes.

more labile bromide ligands (**27**). For the cationic complex **23**, the energy barrier of the decoordination of the imine to free a coordination site might be lowered by the inclusion of electron withdrawing groups (**28**).

CHAPTER 6

Experimental

All reagents, unless specified, were used without further purification as purchased from commercial suppliers. Dry CH_2Cl_2, MeCN and Et_2O were obtained from an MBraun MB SPS-800 Solvent Purification System. Only distilled water was used and aqueous solutions were prepared on site. Pentane was dried over molecular sieves. A SalvisLab VC20 vacuum oven was used to dry K_2CO_3 and to activate molecular sieves. $PhICl_2$ was synthesised according to literature procedure.[82] Argon gas was used to perform reactions under inert atmosphere. All glassware was oven-dried prior to use and cooled under a flow of argon gas. Reactions involving silver or gold species were shielded from light using aluminium foil.

^1H, ^{13}C, ^1H-^1H COSY, NOESY, ROESY, HSQC and HMBC NMR experiments were recorded in $CDCl_3$ or CD_2Cl_2, using either a Bruker Avance DPX200, AVII400, DRX500, AV600 or AVII600 instrument with residual solvent peaks as references ($CHCl_3$ (δH = 7.24 ppm), $CDCl_3$ (δC = 77.0 ppm), $CHDCl_2$ (δH = 5.32 ppm) or CD_2Cl_2 (δC = 53.8 ppm) as an internal standard). Chemical shift (δ) is given in parts per million (ppm) and coupling constants (J) are given in Hertz (Hz). Multiplicities are abbreviated as: s – singlet; d – doublet; t – triplet; m –multiplet; br. - broad. Doublets and triplets with clear signs of additional long-range splitting is marked d* and t*. Distorted apparent triplets (doublets of doublets) are market t* and the average coupling constant (J) is given.

Mass spectra were obtained on a Micromass QTOF II spectrometer (ESI) and on a Fision VG Prospec sector instrument at 70 eV (EI) by Osamu Sekiguchi.

6.1 Synthesis of 24a[8]

Benzoyl chloride (4.60 mL, 39.6mmol, 1.0 eq.) disolved in CH_2Cl_2 (25 mL) was added dropwise over a period of 30 min to a stirred solution of *p*-toluidine (4.30 g, 40.1 mmol, 1.0 eq.) and triethylamine (5.50 mL, 39.4 mmol, 1.0 eq.) in CH_2Cl_2 (35 mL). The reaction mixture was heated at reflux for 48 h. CH_2Cl_2 (50 mL) was added and the rection mixture was washed with water (100 mL), saturated $NaHCO_3$ (100 mL) and 3M HCl (100 mL). The organic phase was dried over $MgSO_4$ before CH_2Cl_2 was removed under reduced pressure and *N*-(*p*-tolyl)-benzamide **24a** was collected as a white solid (7.45 g, 35.5 mmol, 90%).

^{1}H NMR (300 MHz, $CDCl_3$) δ 7.85 (d*, J = 6.7 Hz, 2H, H3), 7.71 (br. s, 1H, H6), 7.57 - 7.43 (m, 5H, H1; H2; H8), 7.16 (d, J = 8.1 Hz, 2H, H9), 2.33 (s, H11, 3H)

MS (EI, MeCN) *m/z*(rel%): 211(M^+, 64) 105(100), 77(53), 51(10)

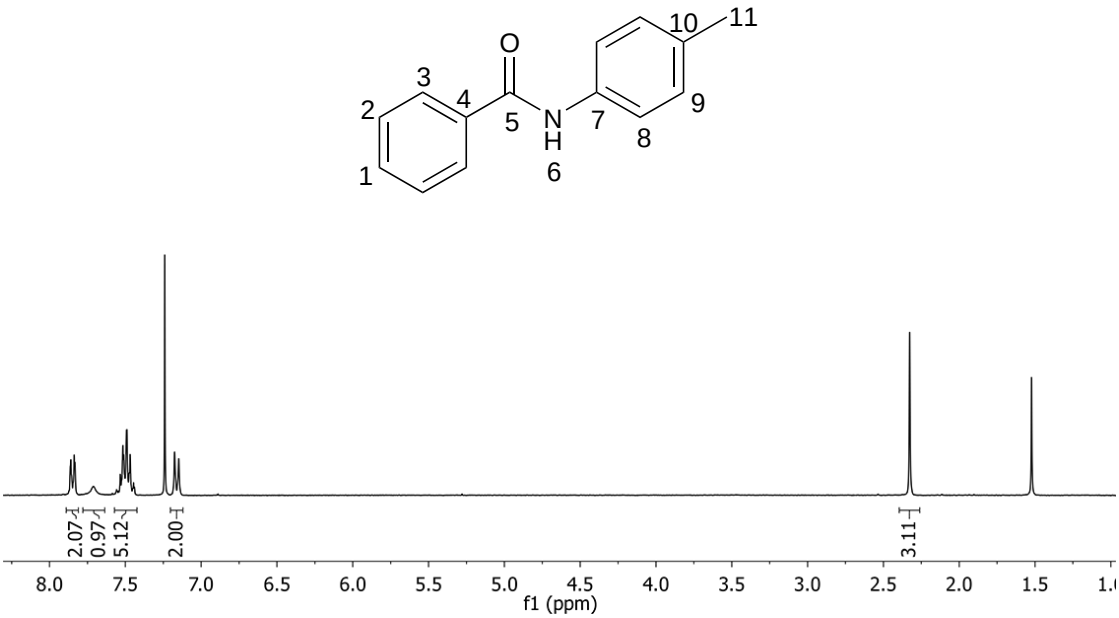

Figure 6.1: ^{1}H NMR (300 MHz, $CDCl_3$) of compound **24a**

6.2 Synthesis of 24b[7,8]

Benzoyl chloride (4.60 mL, 39.6mmol, 1.1 eq.) disolved in CH_2Cl_2 (25 mL) was added dropwise over a period of 30 min to a stirred solution of 2,4,6-trimethylaniline (5.0 mL, 35.6 mmol, 1.0 eq.) and triethylamine (5.50 mL, 39.4, 1.1 eq.) in CH_2Cl_2 (35 mL). The reaction mixture was heated at reflux for 48 h. CH_2Cl_2 (150 mL) was added and the rection mixture was washed with water (100 mL), saturated $NaHCO_3$ (100 mL) and 3M HCl (2×100 mL). The organic phase was dried over $MgSO_4$ before CH_2Cl_2 was removed under reduced pressure and *N*-(2,4,6-trimethylphenyl)-benzamide **24b** was collected as a white solid (7.49 g, 35.5 mmol, 88%)

^{1}H NMR (300 MHz, $CDCl_3$) δ 7.91 (d*, J = 6.6 Hz, 2H, H3), 7.59 - 7.43 (m, 3H, H1; H2), 7.27 (br. s, 1H, H6), 6.92 (s, 2H, H9), 2.33 (s, 3H, H11), 2.23 (s, 6H, H12)

MS (EI, MeCN) m/z(rel%): 239(M^+, 44), 134(16), 105(100), 77(32)

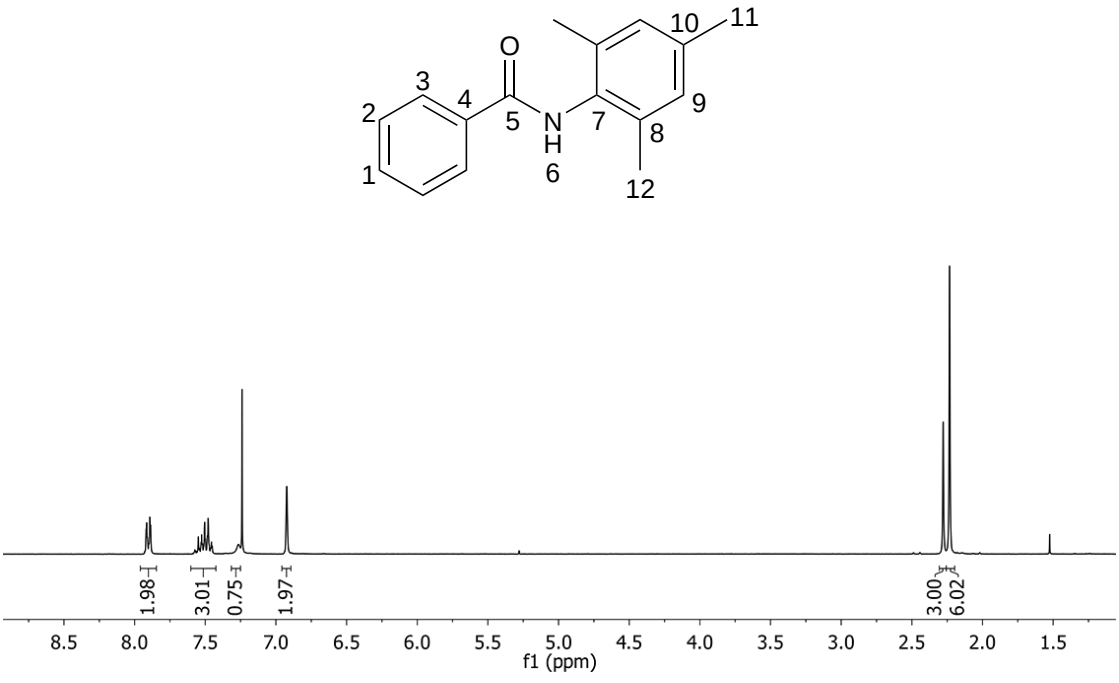

Figure 6.2: ^{1}H NMR (300 MHz, $CDCl_3$) of compound **24b**

6.3 Synthesis of 25a[8,83]

A mixture of*N*-(*p*-tolyl)-benzamide **24a** (3.38 g, 16.0 mmol, 1.0 eq.) and $SOCl_2$ (2.00 mL, 27.5 mmol, 1.7 eq.) was heated at reflux for 4 h. The reaction mixture was cooled to room temperature before HCl and excess $SOCl_2$ was removed under vacuum to yield **25a** as a yellow solid (3.56, 15.5 mmol, 97%).

^{1}H NMR (300 MHz, $CDCl_3$) δ 8.12 (d*, J = 6.9 Hz, 2H, H3), 7.56 - 7.41 (m, 3H, H1 and H2), 6.92 (d, J = 8.0 Hz, 2H, H8), 6.92 (d, J = 8.0 Hz, 2H, H7), 2.36 (s, 3H, H10)

MS (EI, MeCN) m/z(rel%): 229(M^+, 22) 194(M^+-Cl, 100), 91(22), 65(14)

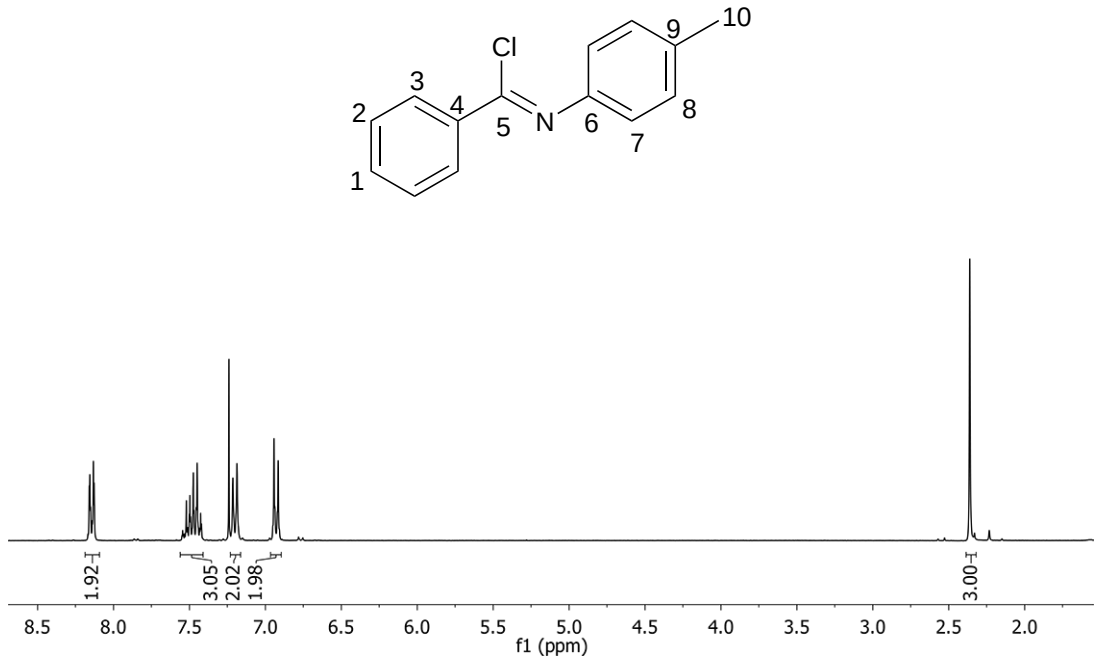

Figure 6.3: ^{1}H NMR (300 MHz, $CDCl_3$) of compound **25a**

6.4 Synthesis of 25b[7,83]

A mixture of *N*-(2,4,6-trimethylphenyl)-benzamide **24b** (1.86 g, 7.77 mmol, 1.0 eq.) and $SOCl_2$ (0.80 mL, 11.0 mmol, 1.4 eq.) was heated at reflux for 4 h. The reaction mixture was cooled to room temperature before HCl and excess $SOCl_2$ was removed under vacuum to yield **25b** as a light brown oil (1.99 g, 7.72 mmol, 99%).

^{1}H NMR (300 MHz, $CDCl_3$) δ 8.22 (d*, J = 7.2 Hz, 2H, H3), 7.60 - 7.42 (m, 3H, H1;H2), 6.90 (s, 2H, H8), 2.29 (s, 3H, H10) 2.06 (s, 6H, H11)

MS (EI, MeCN) m/z(rel%): 257(M^+, 20) 222(M^+-Cl, 100), 207(13), 91(11), 77(10)

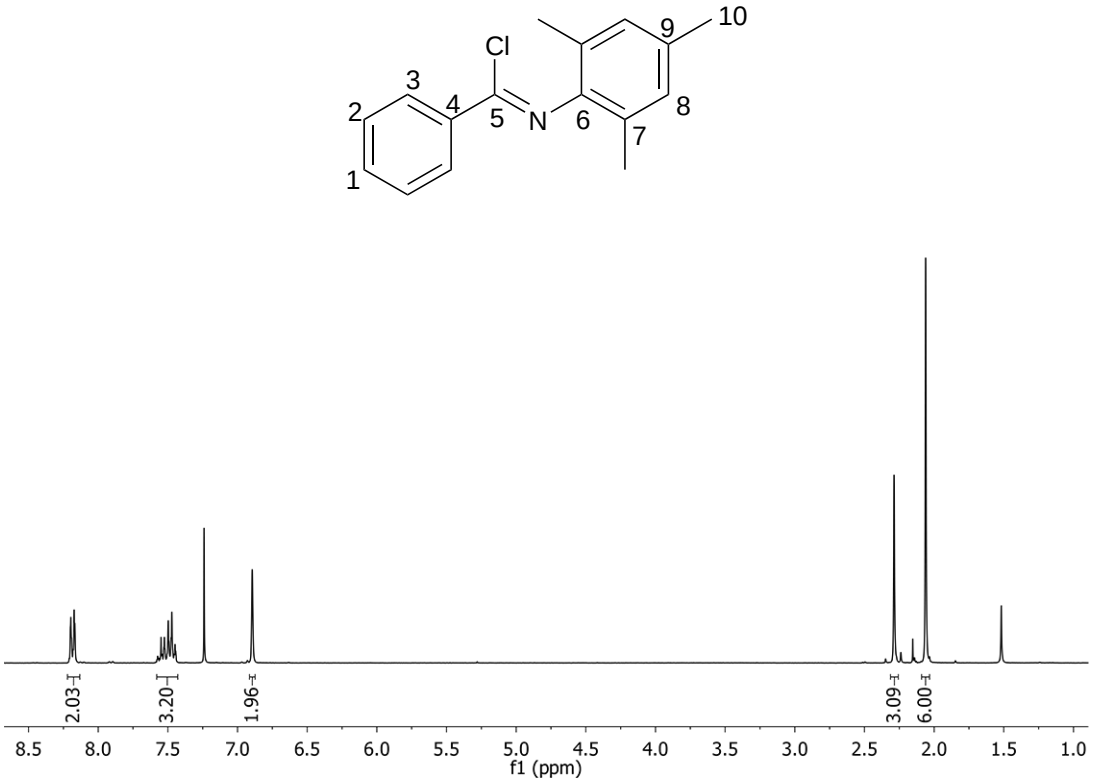

Figure 6.4: ^{1}H NMR (300 MHz, $CDCl_3$) of compound **25b**

6.5 Synthesis of imidazolium chloride 1a[3,8]

1-methylimidazole (1.00 mL, 12.6 mmol, 1.2 eq.) was added dropwise to a solution of **25a** (2.33 g, 10.1 mmol, 1.0 eq.) in THF (40 mL). The solution was stirred for 48 h during which the product precipitated as a white solid. After removal of the solvent by filtration, the product was washed with THF (3×10 mL) and dried under vacuum. The product was redissolved in CH_2Cl_2 and dried under vacuum to remove any trapped THF, yielding **1a** as a white solid (2.63 g, 8.43 mmol, 83%)

^{1}H NMR (600 MHz, CD_2Cl_2) δ 10.55 (s, 1H, H1), 7.84 (t*, J = 1.8 Hz, 1H, H2), 7.64 (t*, J = 1.8 Hz, 1H, H3), 7.55 (tt, J = 7.2 Hz; J = 1.7 Hz, 1H, H9), 7.48 (t*, J = 7.2 Hz, 2H, H8), 7.40 (d*, J = 7.8 Hz, 2H, H7), 7.03 (d, J = 8.0 Hz, 2H, H12), 6.70 (d, J = 8.0 Hz, 2H, H11), 4.30 (s, 3H, H4), 2.26 (s, 3H, H14)

^{13}C NMR (151 MHz, CD_2Cl_2) δ 148.7 (C5), 142.9 (C10), 138.7 (C1), 136.0 (C13), 132.2 (C9), 130.0 (C7), 130.0 (C12), 129.8 (C8), 127.8 (C6), 124.6 (C3), 121.7 (C11), 119.5 (C2), 37.6 (C4), 21.9 (C14)

Additional NMR spectra of **1a** in $CDCl_3$ were recorded so that the ^{13}C NMR resonances could be compared in Section 2.5.

^{13}C NMR (151 MHz, $CDCl_3$) δ 148.6 (C5), 142.2 (C10), 138.0 (C1), 135.6 (C13), 132.2 (C9), 129.7 (C7), 129.7 (C12), 129.6 (C8), 127.1 (C6), 124.5 (C3), 121.6 (C11), 121.6 (C2), 37.7 (C4), 21.0 (C14)

MS (ESI, MeCN) m/z(rel%): 276(M^+-Cl, 98), 194($C_{14}H_{12}N^+$, 100)

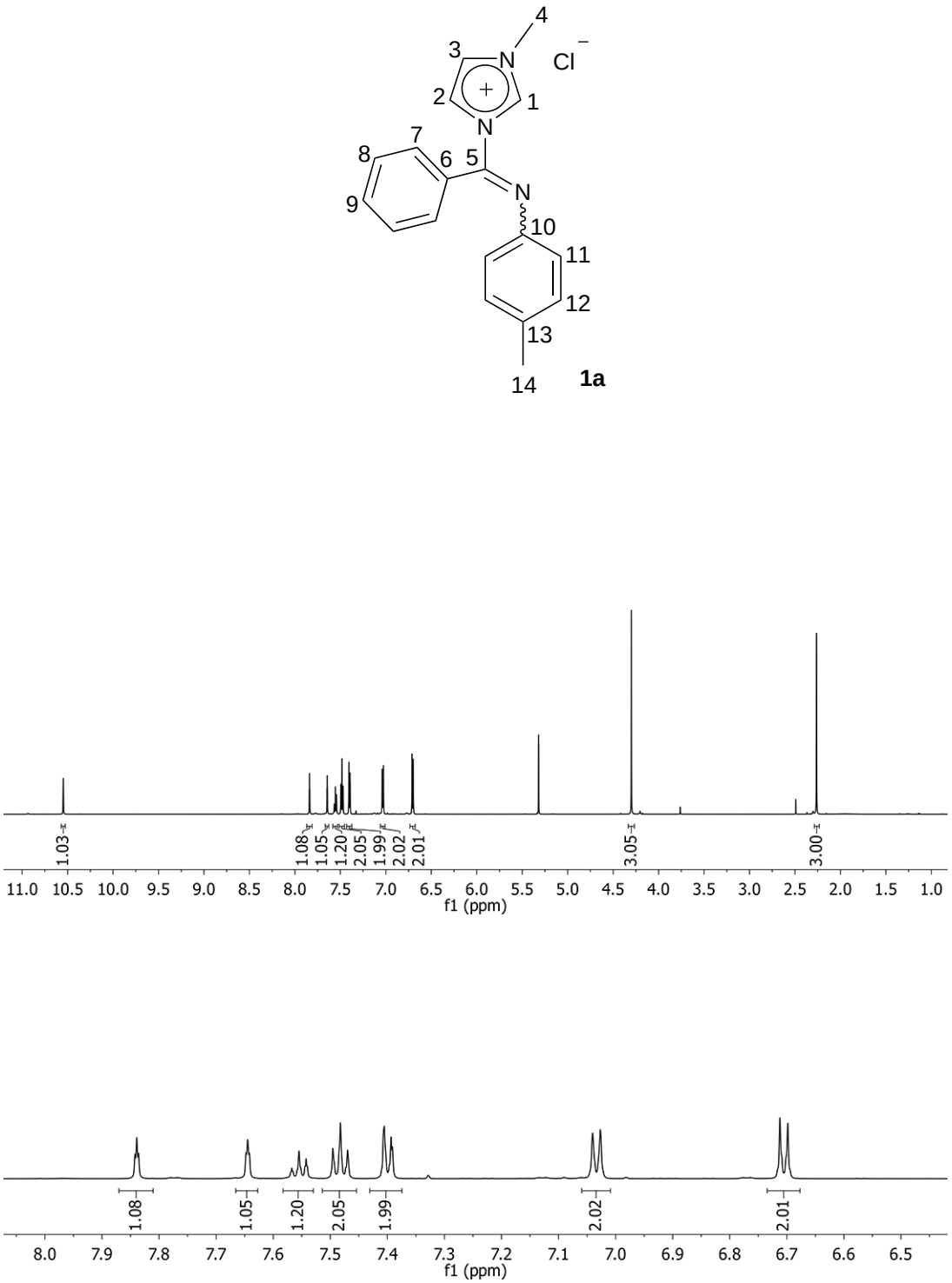

Figure 6.5: ^{1}H NMR (600 MHz, CD_2Cl_2) of compound **1a**

6.6 Synthesis of imidazolium chloride 1b[3,7]

1-methylimidazole (0.35 mL, 4.4 mmol, 1.1 eq.) was added dropwise to a solution of **25b** (1.01 g, 3.93 mmol, 1.0 eq.) in THF (25 mL). The solution was stirred for 48 h during which the product precipitated as a light yellow solid. After removal of the solvent by filtration, the product was washed with THF (3×10 mL) and dried under vacuum. The crude product was dissolved in CH_2Cl_2, precipitated from Et_2O and dried under vacuum to afford a yellow solid (0.529 g, 1.56 mmol, 40%).

^{1}H NMR (600 MHz, $CDCl_3$) δ 10.4 (s, 1H, H1), 7.87 (s, 1H, H2 or H3), 7.86 (s, 1H, H2 or H3), 7.46 (t, J = 7.2 Hz, 1H, H9), 7.46 (t*, J = 7.3 Hz, 2H, H8), 7.29 (d, J = 7.2 Hz, 2H, H7) 6.71 (s, 2H, H12), 4.31 (s, 3H, H4), 2.16(s, 3H, H14), 1.93 (s, 6H, H15)

^{13}C NMR (151 MHz, $CDCl_3$): δ 147.9 (C5), 140.7 (C10), 138.3 (C1), 134.2 (C13), 132.5 (C9), 129.5 (C7), 128.7 (C12), 128.5 (C8), 127.5 (C6), 126.0 (C11), 124.5 (C3), 119.3 (C2), 37.7 (C4), 20.7 (C14), 18.3 (C15)

MS (EI, MeCN) m/z(rel%): 304(M^+-Cl, 98), 222($C_{16}H_{16}N^+$, 100)

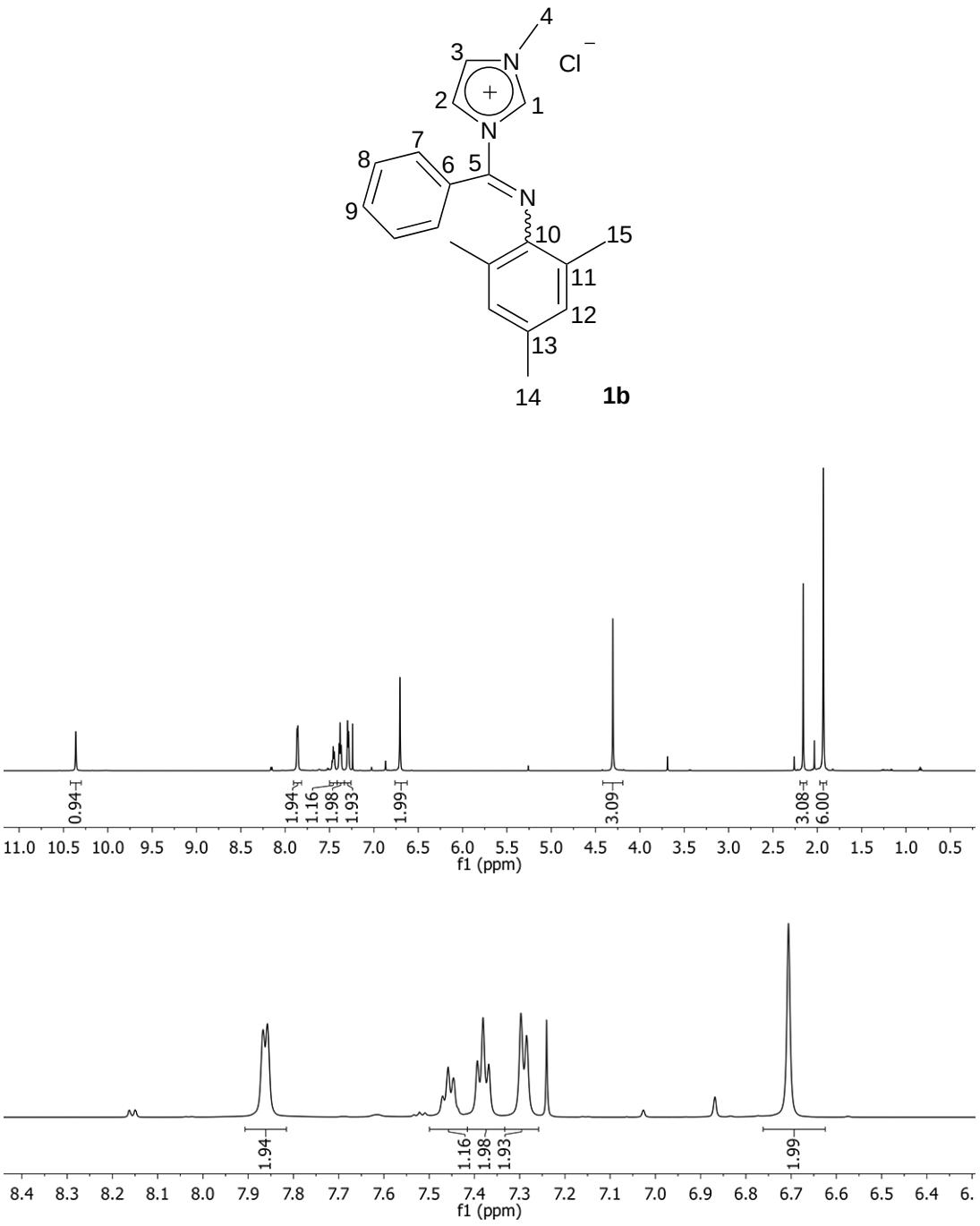

Figure 6.6: ^{1}H NMR (600 MHz, $CDCl_3$) of compound **1b**

6.7 Synthesis of silver(I) complex 2[3]

A mixture of **1a** (599 mg, 1.92 mmol, 1.0 eq.), Ag_2O (554 mg, 2.39 mmol, 1.2 eq.) and activated 4 Å molecular sieves were suspended in CH_2Cl_2 (30 mL) and stirred at room temperature overnight. The solution was filtered using cannula filtration and the solvent was removed under vacuum to yield **2** as greyish yellow solid (401 mg, 0.965 mmol, 50%).

Major isomer
^{1}H NMR (400 MHz, CD_2Cl_2) δ 7.79 (br. s, 1H, H2), 7.53 - 7.44 (m, 1H, H9), 7.39 (t*, J = 7.6 Hz, 2H, H8), 7.23 (d, J = 7.6 Hz, 2H, H7), 7.14 (s, 1H, H3), 6.99 (d, J = 8.0 Hz, 2H, H12), 6.64 (d, J = 8.0 Hz, 2H, H11), 3.84 (s, 1H, H4), 3.26 (s, 1H, H14)
^{13}C NMR (100 MHz, CD_2Cl_2) δ 153.5 (C5), 144.5 (C10), 134.6 (C13), 131.5 (C9), 130.7 (C6), 130.1 (C7), 129.7 (C12), 129.3 (C8), 122.7 (C2), 121.4 (C11), 120.8 (C3), 40.3 (C4), 20.9 (C14)

Minor isomer
^{1}H NMR (400 MHz, CD_2Cl_2) δ 7.69 (d, J = 7.8 Hz, 2H, H7), 7.61 (t, J = 7.4 Hz, 1H, H9), 7.53 - 7.44 (m, 2H, H8), 7.09 - 7.03 (m, 3H, H3; H12), 6.94 (s, 1H, H2), 6.68 (d, J = 8.0 Hz, 2H, H111) 3.80 (s, 1H, H4), 3.29 (s, 1H, H14)
^{13}C NMR (100 MHz, CD_2Cl_2) δ 148.9 (C5), 144.5 (C10), 135.4 (C13), 134.5 (C6), 132.9 (C9), 130.1 (C12), 129.6 (C7), 129.1 (C8), 122.6 (C2), 122.3 (C3), 121.0 (C11), 39.5 (C4), 21.0 (C14)

The C1 carbon was not observed in the ^{13}C NMR spectrum of **2** in CD_2Cl_2. A spectrum was recorded of **2** in $CDCl_3$. Signals corresponding to the carbenic carbons of the major and minor isomer were at 184.2 and 182.1 ppm respectively.

MS (ESI, MeCN) *m/z*(rel%): 657/659($(NHC)_2Ag^+$, 13/13), 276($(NHC)H^+$, 80), 194($C_{14}H_{12}N^+$, 100)

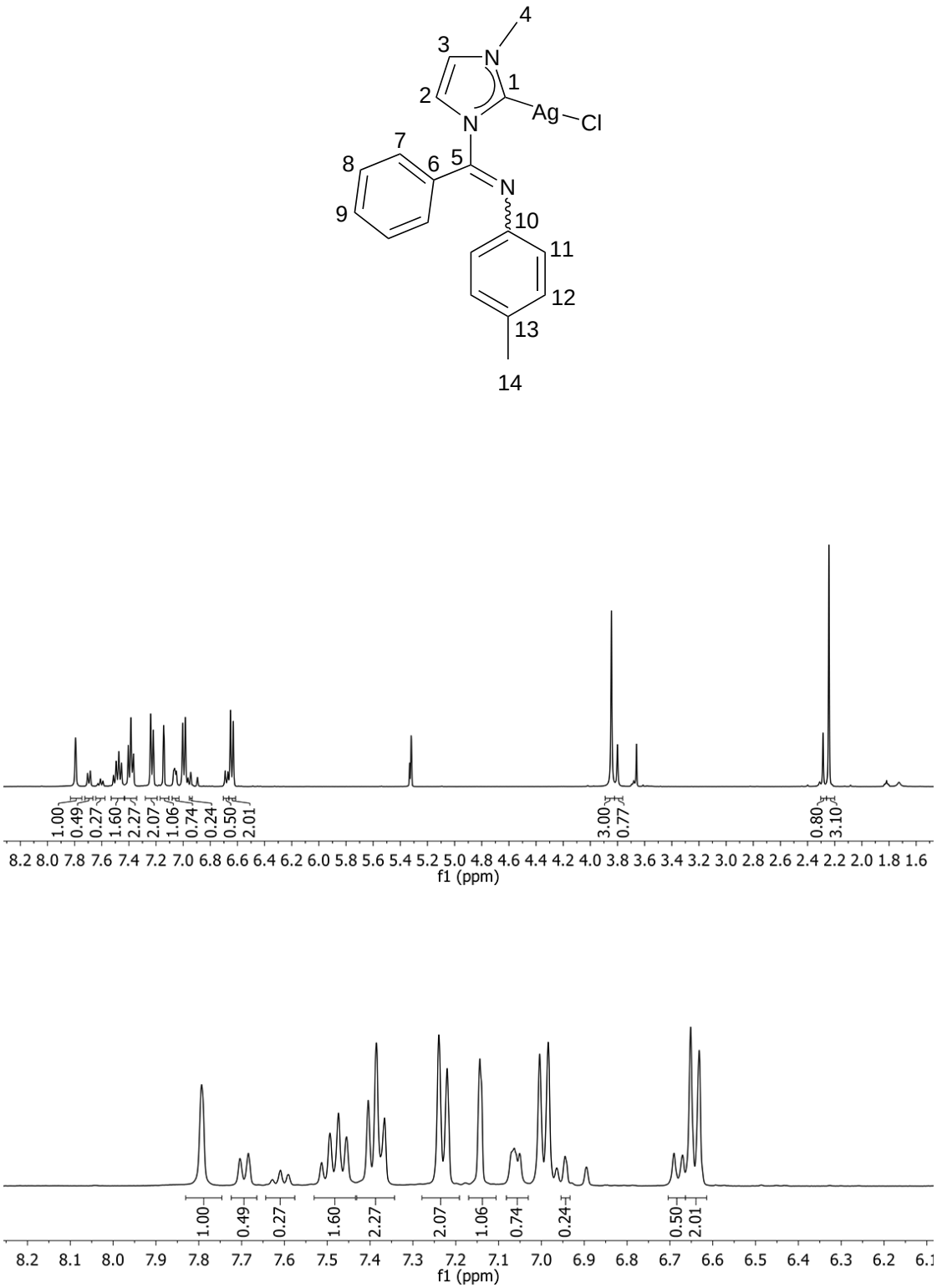

Figure 6.7: ^{1}H NMR (400 MHz, CD_2Cl_2) of compound **2**

6.8 Silver-free synthesis of gold(I) complex 3a

Imidazolium salt **1a** (23.4 mg, 0.0750 mmol, 1.0 eq.), $(SMe_2)AuCl$ (22.6 mg, 0.0767 mmol, 1.0 eq.) and K_2CO_3 (20.1 mg, 0.151 mmol, 2.0 eq.) were suspended in MeCN (3 mL) and stirred for 2.5 h at 40 °C. The solvent and SMe_2 was removed under vacuum before a small portion of CH_2Cl_2 was added and the mixture was filtered through a pad of Celite. The solution was concentrated to about 1 mL and pentane (5 mL) was added. The precipitate was dried under vacuum affording **3a** as a light yellow solid (37.6 mg, 0.0740 mmol, 99%).

Major isomer
^{1}H NMR (600 MHz, $CDCl_3$): δ 7.81 (1H, H2), 7.47 (t, J = 7.2 Hz, 1H, H9), 7.33 (t*, J = 7.2 Hz, 2H, H8), 7.17 (d, J = 7.2 Hz, 2H, H7), 7.04 (s, 1H, H3), 6.98-6.94 (m, 1H, H12), 6.61 (d, J = 7.3 Hz, 2H, H11), 3.86 (s, 3H, H4), 2.23 (s, 3H, H14)

^{13}C NMR (151 MHz, $CDCl_3$) δ 174.5 (C1), 147.8 (C5), 144.0 (C13), 134.4 (C10), 131.3 (C9), 130.1 (C7), 130.0 (C6), 129.5 (C12), 128.8 (C8), 121.7 (C3), 121.0 (C11), 120.5 (C2), 39.8 (C4), 20.8 (C14),

Minor isomer
^{1}H NMR (600 MHz, $CDCl_3$) δ 7.66 (d, J = 7.9 Hz, 2H, H7), 7.53 (t, J = 7.1 Hz, 1H, H9), 7.34 (t*, J = 7.5 Hz, 2H, H8), 7.01 (d, J = 7.6 Hz, 2H, H12), 6.96 (s, 1H, H3), 6.82 (s, 1H, H2), 6.74 (d, J = 7.6 Hz, 2H, H11), 3.81 (s, 3H, H4), 2.25 (s, 3H, H14)
^{13}C NMR (151 MHz, $CDCl_3$) δ 172.6 (C1), 152.9 (C5), 144.0 (C13), 135.0 (C10), 133.7 (C6), 132.7 (C9), 129.7 (C12), 129.0 (C7), 128.8 (C8), 121.5 (C3), 121.4 (C2), 120.4 (C11), 39.8 (C4), 20.8 (C14)

MS (ESI, MeCN) m/z(rel%): 1037($2M{\cdot}Na^+$, 28), 979($(NHC)_2Au_2Cl^+$, 100), 747($(NHC)_2Au^+$, 26), 554($(NHC)_2Au^+$-($C_{14}H_{11}N$), 34), 194($C_{14}H_{12}N^+$, 19)
HR-MS (EI, MeCN): 979.1859,
calculated for $C_{36}H_{34}N_6ClAu_2$: 979.1864 (-0.57 ppm)

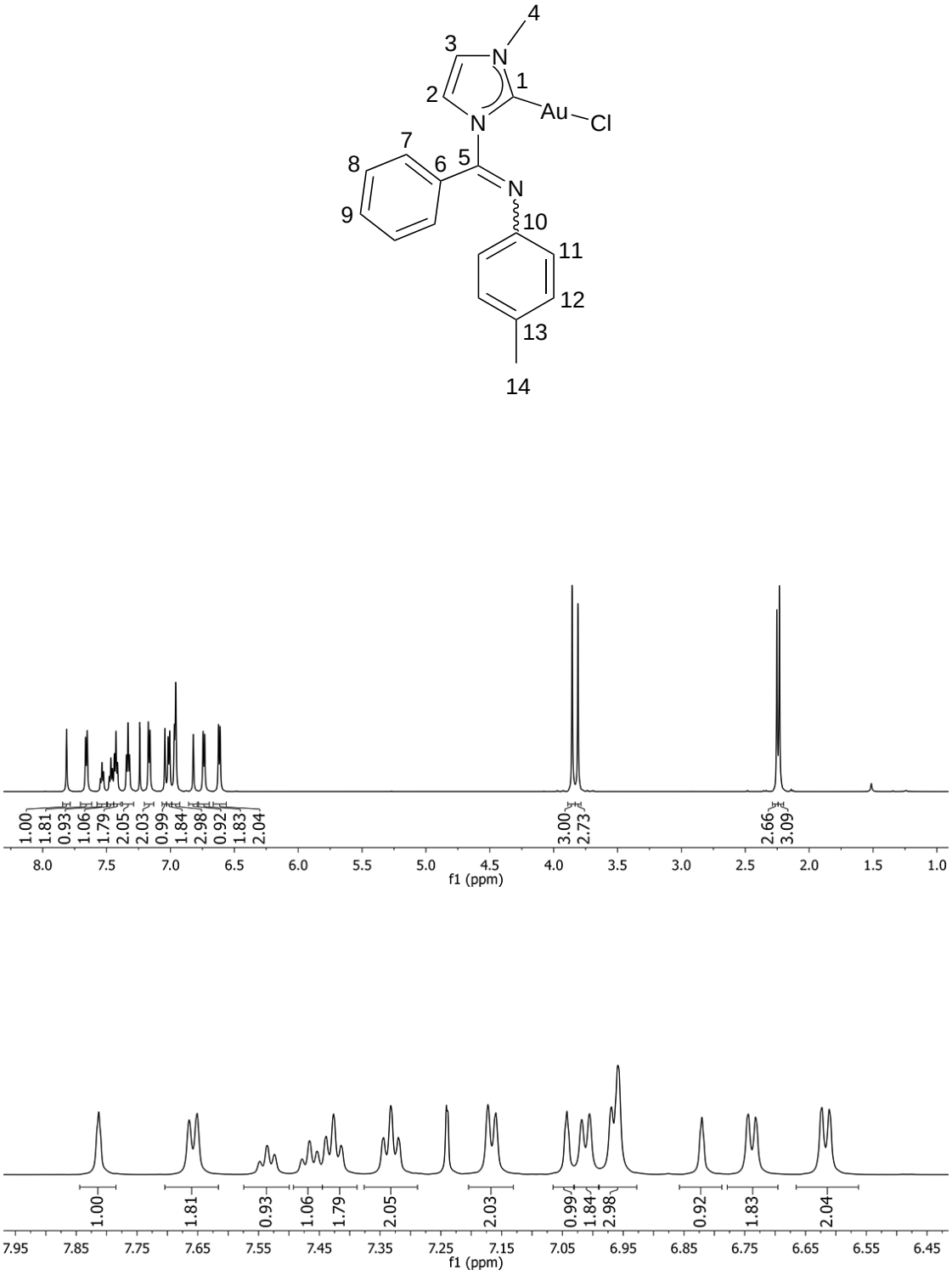

Figure 6.8: ^{1}H NMR (600 MHz, $CDCl_3$) of compound **3a**

6.9 Synthesis of gold(I) complex 3a by transmetalation from 2

Silver(I) carbene **2** (93.0 mg, 0.222 mmol, 1.0 eq.) and (SMe_2)AuCl (66.2 mg, 0.225 mmol, 1.0s eq.) were dissolved in CH_2Cl_2 and stirred for 4 h at room temperature. The solution was filtered using canula filtration and passed through a pad of Celite. The solvent was removed under vacuum and the crude was recrystallised by layering a nearly saturated solution of CH_2Cl_2 solution with pentane. The precipitate was collected and dried under vacuume to yield **3a** as a light yellow solid (95.7 mg, 0.188 mmol, 85%).
For characterisation, please see Section 6.8.

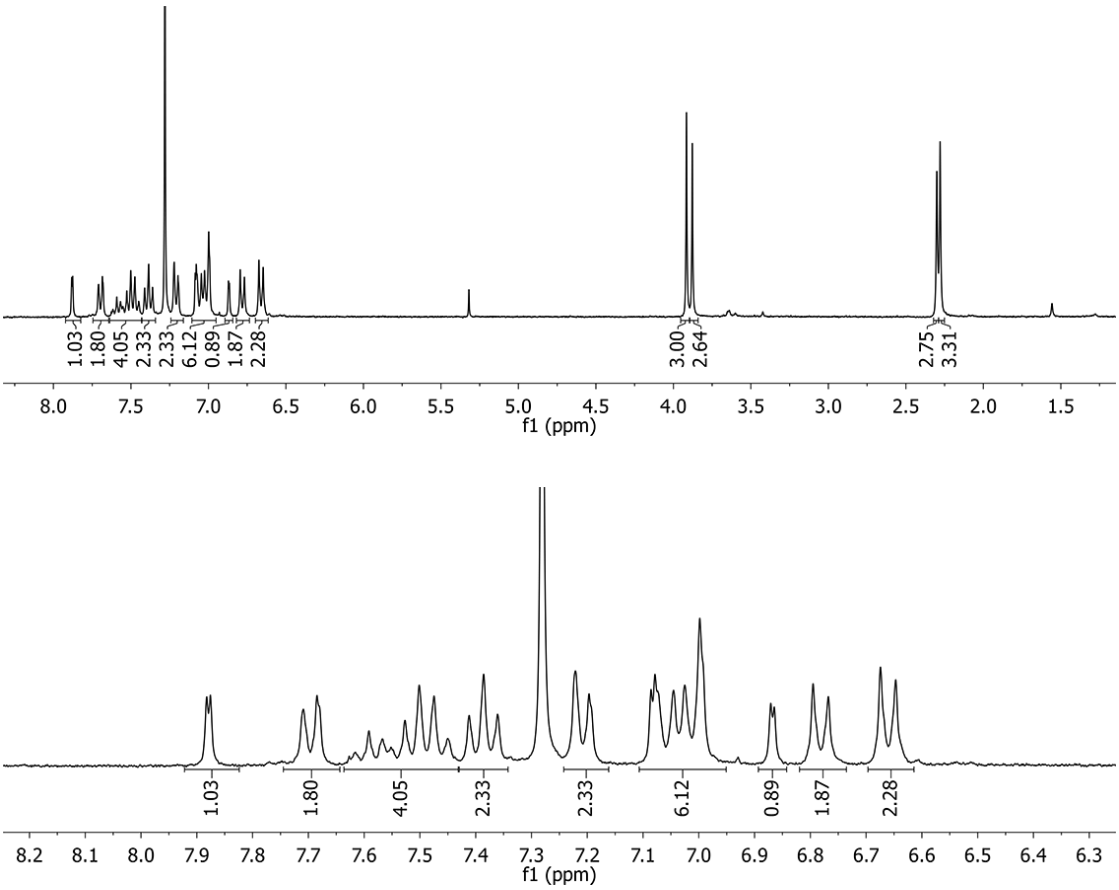

Figure 6.9: ^{1}H NMR (300 MHz, $CDCl_3$) of compound**3a** synthesised by transmetallation from **2**

6.10 Synthesis of gold(I) complex 3a in a one-pot reaction using a silver base

A mixture of **1a** (156 mg, 0.500 mmol, 1.0 eq.), Ag_2O (116 mg, 0.501 mmol, 1.0 eq.), $(SMe_2)AuCl$ (147 mg, 0.500 mmol, 1.0 eq.) and activated 3 Å molecular sieves was suspended in CH_2Cl_2 (25 mL) and stirred at room temperature overnight. The solution was filtered through Celite and the solvent was removed under vacuum. A small portion of CH_2Cl_2 was added and the solution was layered by pentane (15 mL). The resultant precipitate was collected and dried to yield **3a** as light yellow crystals (209 mg, 0.412 mmol, 83%).
For characterisation, please see Section 6.8.

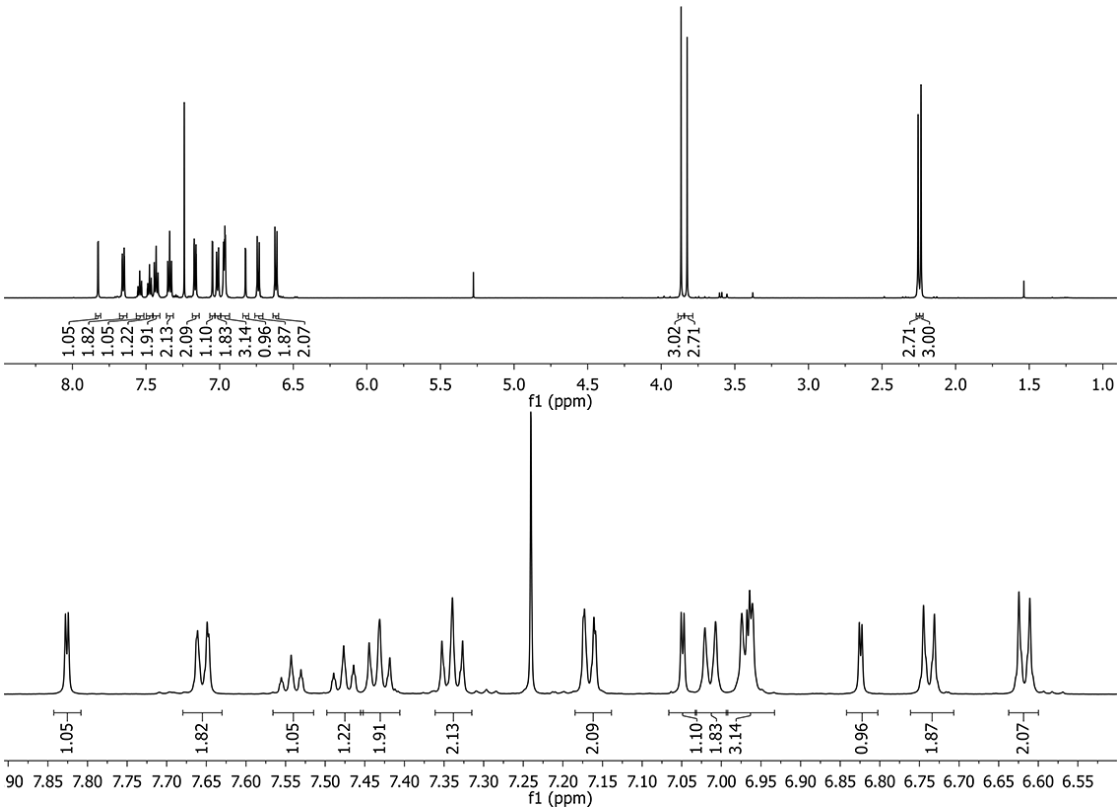

Figure 6.10: ^{1}H NMR (600 MHz, $CDCl_3$) of compound **3a** synthesised from **1a** in a one-pot reaction using Ag_2O

6.11 Synthesis of imidazolium dichloroaurate(I) 4

Imidazolium salt **1a** (6.5 mg, 0.021 mmol, 1.0 eq.) and (SMe_2)AuCl (6.1 mg, 0.021 mmol, 1.0 eq.) was stirred in CH_2Cl_2 (1 mL) for 10 min before CH_2Cl_2 and SMe_2 were removed under vacuum to yield **4** as a yellow solid (11.4 mg, 0.021 mmol, 99%).

^{1}H NMR (600 MHz, $CDCl_3$) δ 9.28 (br. s, 1H, H1), 7.75 (br. s, 1H, H2), 7.56 (br. s, 1H, H3), 7.52 - 7.48 (m, 1H, H9), 7.47 - 7.44 (m, 4H, H8; H7), 6.98 (d, J = 8.1 Hz, 2H, H12), 6.70 (d, J = 8.1 Hz, 2H, H11), 4.18 (s, 1H, H4), 2.23 (s, 1H, H14)

^{13}C NMR (151 MHz, $CDCl_3$) δ 147.8 (C5), 142.2 (C13), 136.1 (C10), 135.8 (C1), 132.2 (C9), 129.4 (C12), 129.7 (C7), 129.7 (C8), 127.1 (C6), 124.2 (C3), 121.6 (C11), 120.0 (C2), 37.8 (C4), 21.0 (C14),

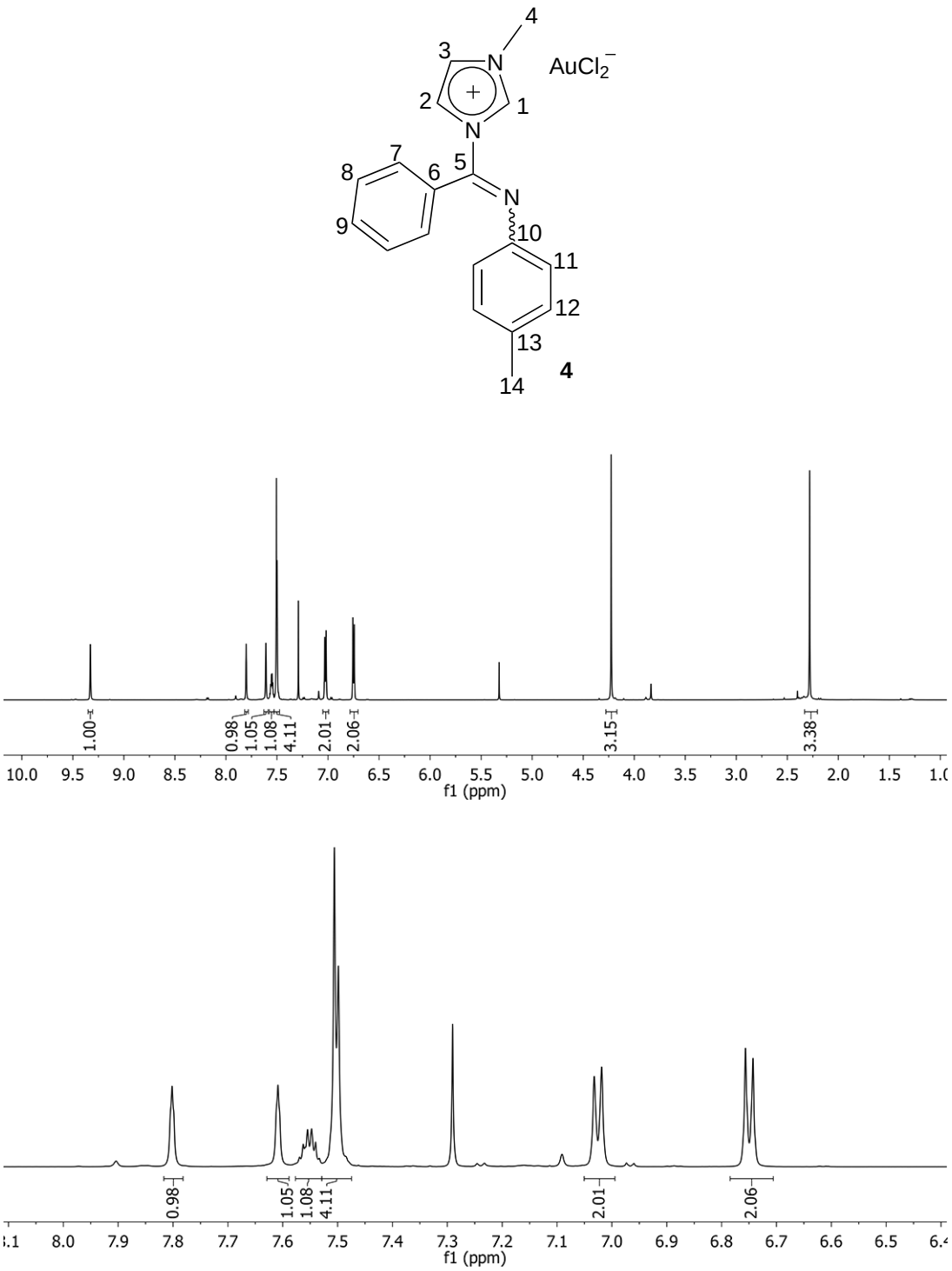

Figure 6.11: ^{1}H NMR (600 MHz, $CDCl_3$) of compound **4**

6.12 Synthesis of gold(I) complex 3b

Imidazolium salt **1b** (25.7 mg, 0.756 mmol, 1.0 eq.), (SMe_2)AuCl (22.2 mg, 0.0754 mmol, 1.0 eq.) and K_2CO_3 (20.1 mg, 0.151 mmol, 2.0 eq.) were suspended in MeCN (3 mL) and stirred for 1.5 h at 40 °C. The solvent and SMe_2 was removed under vacuum before a small portion of CH_2Cl_2 was added and the mixture was and filtered through a pad of Celite. The solvent was concentrated to about 1 mL and pentane (5 mL) was added. The precipitate was dried under vacuum affording **3b** as a light yellow solid (41.3 mg). By integration of NMR signals it was calculated that the product contained approximately 3% CH_2Cl_2 by weight. Yield: 40.0 mg, 0.0747 mmol, 99%.

Major isomer
^{1}H NMR (600 MHz, CD_2Cl_2) δ 7.79 (d, J = 1.9 Hz, 1H, H2), 7.47 (t, J = 7.5 Hz, 1H, H9), 7.32 (t*, J = 7.8 Hz, 2H, H8), 7.16 (d, J = 7.4 Hz, 2H, H7), 7.13 (d, J = 1.9 Hz, 1H, H3) 6.80 (s, 2H, H12), 3.91 (s, 3H, H4), 2.20(s, 3H, H14), 2.02 (s, 6H, H15)
^{13}C NMR (151 MHz, CD_2Cl_2) δ 174.4 (C1), 152.7 (C5), 142.5 (C10), 133.8 (C13), 132.2 (C9), 131.8 (C6), 129.5 (C7), 128.1 (C12), 128.9 (C8), 126.3 (C11), 122.2 (C3), 121.0 (C2), 39.8 (C4), 20.8 (C14), 18.55 (C15)

Minor isomer
^{1}H NMR (600 MHz, CD_2Cl_2) 7.71 (d*, J = 7.4 Hz, 2H, H7), 7.64 (t, J = 7.0 Hz, 1H, H9), 7.33 (t*, J = 7.5 Hz, 2H, H8), 6.89 (s, 1H, H2), 6.80 (s, 2H, H12), 6.89 (s, 1H, H3), 3.81 (s, 3H, H4), 2.22(s, 3H, H14), 2.21 (s, 6H, H15)
The minor isomer was not characterised by ^{13}C NMR since the signals were too weak.

MS (ESI, MeCN) m/z(rel%): 1035($(NHC)_2Au_2Cl^+$, 19), 803($(NHC)_2Au^+$, 10), 558($M{\cdot}Na^+$, 14), 222($C_{16}H_{16}N^+$, 100)
HR-MS (EI, MeCN): 1035.2474,
calculated for $C_{40}H_{42}N_6ClAu_2$: 1035.2490 (-1.61 ppm)

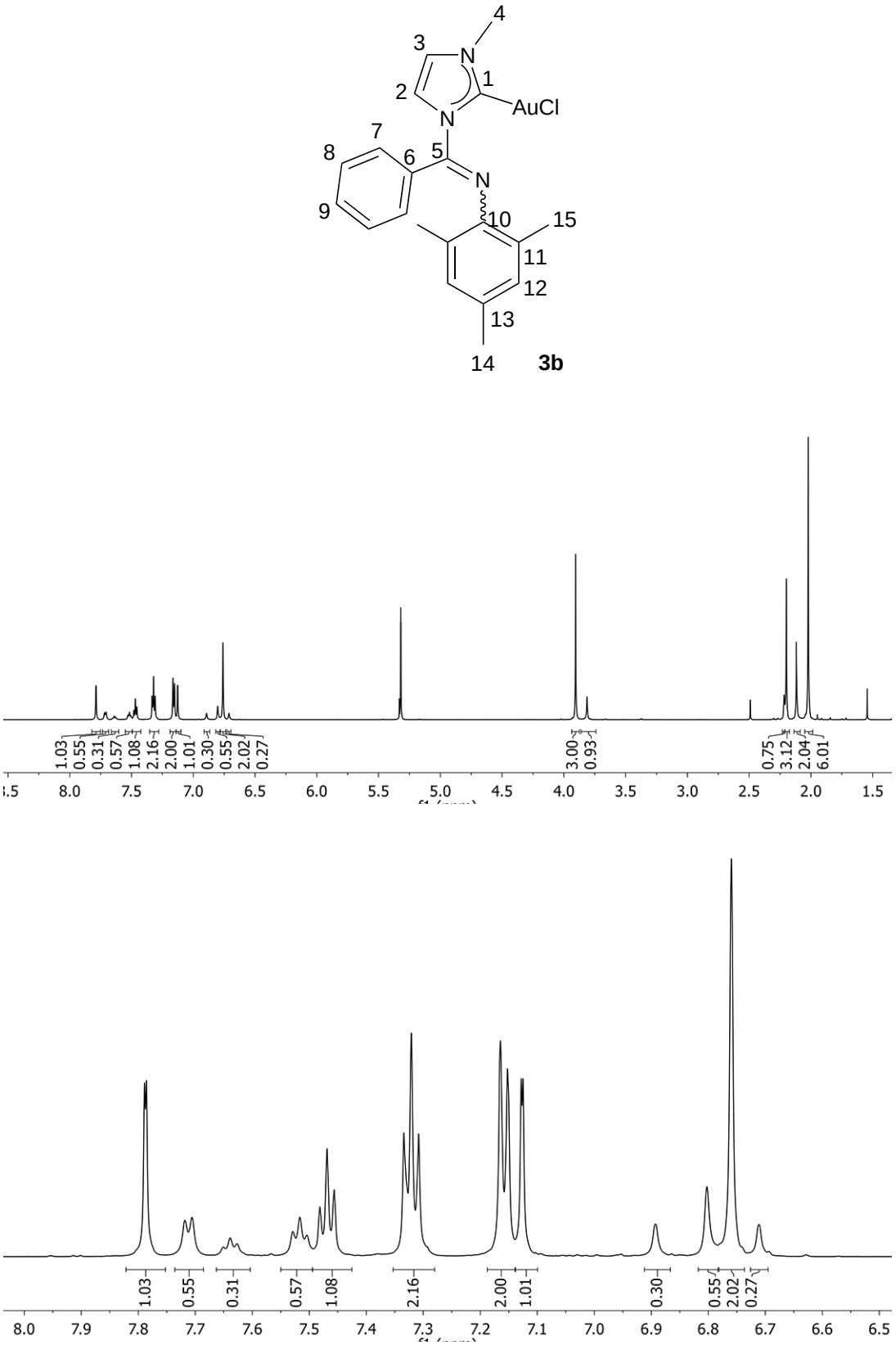

Figure 6.12: ^{1}H NMR (600 MHz, CD_2Cl_2) of compound **3b**

6.13 Synthesis of gold(III) complex 5a

A solution of gold(I) complex **3a** (159 mg, 0.313 mmol, 1.0 eq.) and $PhICl_2$ (106 mg, 0.386 mmol, 1.2 eq.) in CH_2Cl_2 was stirred overnight at ambient temperature. The solvent was removed under vacuum. The crude was dissolved in CH_2Cl_2 (2 mL) and the mixture was layered with pentane (25 mL). The resulting precipitate was collected and dried under a flow of Ar(g) to afford gold(III) complex **5a** as orange crystals (177 mg, 0.306 mmol, 98%).

^{1}H NMR (600 MHz, CD_2Cl_2): δ 7.55 (t, J = 7.5 Hz, 1H, H9), 7.43 (t*, J = 7.7 Hz, 2H, H8), 7.32 (d*, J = 7.4 Hz, 2H, H7), 7.22 (s, 1H, H3), 7.21 (s, 1H, H2), 7.06 (d, J = 8.1 Hz, 2H, H12), 6.83 (d, J = 8.1 Hz, 2H, H11), 4.11 (s, 3H, H4), 2.28 (s, 3H, H14)
^{13}C NMR (151 MHz, CD_2Cl_2) δ 151.0 (C5), 144.4 (C1), 143.0 (C13), 136.0 (C10), 132.1 (C9), 130.3 (C7), 130.0 (C12), 129.6 (C8), 129.0 (C6), 124.8 (C3), 123.0 (C2), 121.6 (C11), 39.4 (C4), 21.0 (C14)

Additional NMR spectra of **5a** in $CDCl_3$ were recorded so that the ^{13}C NMR resonances could be compared in Section 2.5.

^{13}C NMR (151 MHz, $CDCl_3$) δ 150.1 (C5), 144.0 (C1), 142.5 (C13), 135.5 (C10), 131.8 (C9), 129.9 (C7), 129.6 (C12), 129.3 (C8), 128.6 (C6), 124.5 (C3), 122.4 (C2), 121.5 (C11), 39.0 (C4), 21.0 (C14)

MS (ESI, MeCN) m/z(rel%): 1177/1179/1181/1183(2M·Na^+, 26/56/43/16), 542/544/546(M^+-Cl, 54/23/11), 314/315(M^+-($C_{14}H_{11}NCl_2$), 49/12), 194($C_{14}H_{12}N^+$, 100)
HR-MS (EI, MeCN): 542.0472,
calculated for $C_{18}H_{17}N_3Cl_2Au$: 542.0465 (1.26 ppm)

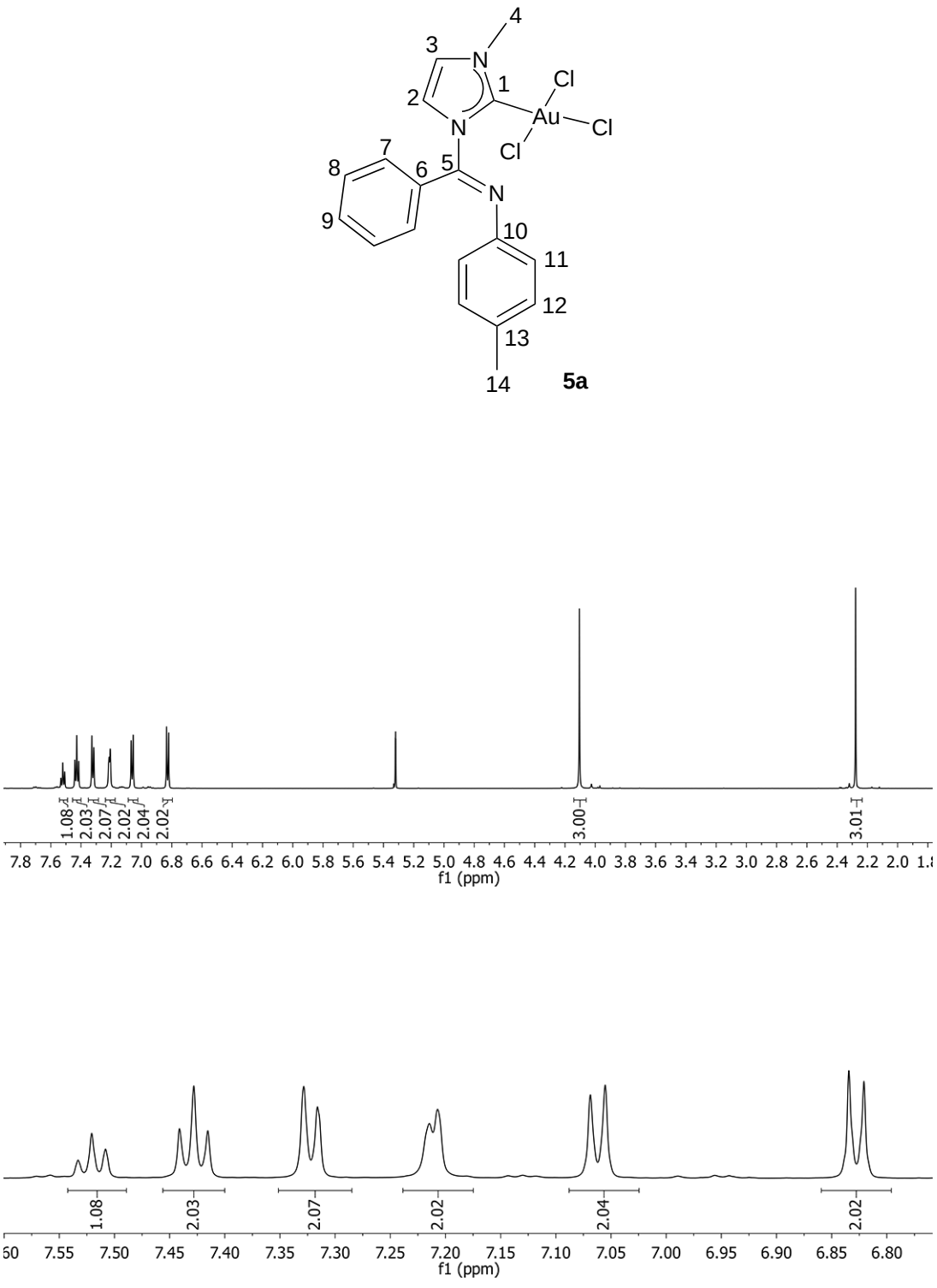

Figure 6.13: ^{1}H NMR (600 MHz, CD_2Cl_2) of compound **5a**

6.14 Synthesis of gold(III) complex 5b

A solution of gold(I) complex **3b** (61.7 mg, 0.115 mmol, 1.0 eq.) and $PhICl_2$ (41.2 mg, 0.150 mmol, 1.3 eq.) in CH_2Cl_2 was stirred overnight at ambient temperature. The solvent was removed under vacuum. The crude was dissolved in CH_2Cl_2 (1 mL) and the mixture was layered with pentane (15 mL). The resulting precipitate contained unreacted $PhICl_2$ and other impurities. From slow diffusion of pentane onto a solution of the crude in CH_2Cl_2, a few orange crystals were grown, (1.4 mg, 0.002 mmol, 2%). The product was not clean by NMR. A complete set of NMR spectra has not yet been obtained. ^{13}C shift values are collected from HSQC and HMBC spectra.

^{1}H NMR (600 MHz, CD_2Cl_2) δ 7.58 (d, J = 2.0 Hz, H3), 7.52 (t*, J = 7.6 Hz, 1H, H9), 7.40 (t*, J = 7.7 Hz, 2H, H8), 7.27 (d, J = 2.1 Hz, 1H, H3), 7.24 (d*, J = 7.6 Hz, 2H, H7), 6.78 (s, 2H, H12), 4.10(s, 3H, H4), 2.12 (s, 3H, H14), 2.05 (s, 6H, H15)

^{13}C NMR (151 MHz, CD_2Cl_2) δ 149.8 (C5), 143.8 (C1), 140.8 (C10), 134.1 (C13), 132.1 (C9), 129.1 (C8), 128.7 (C12), 127.5 (C7), 126.5 (C11), 124.3 (C3), 123.1 (C2), 38.9 (C4), 21.3 (C14), 18.3 (C15)

MS (ESI, MeCN) m/z(rel%): 570/572/574(M^+-Cl, 63/38/10),
222($C_{16}H_{16}N^+$, 100)
HR-MS (EI, MeCN: 570.0757,
calculated for $C_{20}H_{21}N_3Cl_2Au$: 570.0078 (-3.70 ppm)

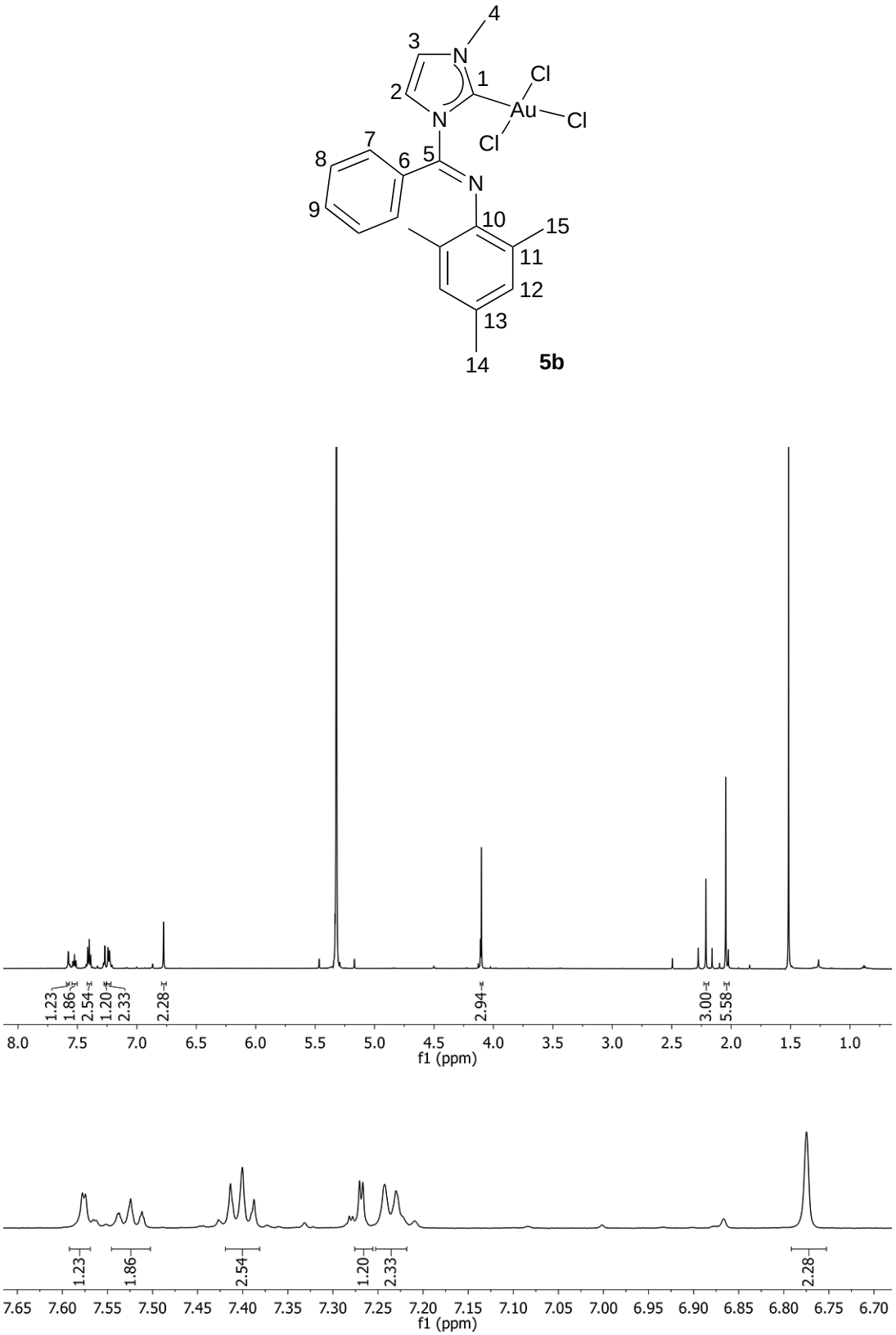

Figure 6.14: ^{1}H NMR (600 MHz, CD_2Cl_2) of compound **5b**

CHAPTER 7

Appendix

7.1 Compound 1a

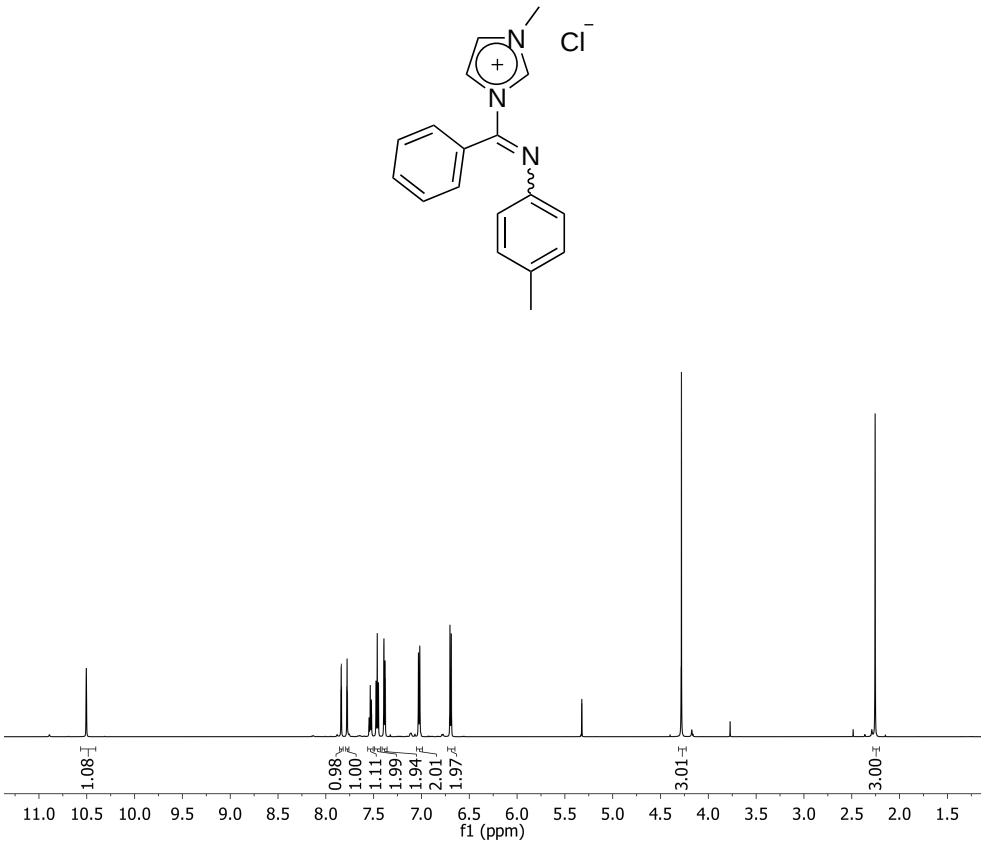

Figure 7.1: ^{1}H NMR (CD_2Cl_2, 600 MHz) of compound **1a**

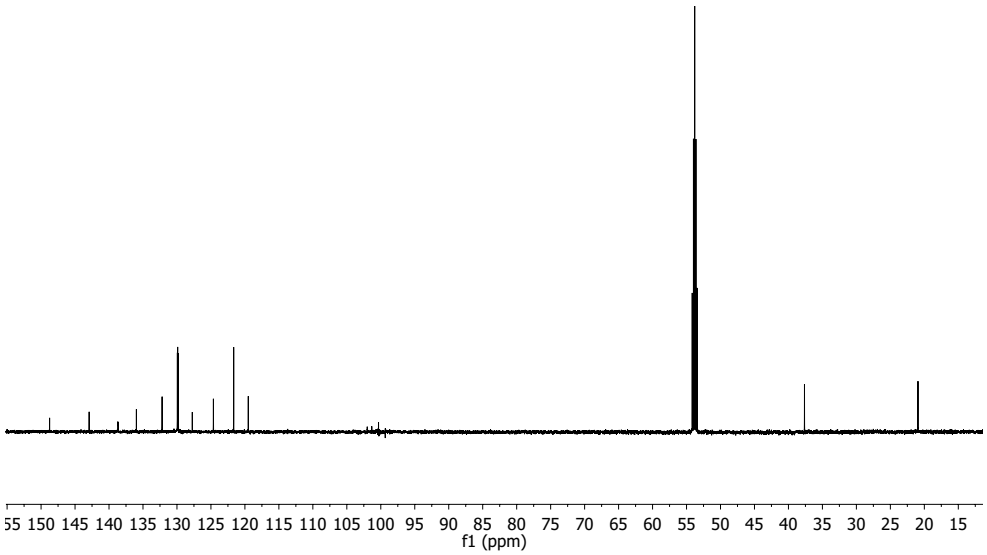

Figure 7.2: ^{13}C NMR (CD_2Cl_2, 151 MHz) of compound **1a**

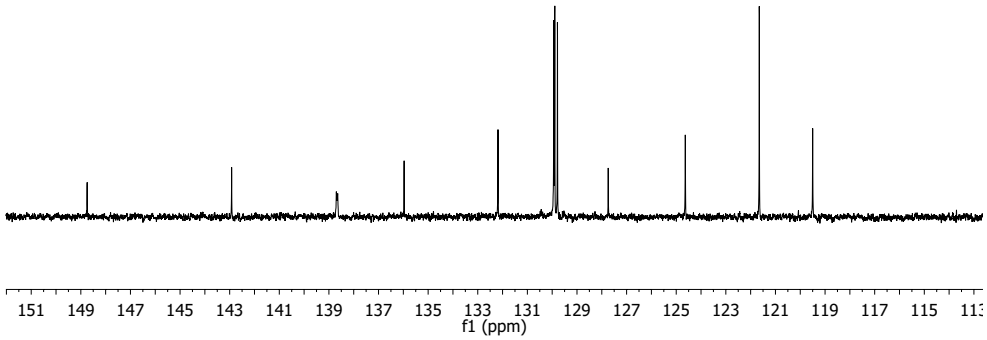

Figure 7.3: ^{13}C NMR (CD_2Cl_2, 151 MHz) of compound **1a** (zoomed)

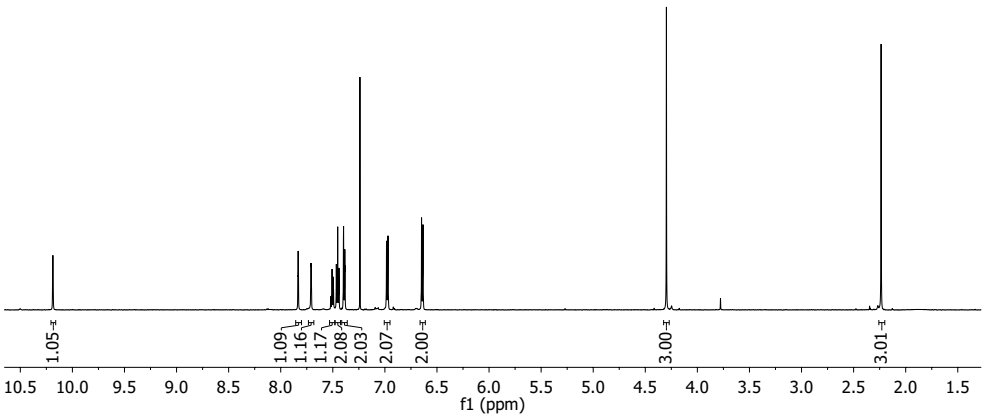

Figure 7.4: ^{1}H NMR ($CDCl_3$, 600 MHz) of compound **1a**

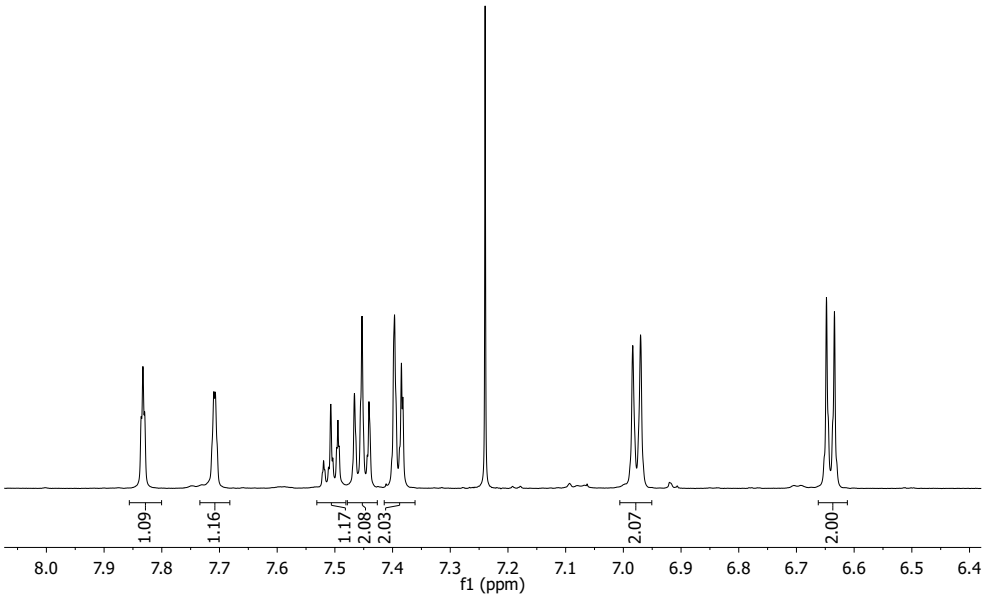

Figure 7.5: ^{1}H NMR ($CDCl_3$, 600 MHz) of compound **1a** (zoomed)

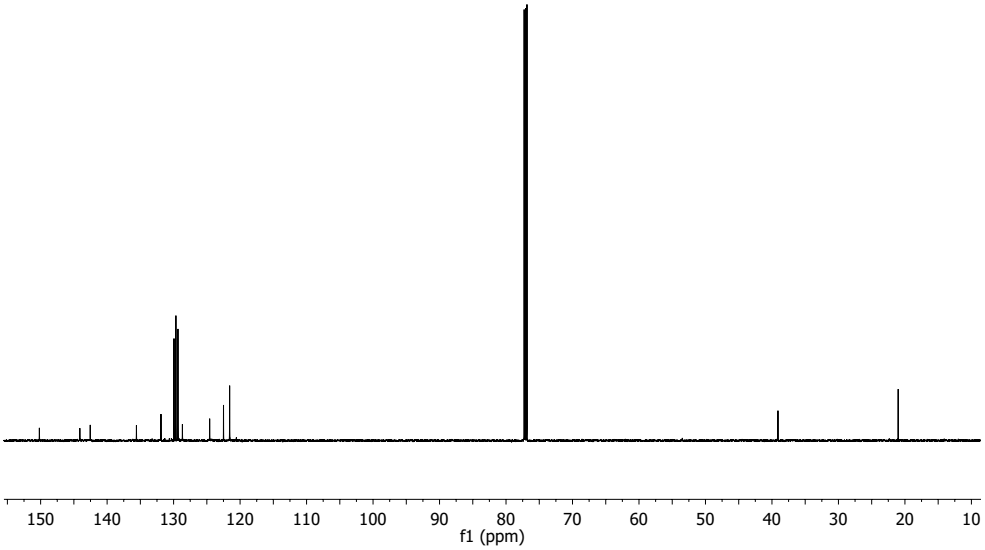

Figure 7.6: ^{13}C NMR ($CDCl_3$, 151 MHz) of compound **1a**

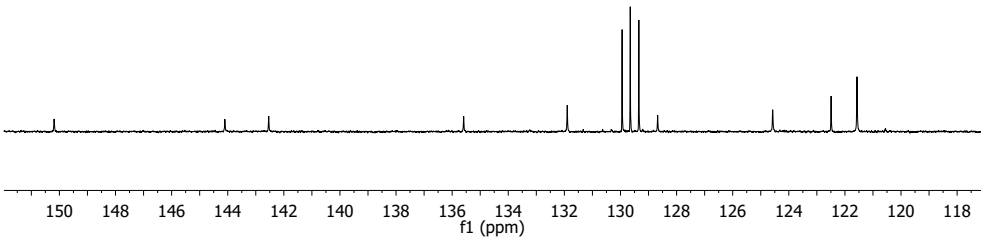

Figure 7.7: ^{13}C NMR ($CDCl_3$, 151 MHz) of compound **1a** (zoomed)

7.2 Compound 1b

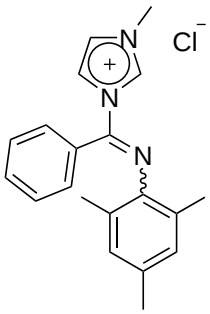

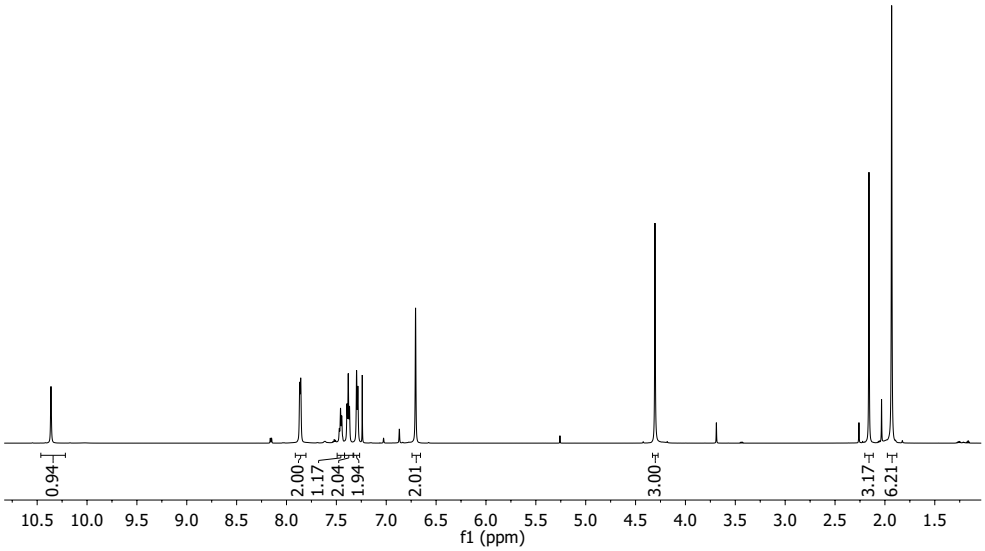

Figure 7.8: ^{1}H NMR ($CDCl_3$, 600 MHz) of compound **1b**

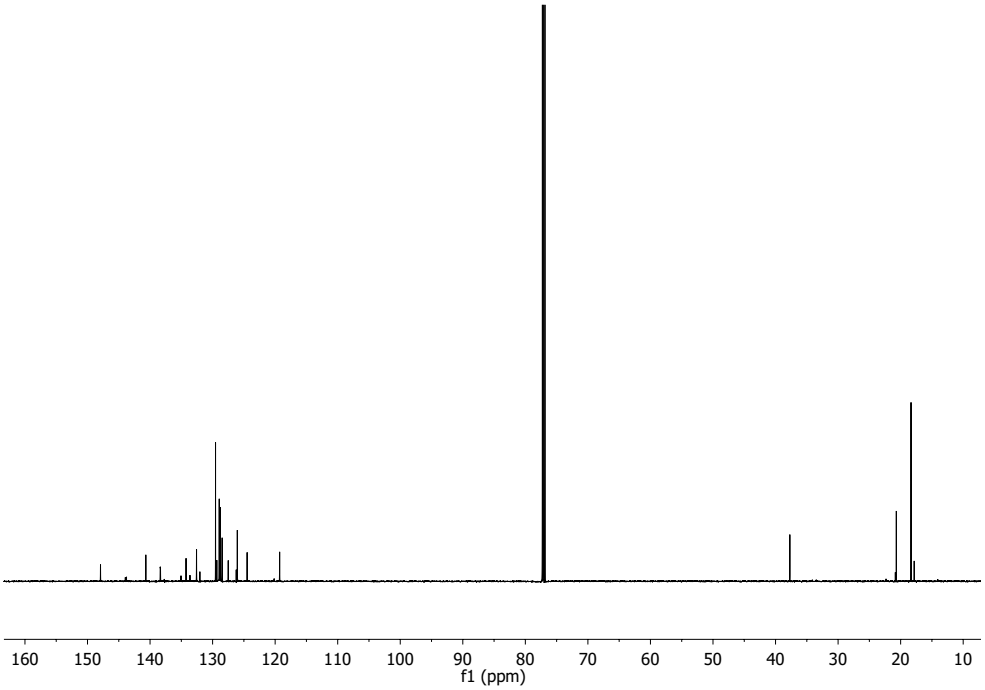

Figure 7.9: ^{13}C NMR ($CDCl_3$, 151 MHz) of compound **1b**

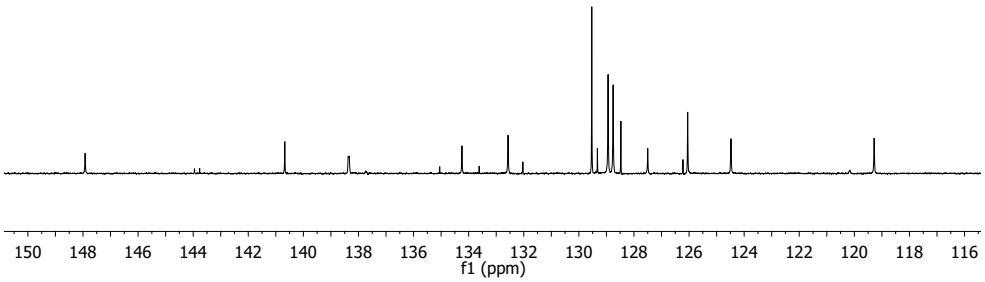

Figure 7.10: ^{13}C NMR ($CDCl_3$, 151 MHz) of compound **1b** (zoomed)

7.3 Compound 4

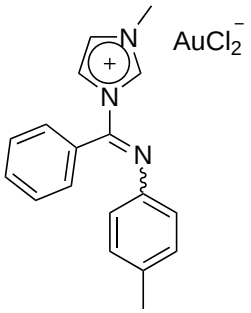

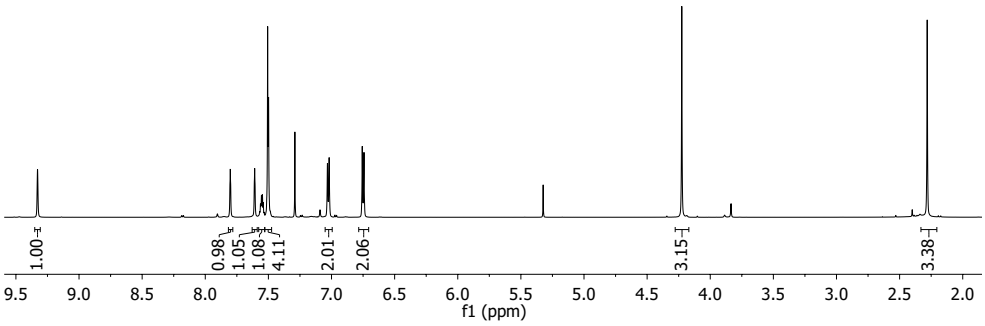

Figure 7.11: ^{1}H NMR ($CDCl_3$, 600 MHz) of compound **4**

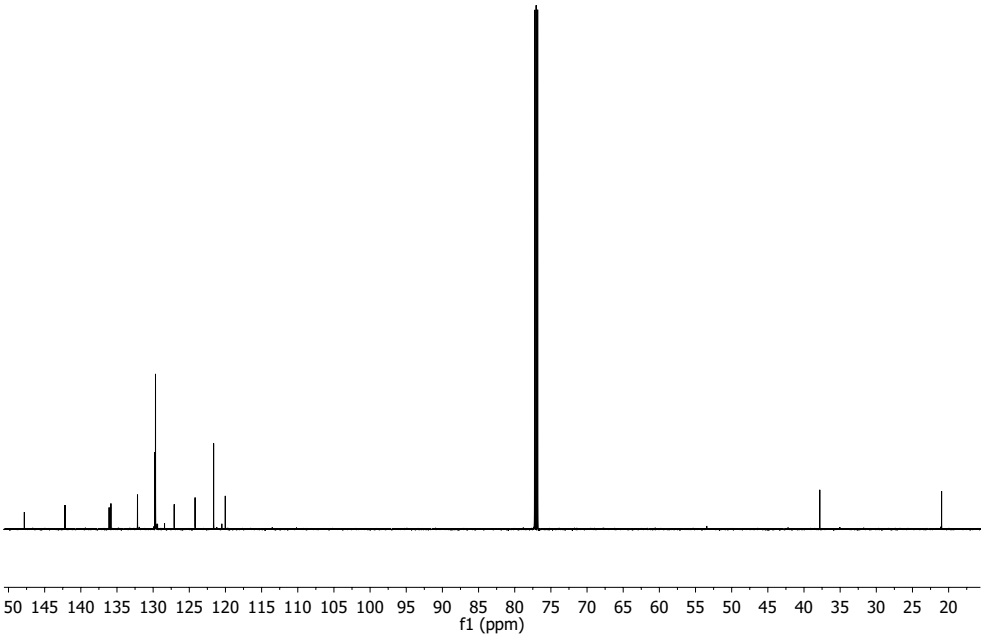

Figure 7.12: ^{13}C NMR ($CDCl_3$, 151 MHz) of compound **4**

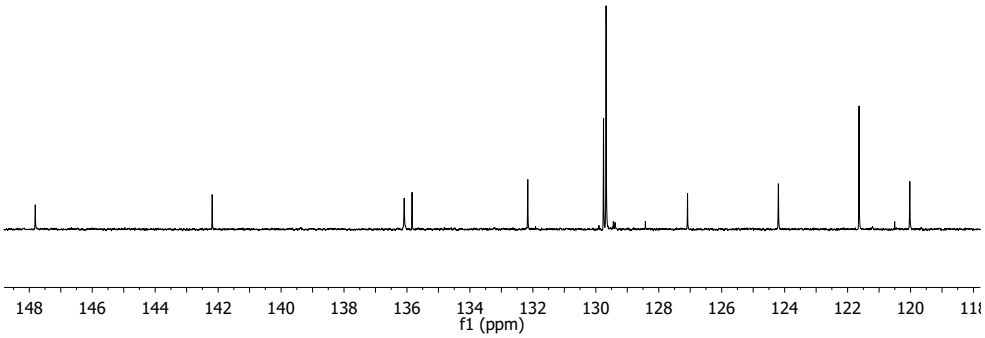

Figure 7.13: ^{13}C NMR ($CDCl_3$, 151 MHz) of compound **4** (zoomed)

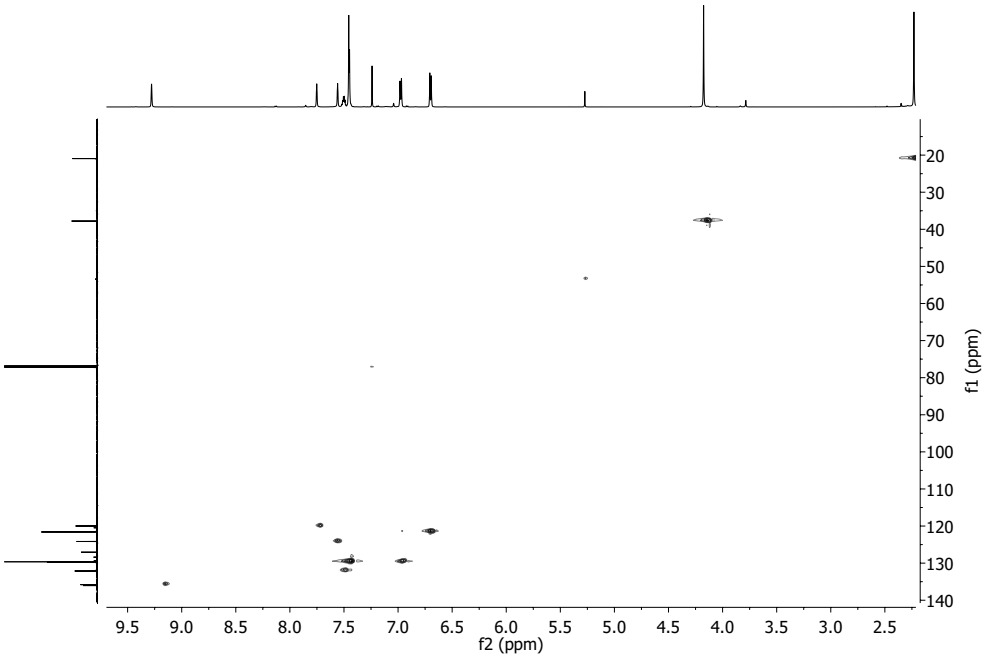

Figure 7.14: HSQC NMR ($CDCl_3$, 600 MHz) of compound **4**

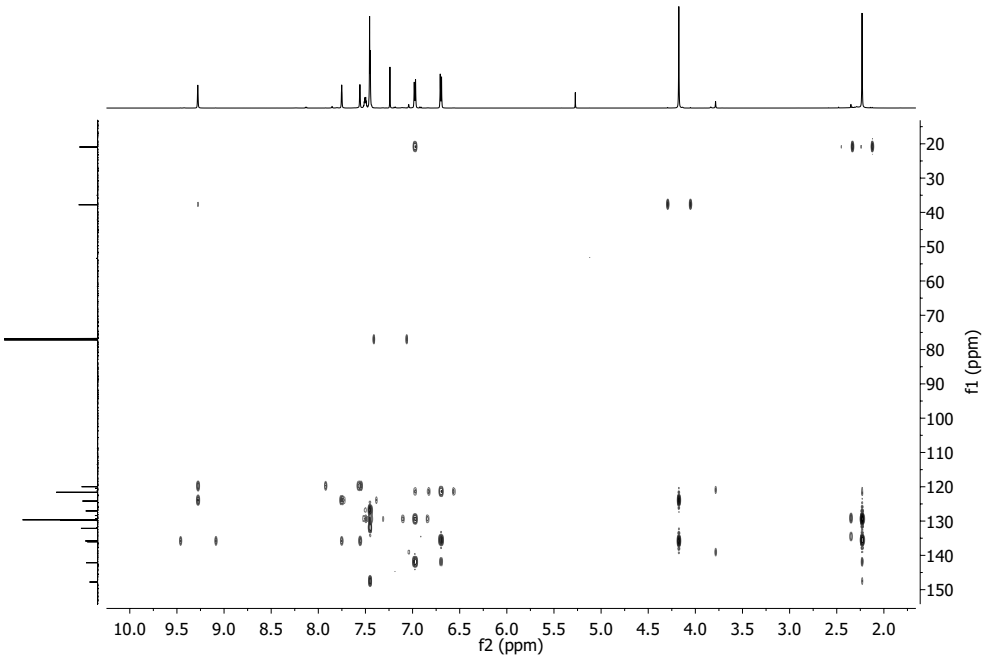

Figure 7.15: HMBC NMR ($CDCl_3$, 600 MHz) of compound **4**

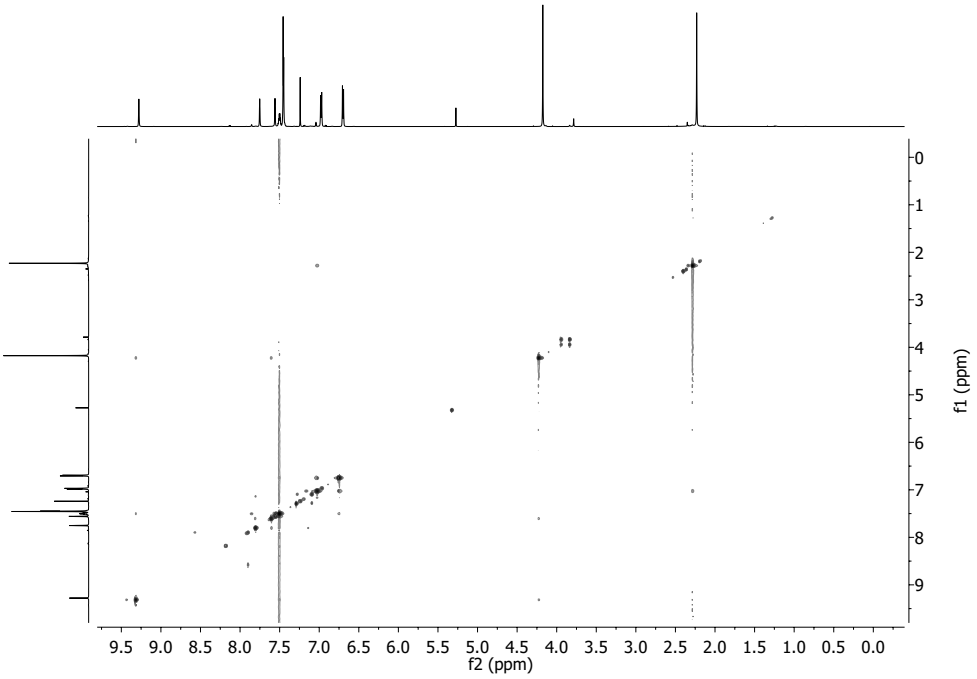

Figure 7.16: NOESY NMR ($CDCl_3$, 600 MHz) of compound **4**

7.4 Compound 2a

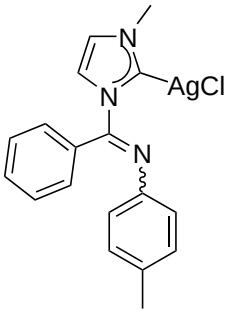

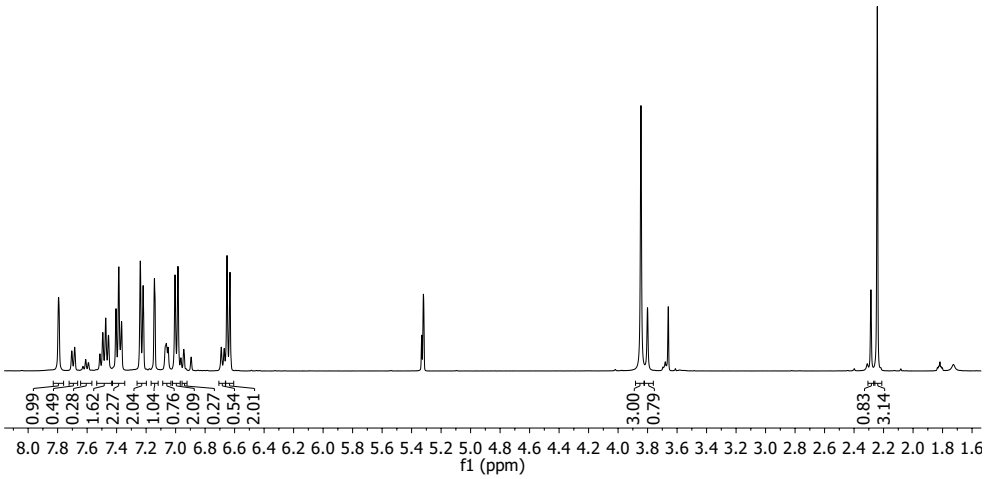

Figure 7.17: ^{1}H NMR (CD_2Cl_2, 400 MHz) of compound **2a**

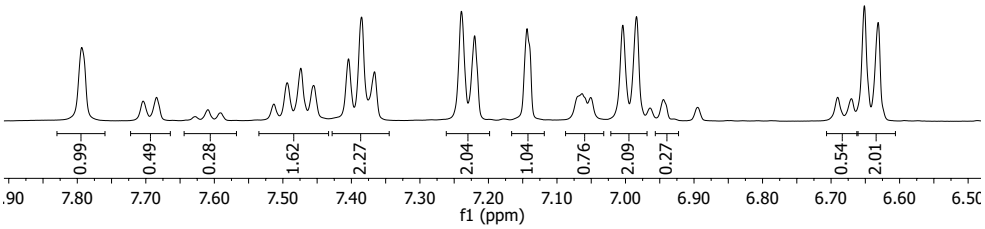

Figure 7.18: ^{1}H NMR (CD_2Cl_2, 400 MHz) of compound **2a** (zoomed)

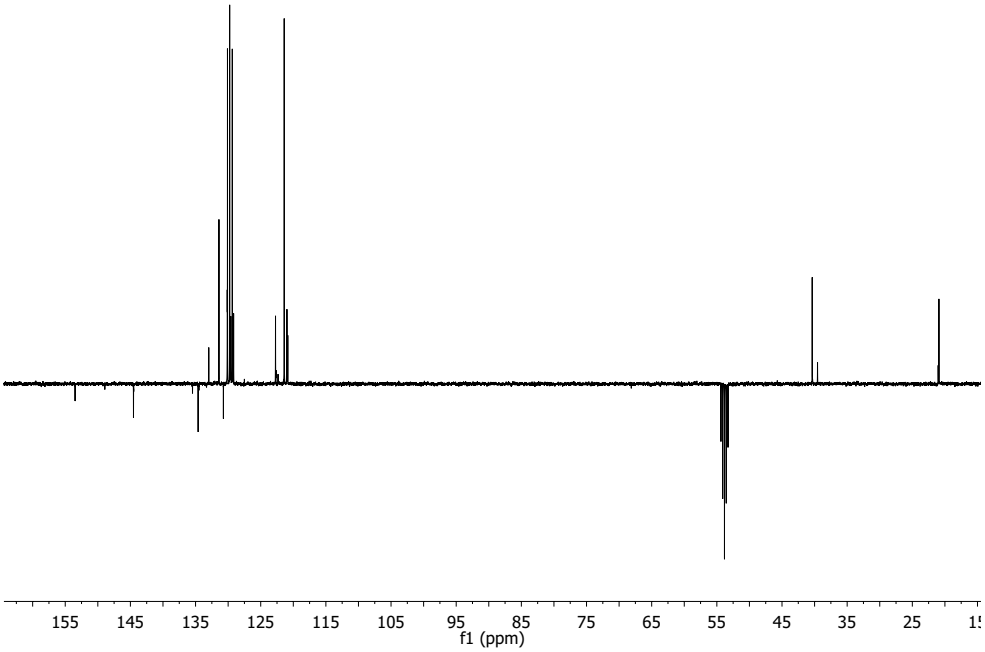

Figure 7.19: ^{13}C NMR (CD_2Cl_2, 100 MHz) of compound **2a**

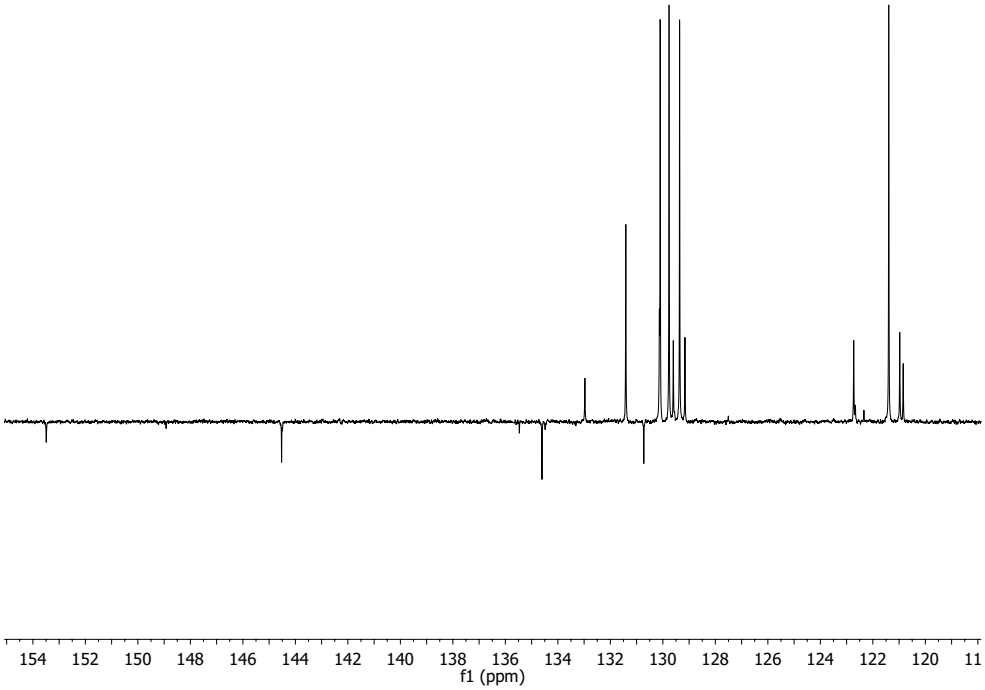

Figure 7.20: ^{13}C NMR (CD_2Cl, 100 MHz) of compound **2a** (zoomed)

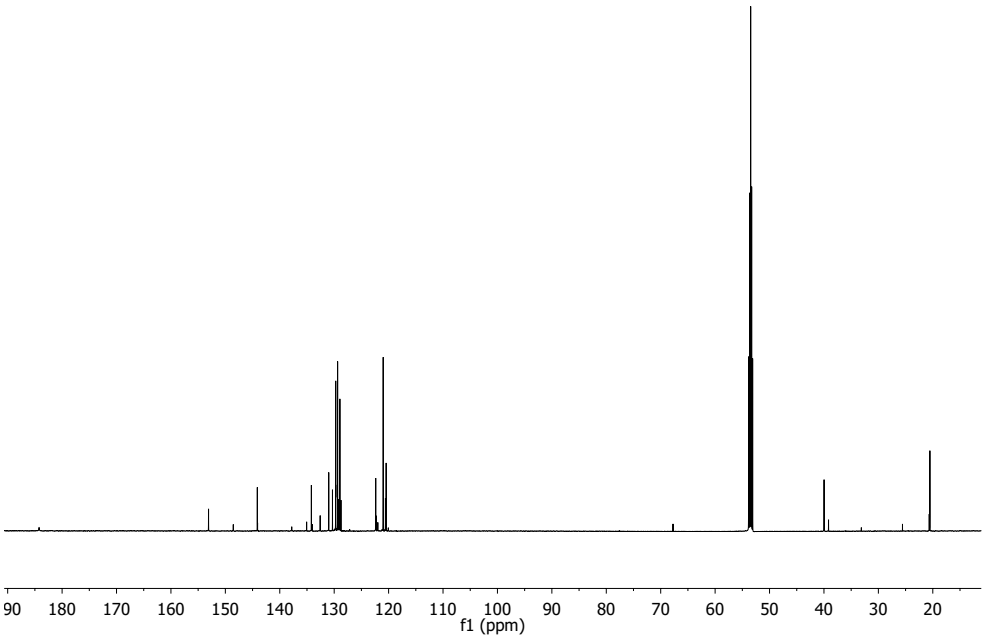

Figure 7.21: ^{13}C NMR ($CDCl_3$, 151 MHz) of compound **2a**

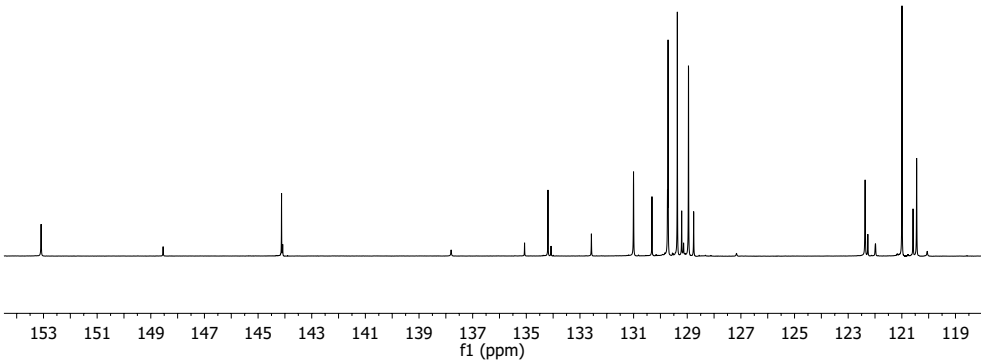

Figure 7.22: ^{13}C NMR ($CDCl_3$, 151 MHz) of compound **2a** (zoomed)

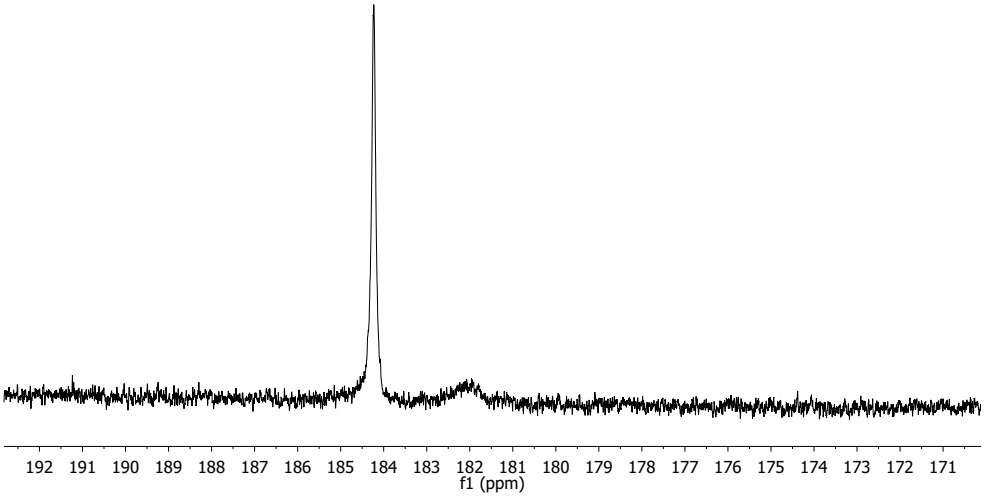

Figure 7.23: ^{13}C NMR ($CDCl_3$, 151 MHz) of compound **2a** (zoomed)

7.5 Compound 3a

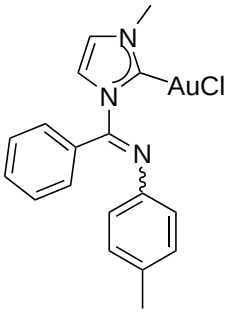

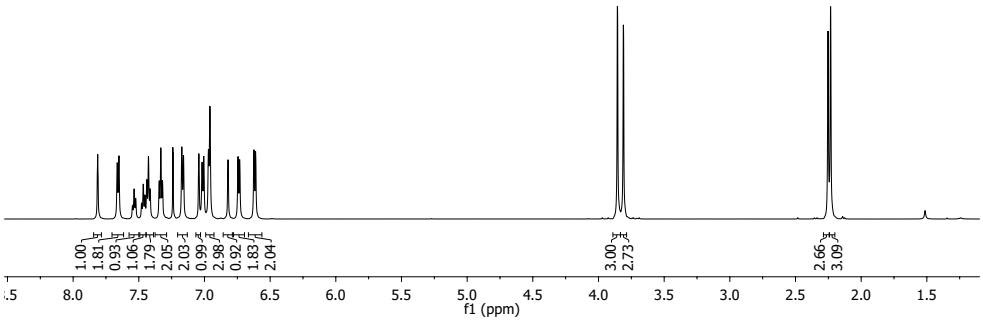

Figure 7.24: ^{1}H NMR ($CDCl_3$, 600 MHz) of compound **3a**

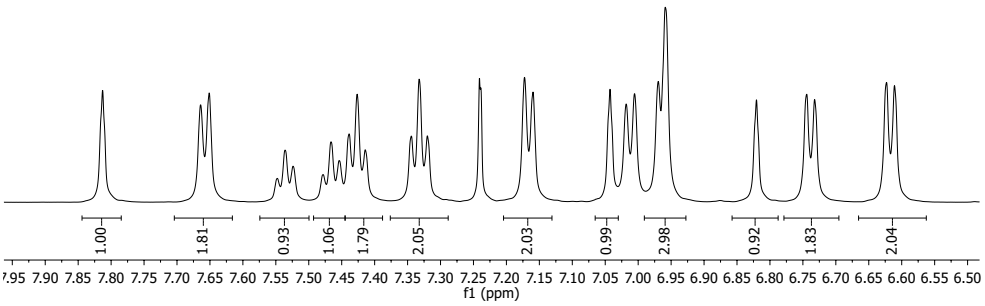

Figure 7.25: ^{1}H NMR ($CDCl_3$, 600 MHz) of compound **3a** (zoomed)

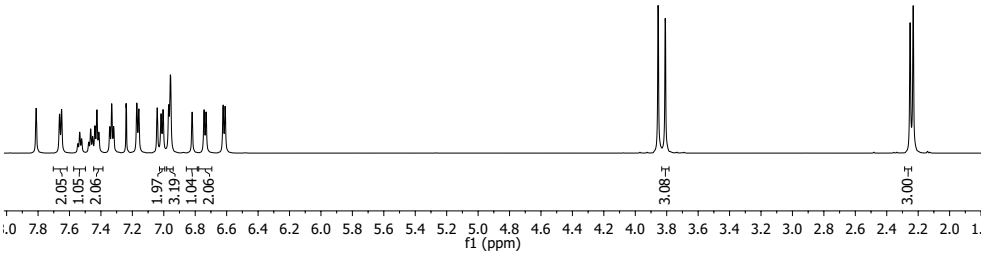

Figure 7.26: ^{1}H NMR ($CDCl_3$, 600 MHz) of compound **3a** with integration on the minor isomer

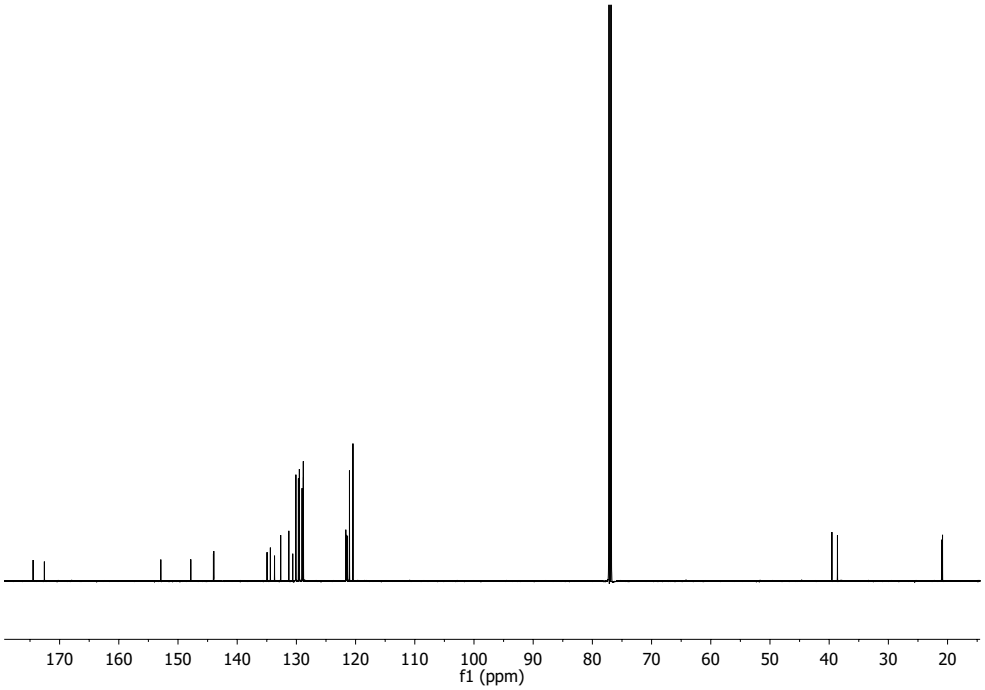

Figure 7.27: ^{13}C NMR ($CDCl_3$, 151 MHz) of compound **3a**

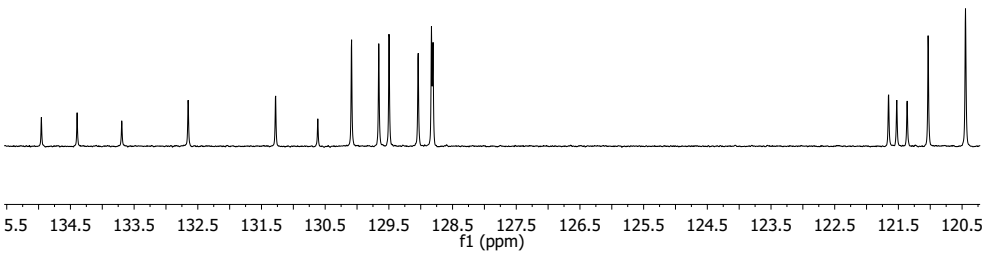

Figure 7.28: ^{13}C NMR ($CDCl_3$, 151 MHz) of compound **3a** (zoomed)

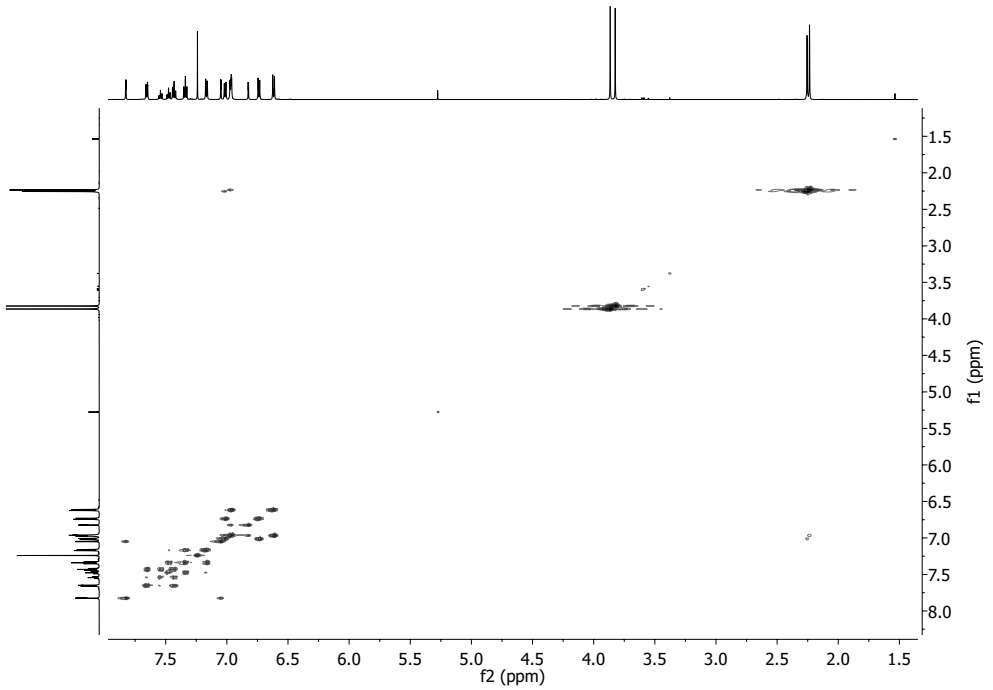

Figure 7.29: COSY NMR ($CDCl_3$, 600 MHz) of compound **3a**

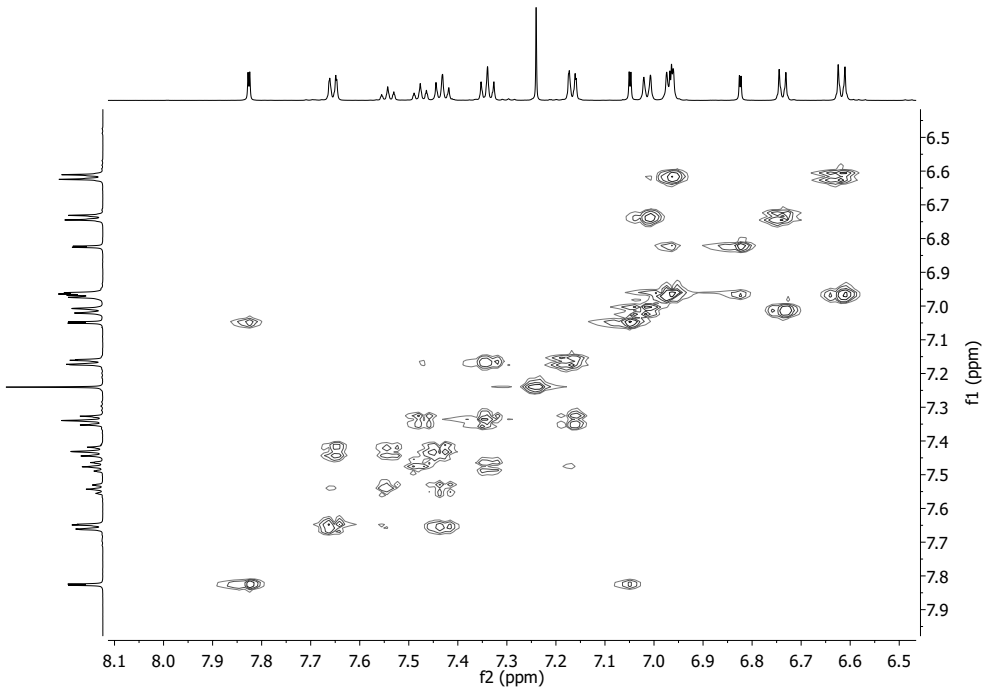

Figure 7.30: COSY NMR ($CDCl_3$, 600 MHz) of compound **3a** (zoomed)

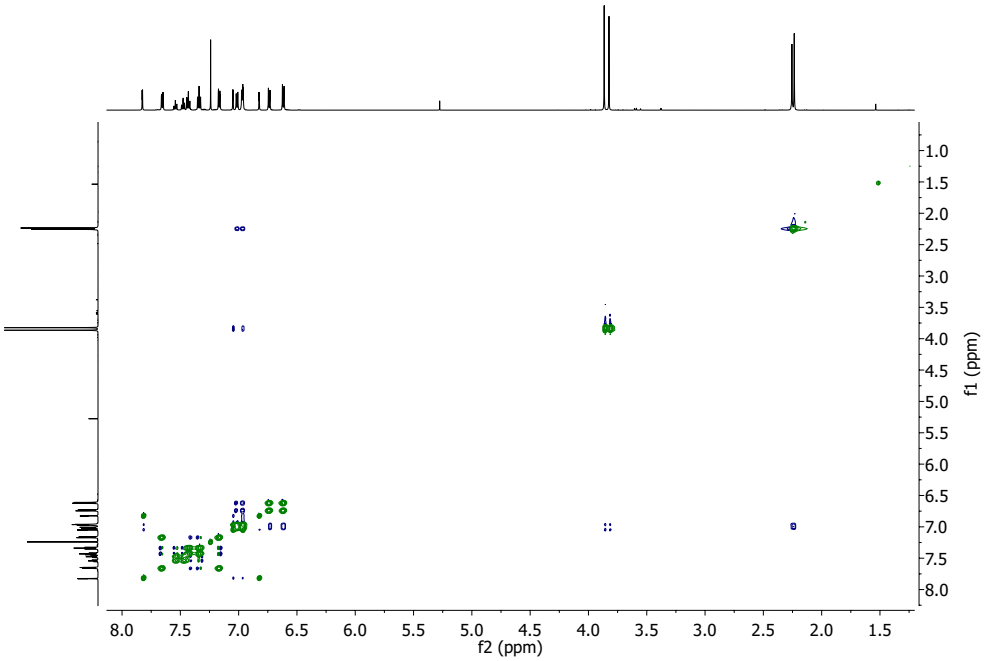

Figure 7.31: NOESY NMR ($CDCl_3$, 600 MHz) of compound **3a**

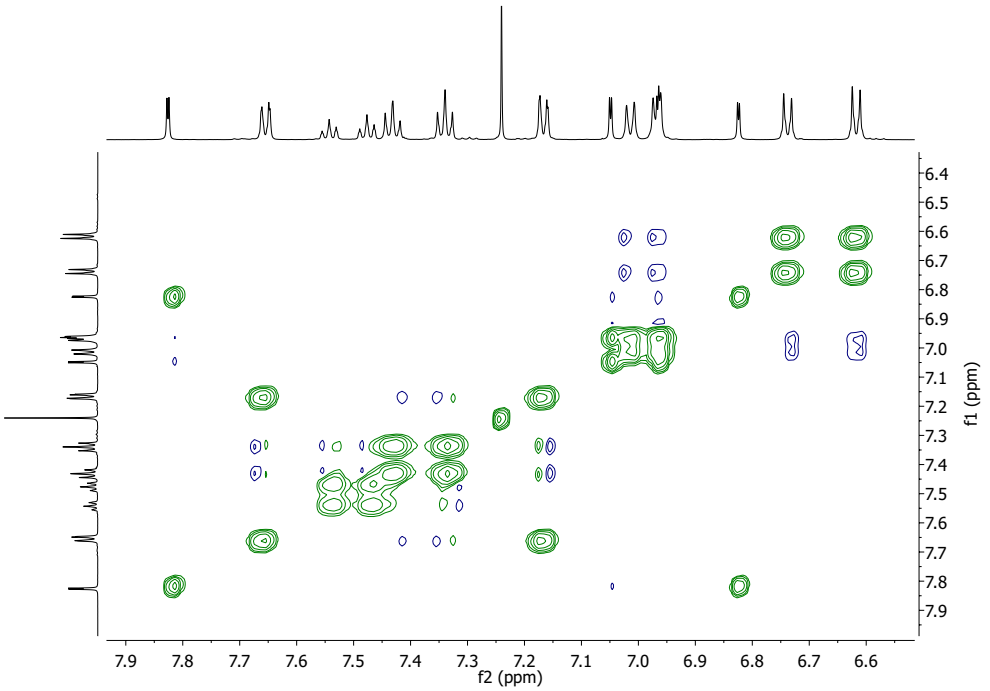

Figure 7.32: NOESY NMR ($CDCl_3$, 600 MHz) of compound **3a** (zoomed)

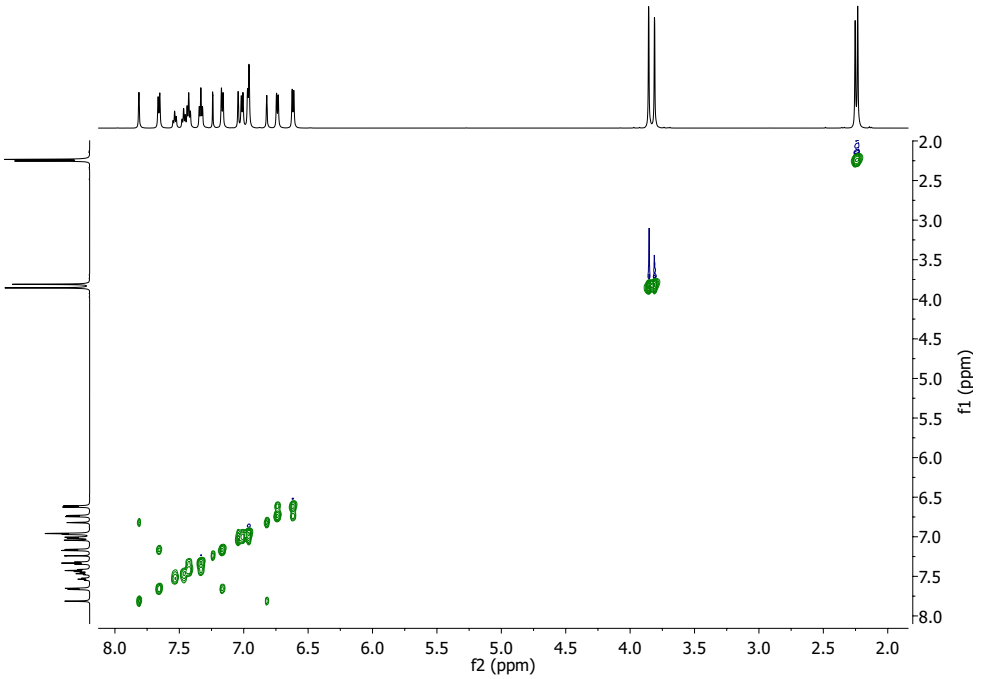

Figure 7.33: ROESY NMR ($CDCl_3$, 600 MHz) of compound **3a**

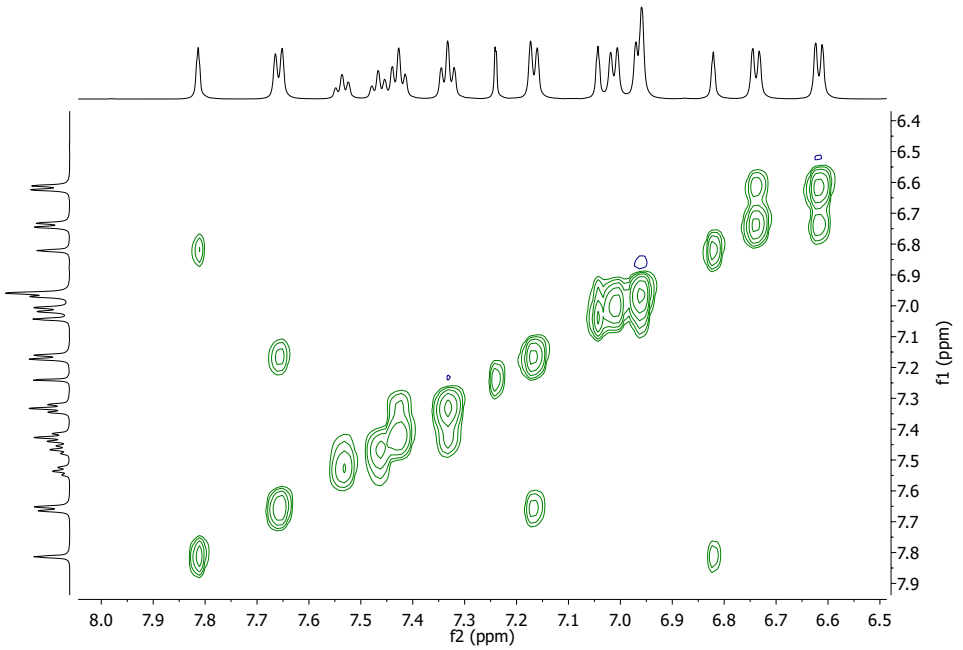

Figure 7.34: ROESY NMR ($CDCl_3$, 600 MHz) of compound **3a** (zoomed)

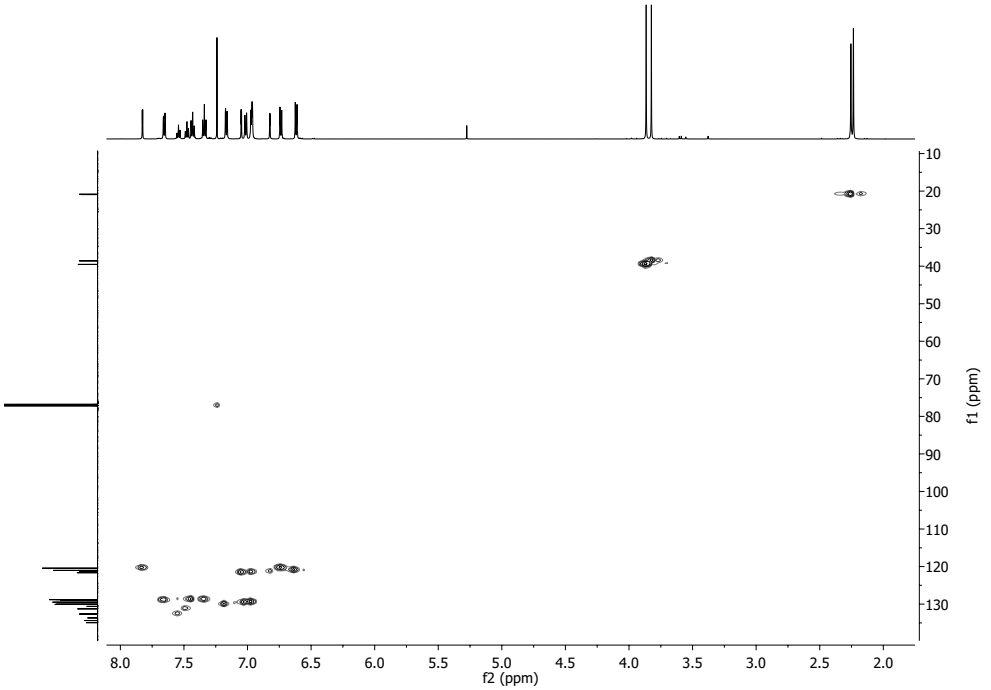

Figure 7.35: HSQC NMR ($CDCl_3$, 600 MHz) of compound **3a**

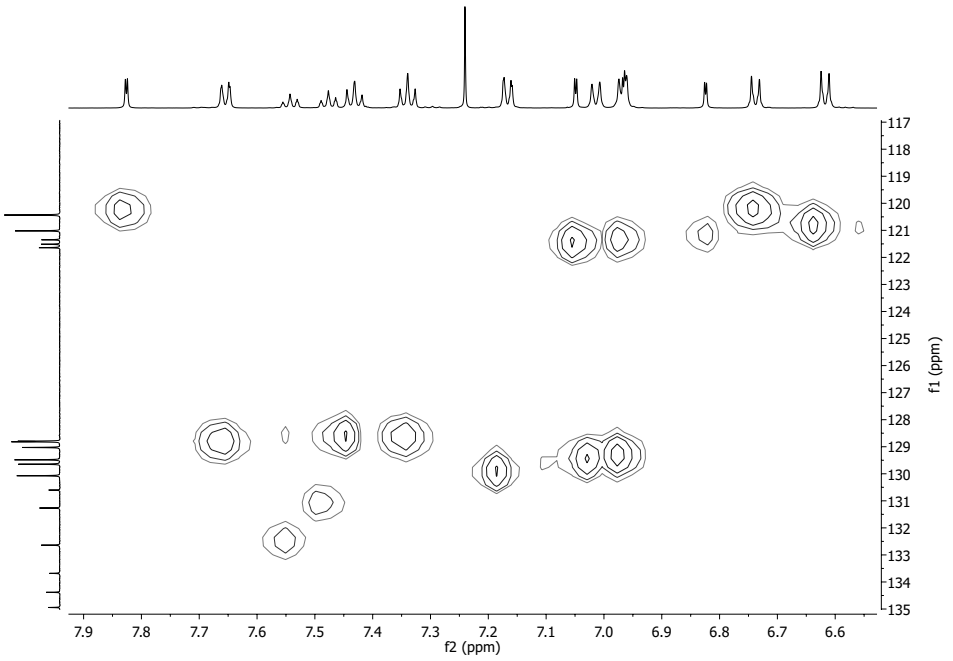

Figure 7.36: HSQC NMR ($CDCl_3$, 600 MHz) of compound **3a** (zoomed)

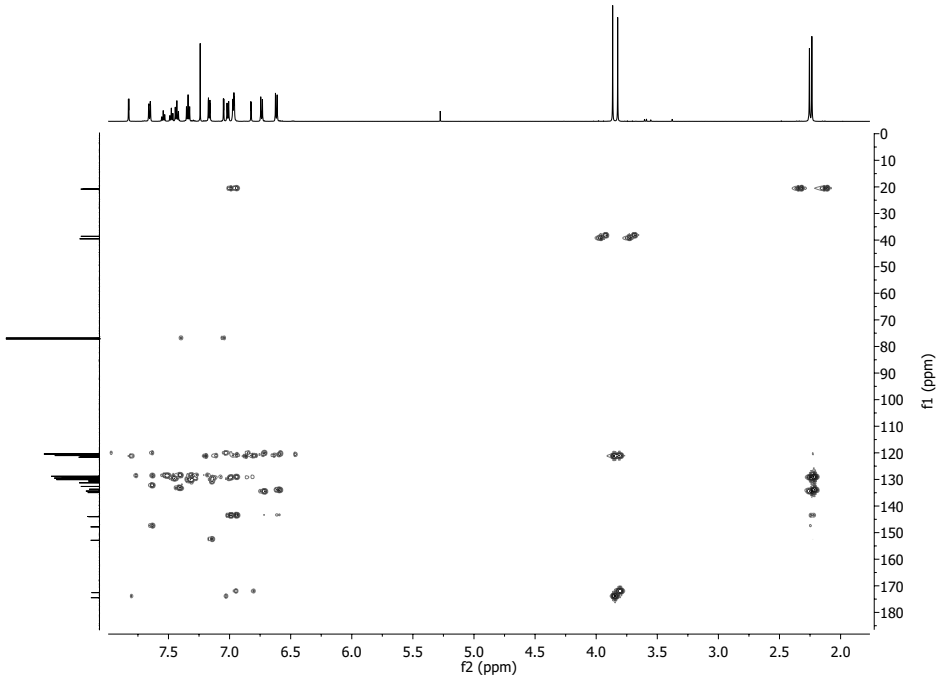

Figure 7.37: HMBC NMR ($CDCl_3$, 600 MHz) of compound **3a**

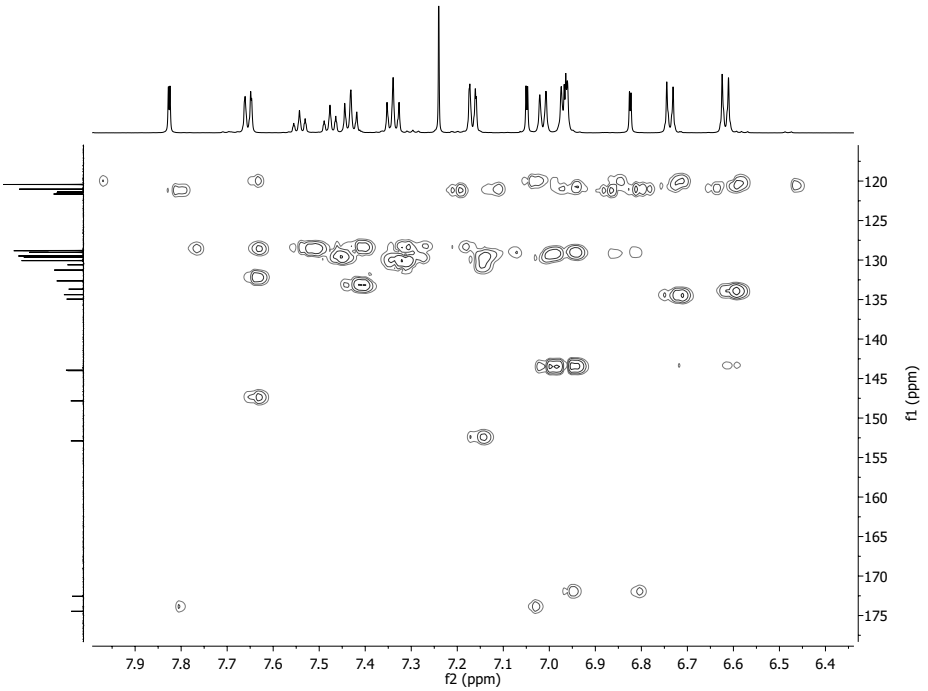

Figure 7.38: HMBC NMR ($CDCl_3$, 600 MHz) of compound **3a** (zoomed)

7.6 Compound 3b

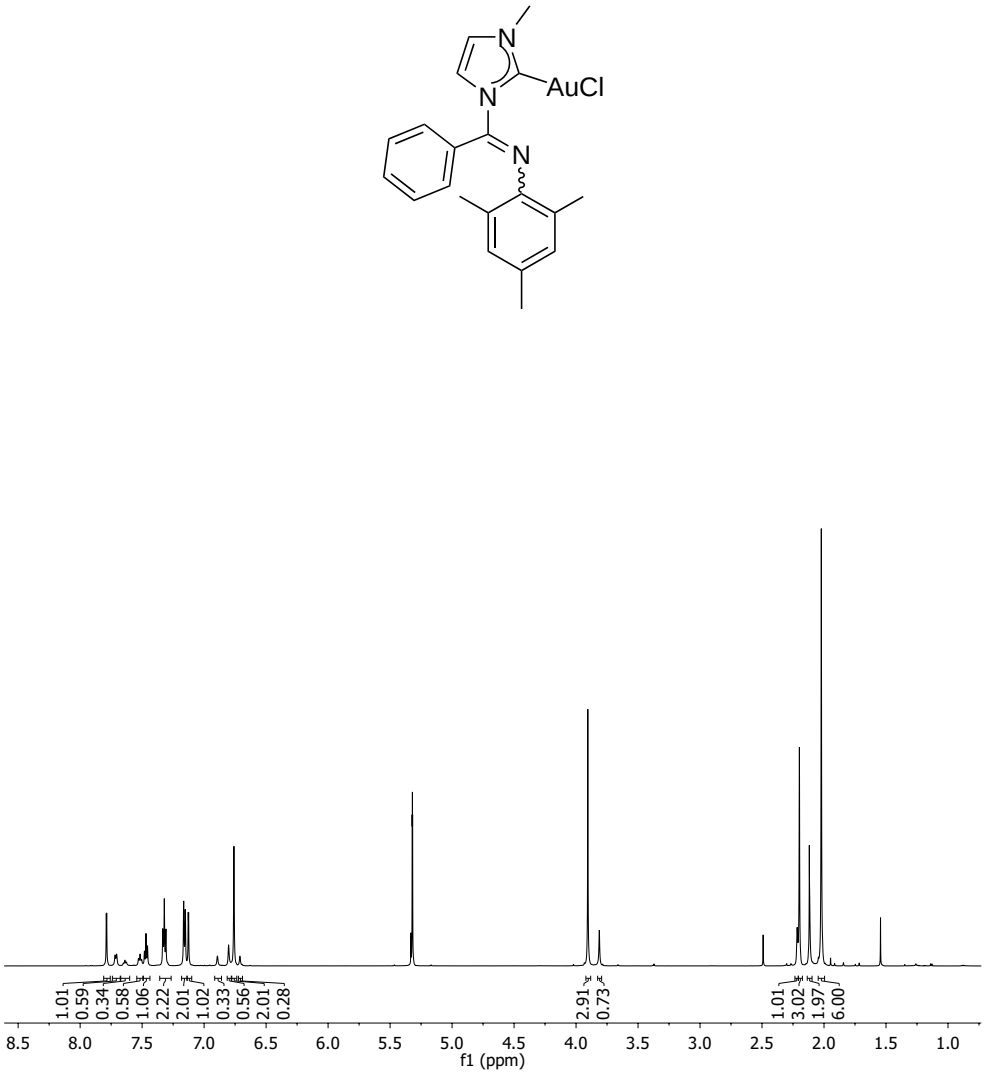

Figure 7.39: ^{1}H NMR (CD_2Cl_2, 600 MHz) of compound **3b**

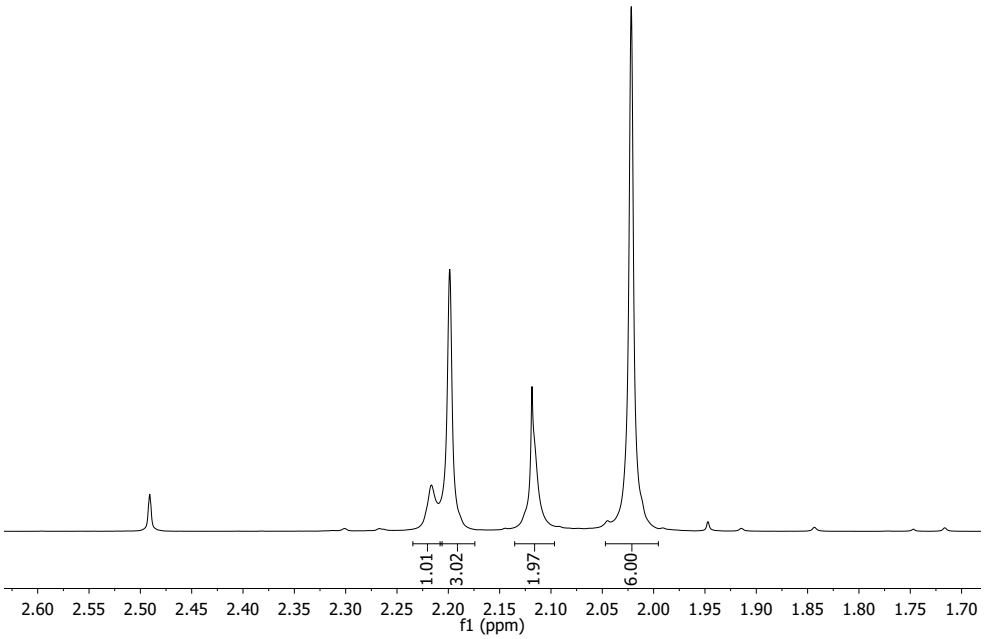

Figure 7.40: ^{1}H NMR (CD_2Cl_2, 600 MHz) of compound **3b** (zoomed)

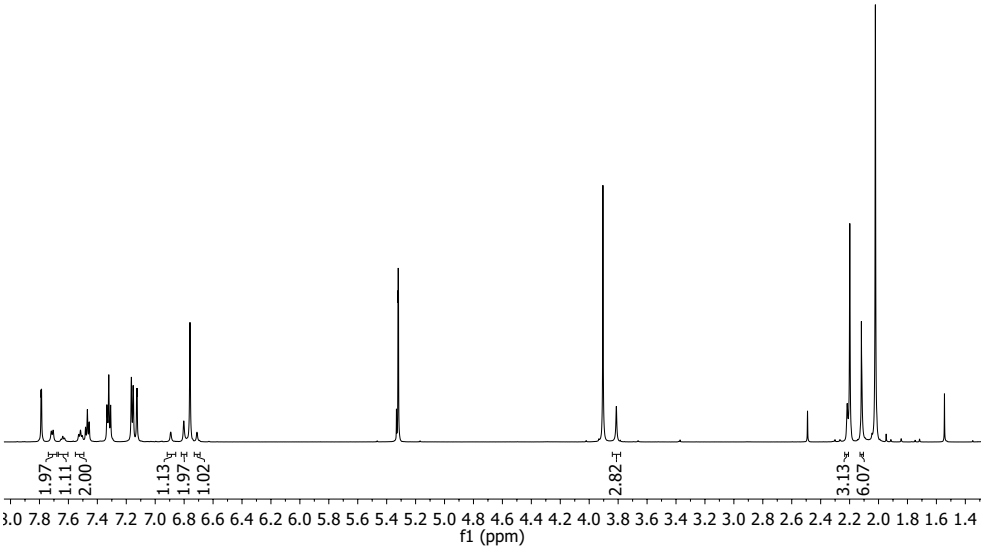

Figure 7.41: ^{1}H NMR (CD_2Cl_2, 600 MHz) of compound **3b** with integration on the minor isomer

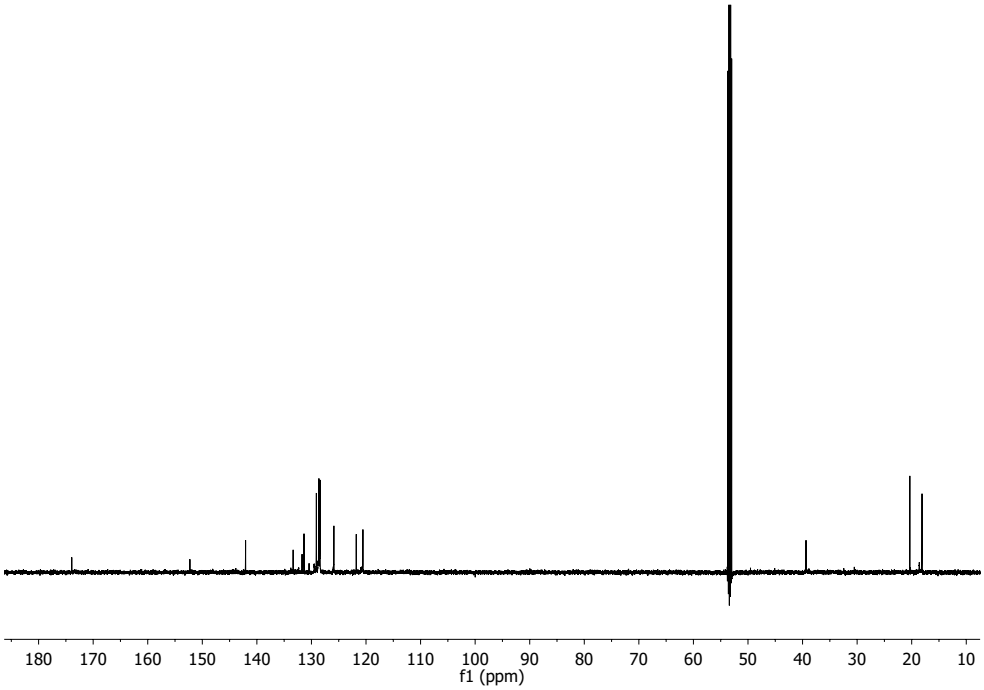

Figure 7.42: ^{13}C NMR (CD_2Cl_2, 151 MHz) of compound **3b**

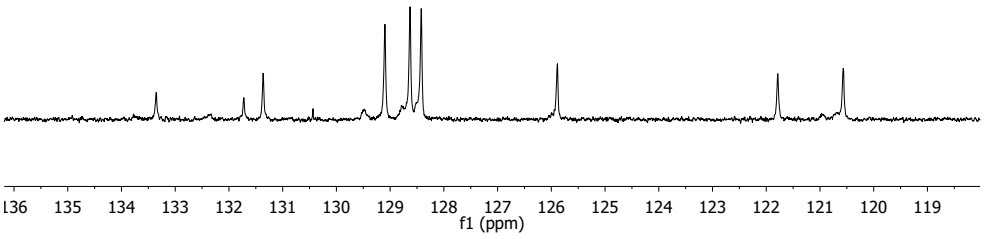

Figure 7.43: ^{13}C NMR (CD_2Cl_2, 151 MHz) of compound **3b** (zoomed)

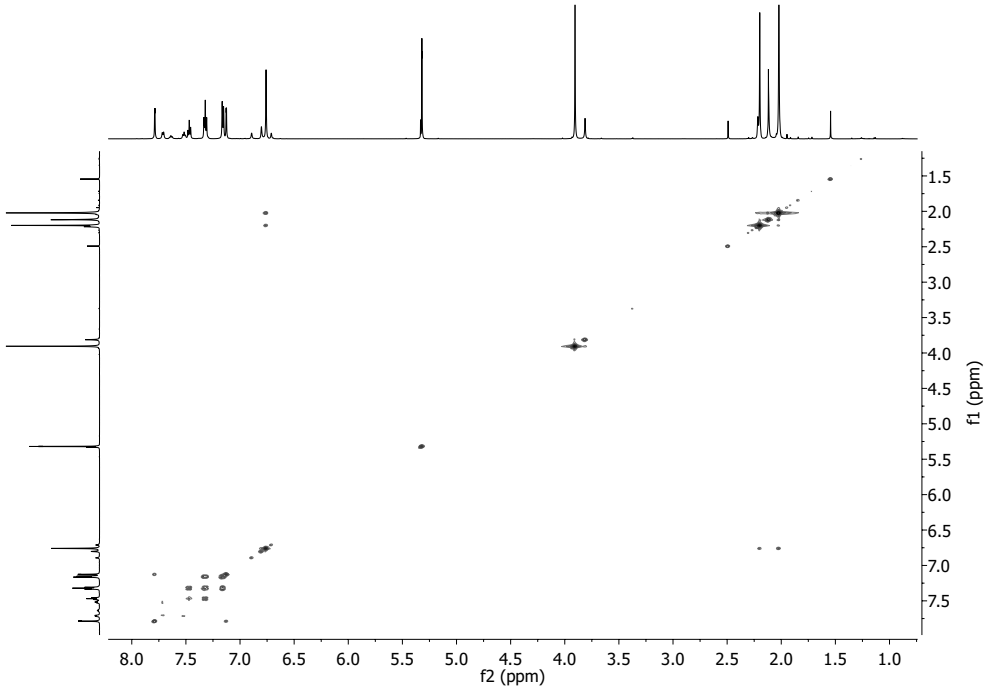

Figure 7.44: COSY NMR (CD_2Cl_2, 600 MHz) of compound **3b**

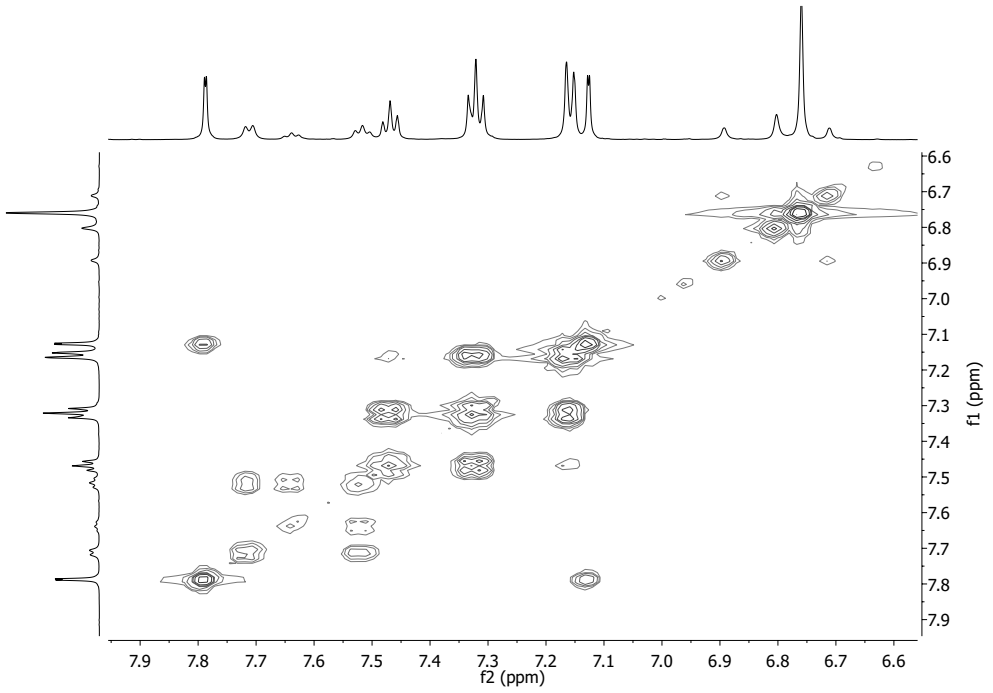

Figure 7.45: COSY NMR (CD_2Cl_2, 600 MHz) of compound **3b** (zoomed)

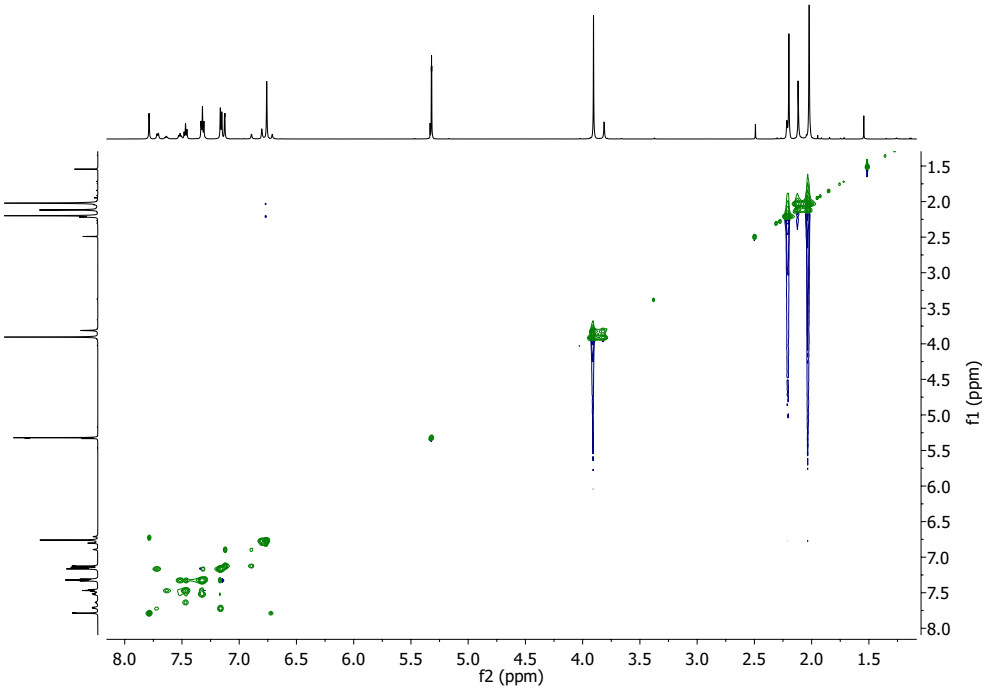

Figure 7.46: NOESY NMR (CD_2Cl_2, 600 MHz) of compound **3b**

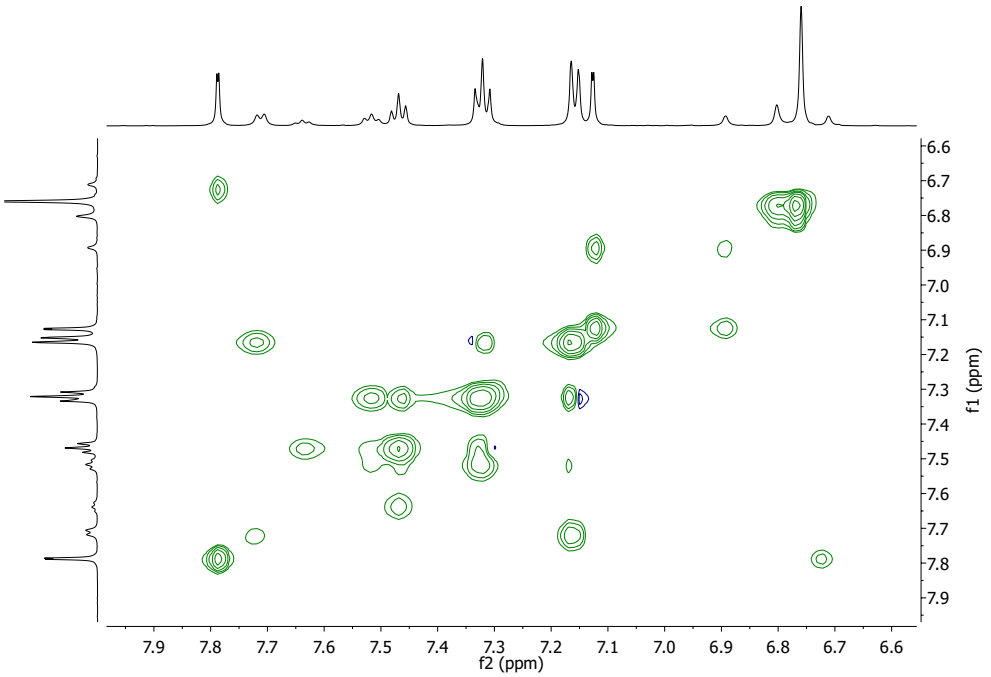

Figure 7.47: NOESY NMR (CD_2Cl_2, 600 MHz) of compound **3b** (zoomed)

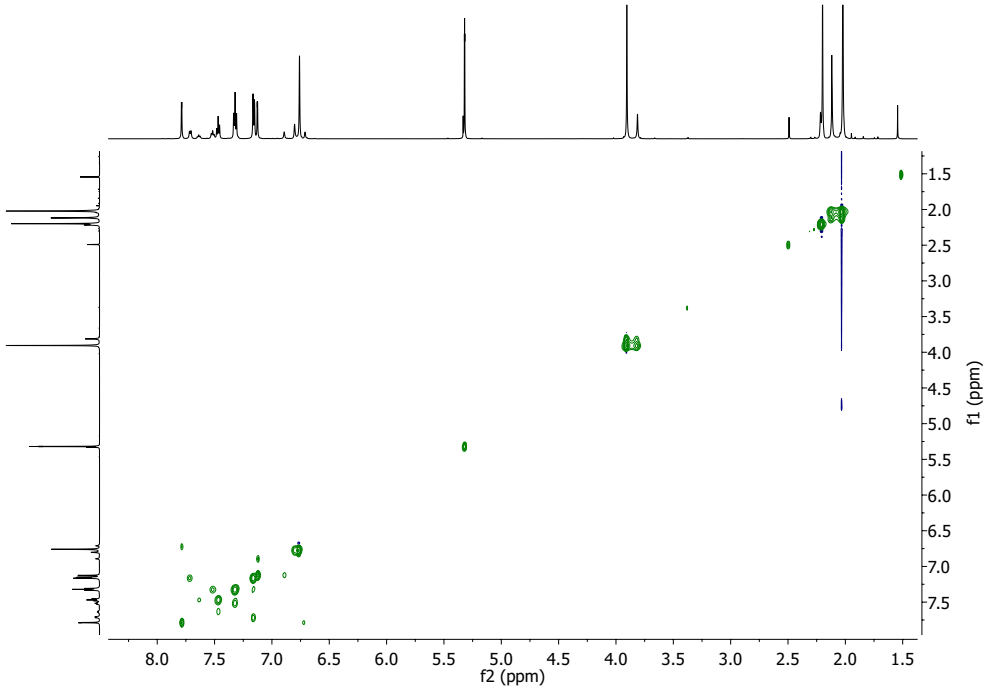

Figure 7.48: ROESY NMR (CD_2Cl_2, 600 MHz) of compound **3b**

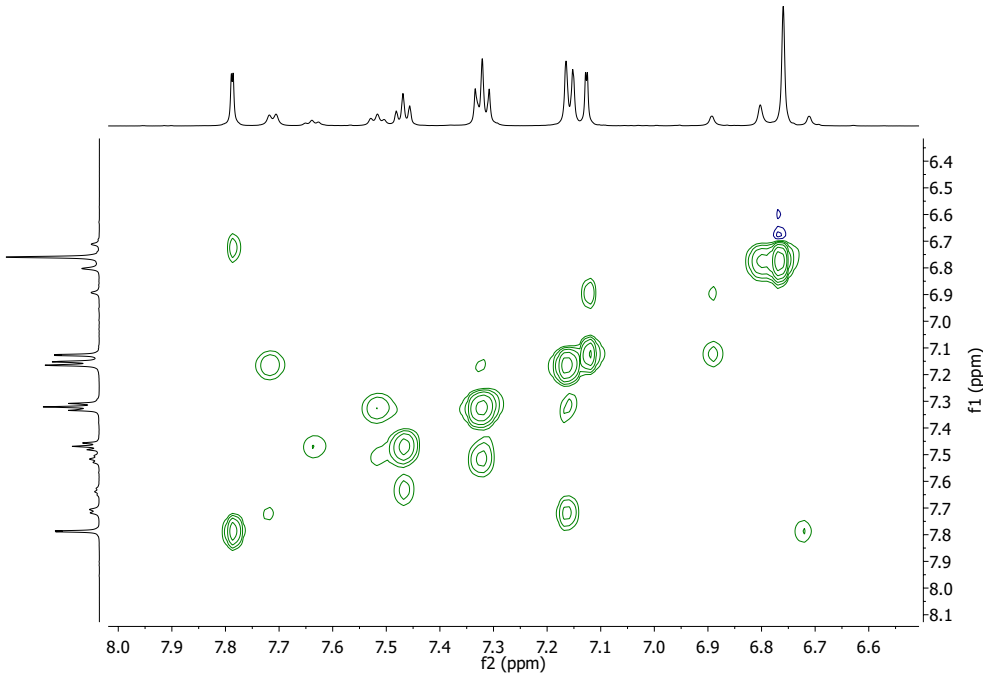

Figure 7.49: ROESY NMR (CD_2Cl_2, 600 MHz) of compound **3b** (zoomed)

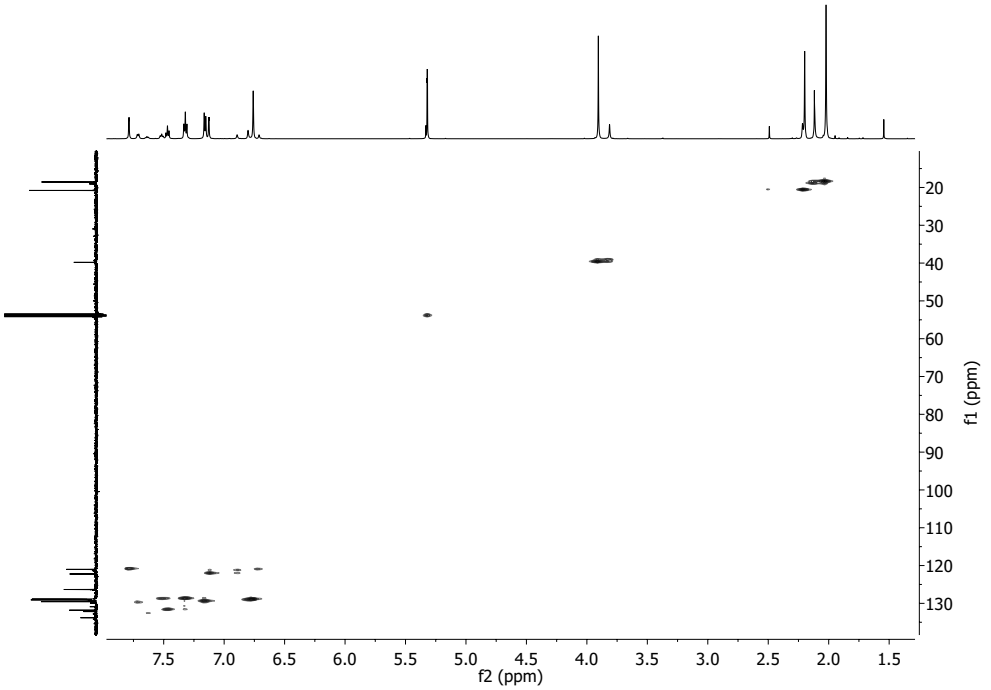

Figure 7.50: HSQC NMR (CD_2Cl_2, 600 MHz) of compound **3b**

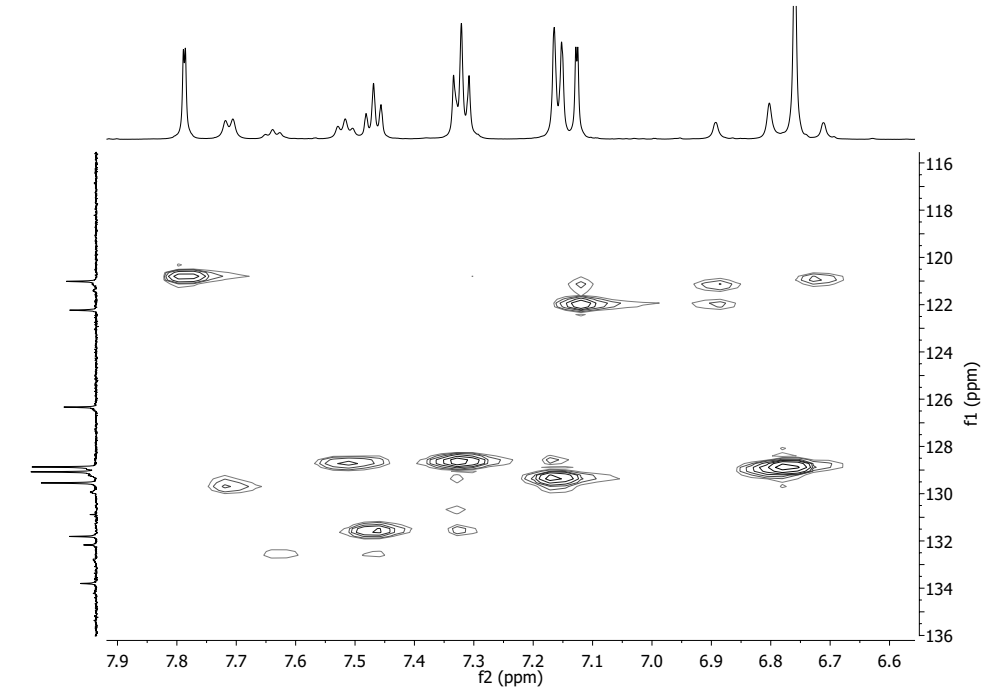

Figure 7.51: HSQC NMR (CD_2Cl_2, 600 MHz) of compound **3b** (zoomed)

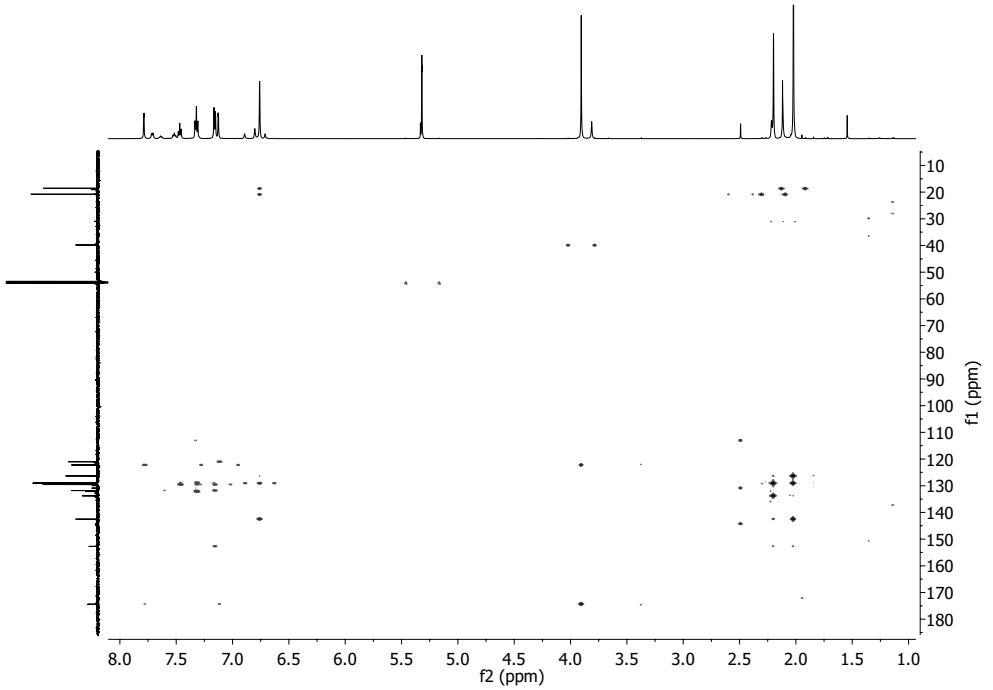

Figure 7.52: HMBC NMR (CD_2Cl_2, 600 MHz) of compound **3b**

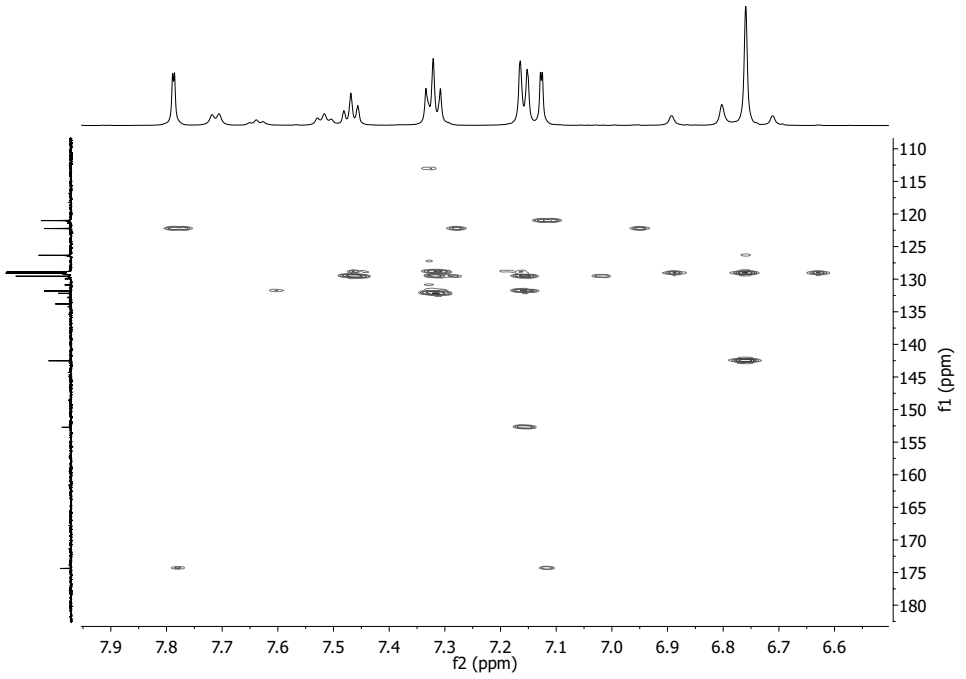

Figure 7.53: HMBC NMR (CD_2Cl_2, 600 MHz) of compound **3b** (zoomed)

7.7 Compound 5a

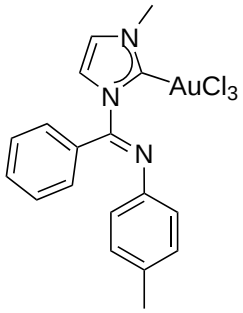

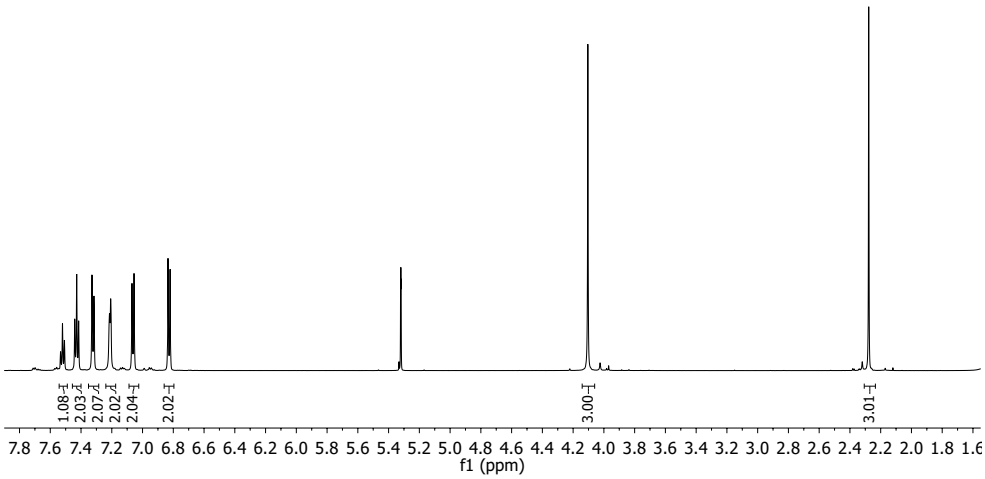

Figure 7.54: ^{1}H NMR (CD_2Cl_2, 600 MHz) of compound **5a**

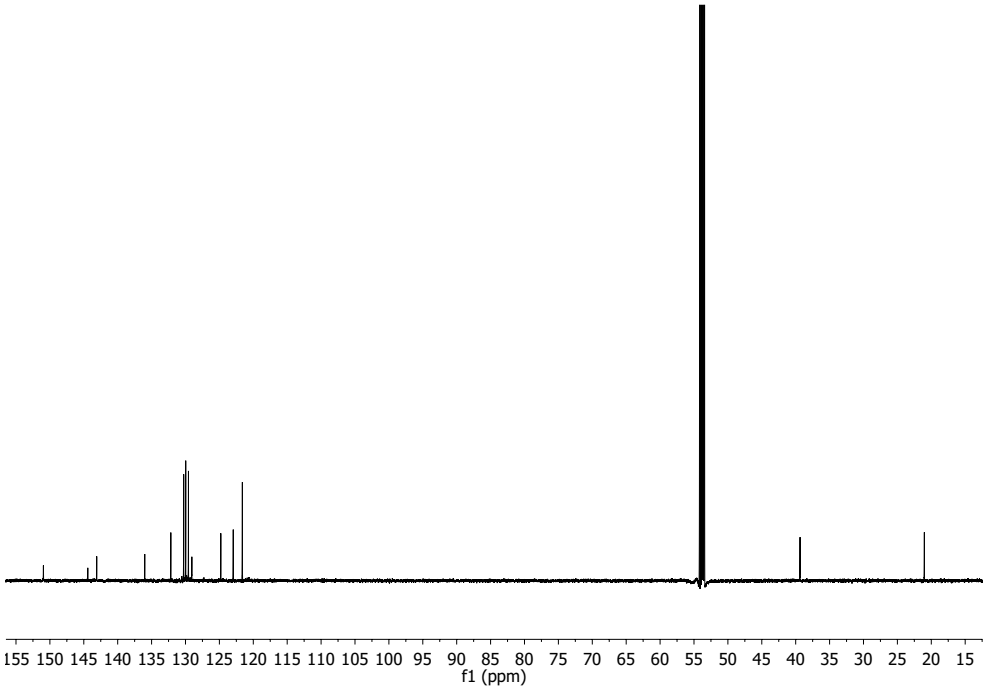

Figure 7.55: ^{13}C NMR (CD_2Cl_2, 151 MHz) of compound **5a**

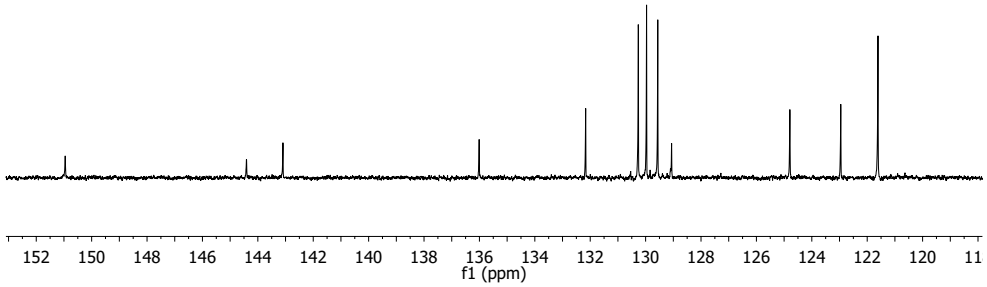

Figure 7.56: ^{13}C NMR (CD_2Cl_2, 151 MHz) of compound **5a** (zoomed)

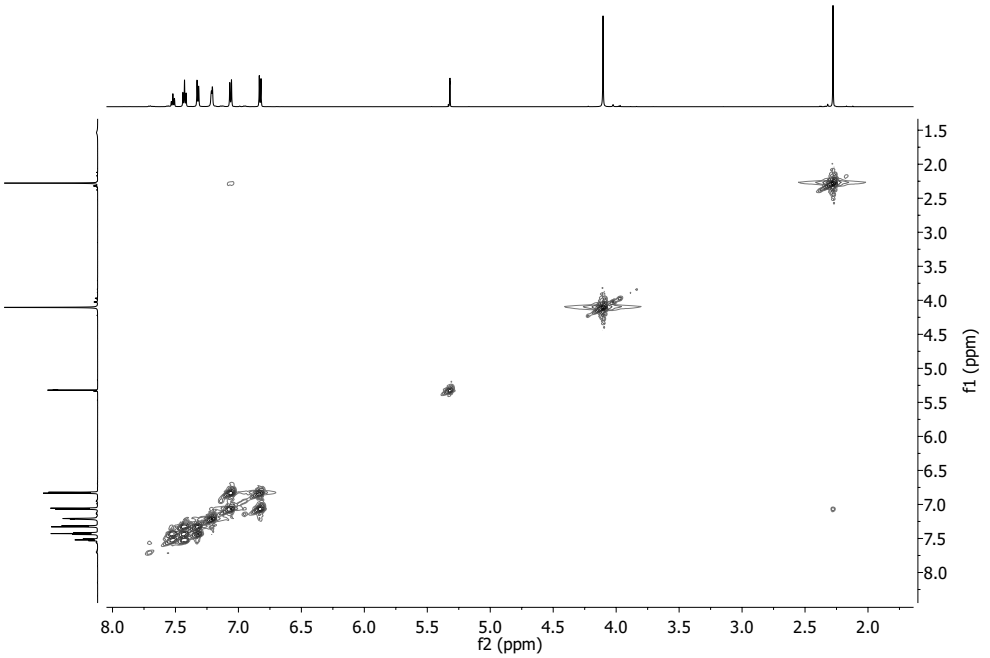

Figure 7.57: COSY NMR (CD_2Cl_2, 600 MHz) of compound **5a**

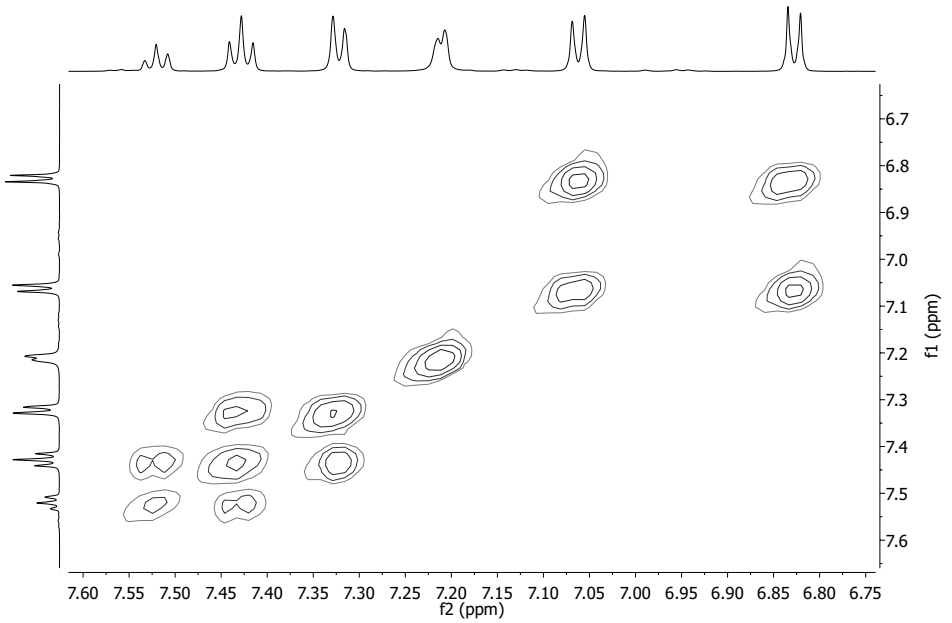

Figure 7.58: COSY NMR (CD_2Cl_2, 600 MHz) of compound **5a** (zoomed)

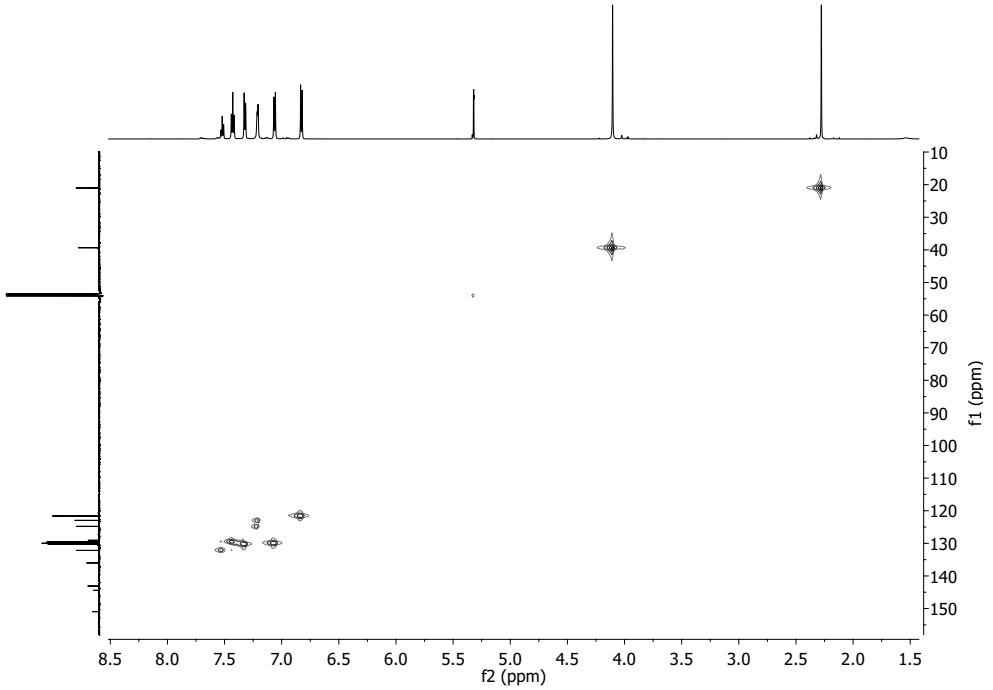

Figure 7.59: COSY NMR (CD_2Cl_2, 600 MHz) of compound **5a**

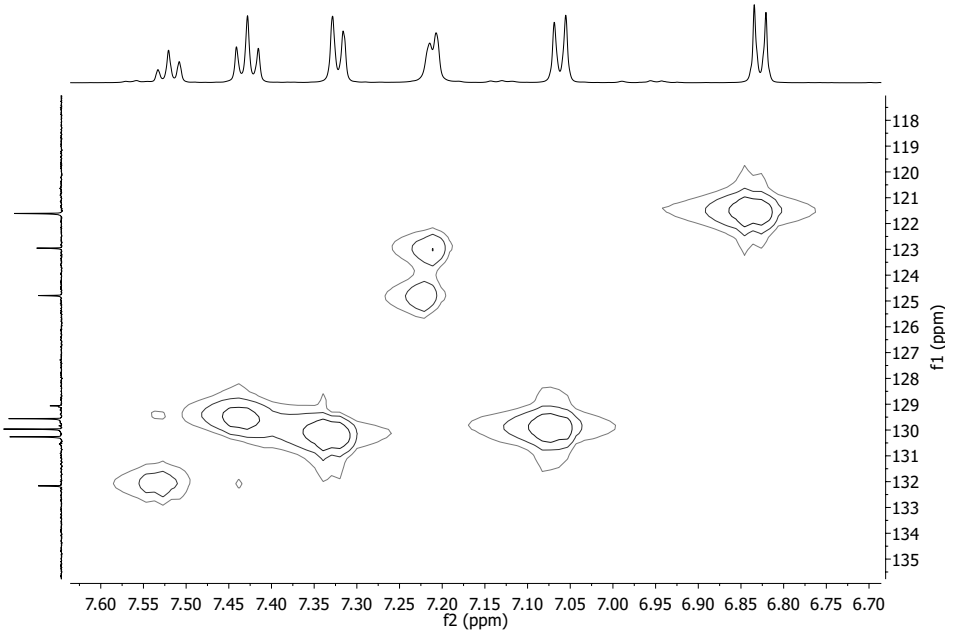

Figure 7.60: COSY NMR (CD_2Cl_2, 600 MHz) of compound **5a** (zoomed)

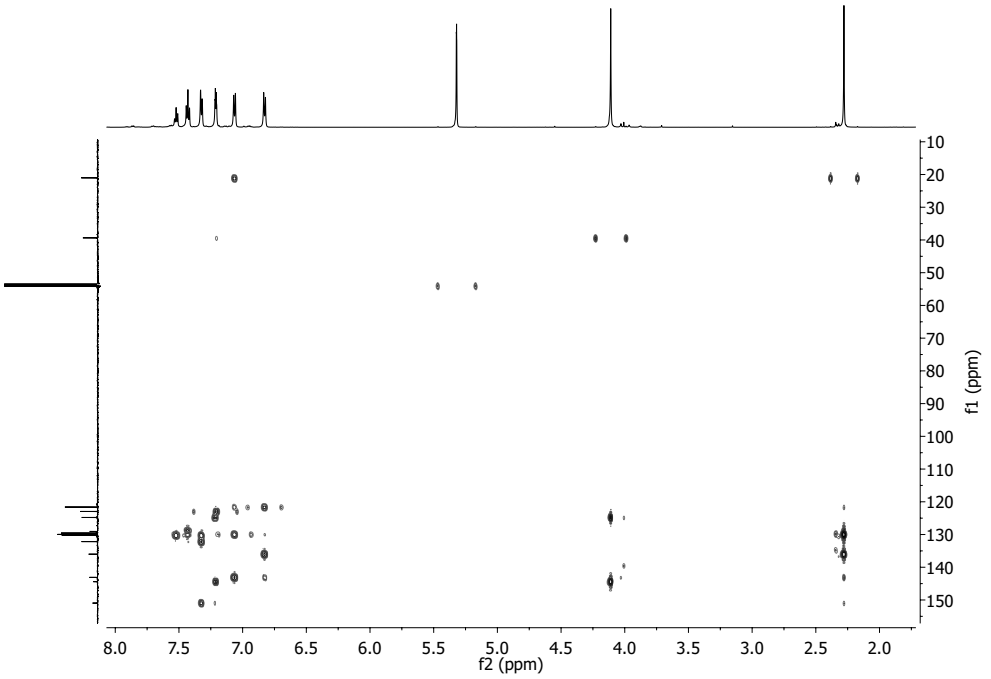

Figure 7.61: HMBC NMR (CD_2Cl_2, 600 MHz) of compound **5a**

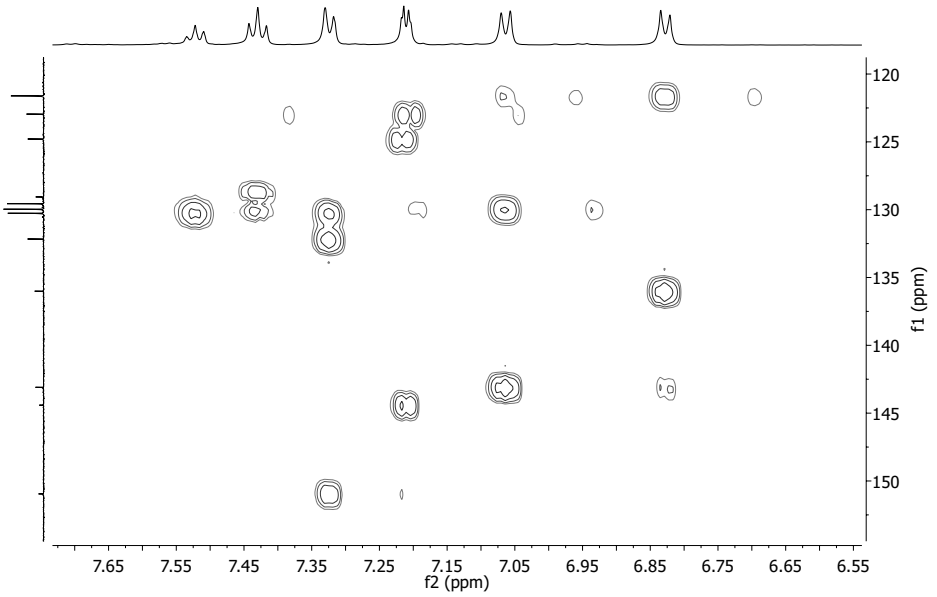

Figure 7.62: HMBC NMR (CD_2Cl_2, 600 MHz) of compound **5a** (zoomed)

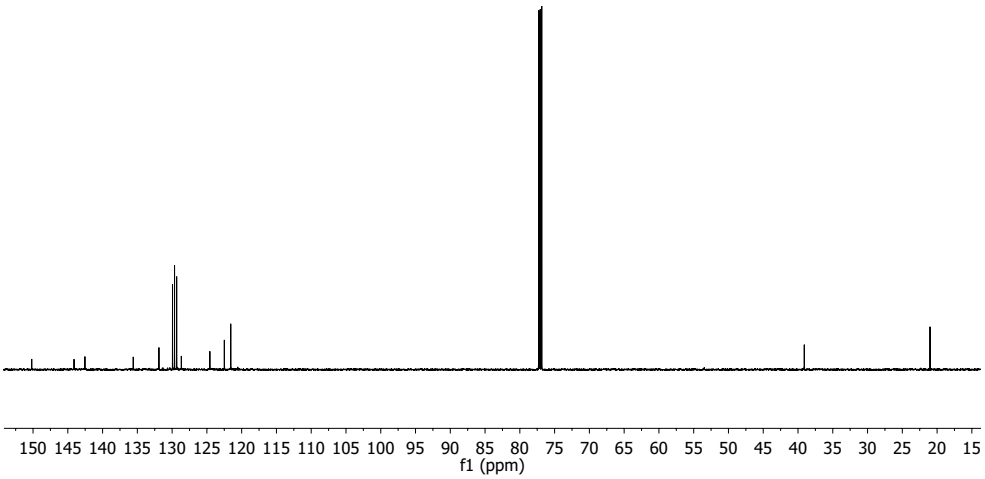

Figure 7.63: ^{13}C NMR ($CDCl_3$, 600 MHz) of compound **5a**

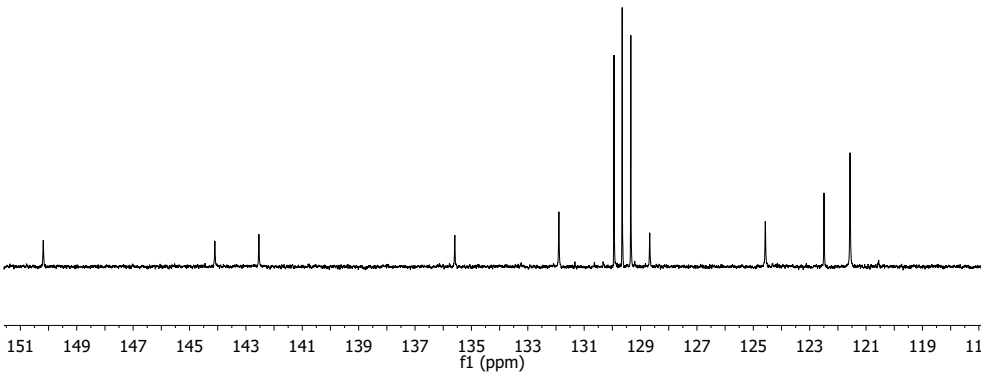

Figure 7.64: ^{13}C NMR ($CDCl_3$, 600 MHz) of compound **5a**

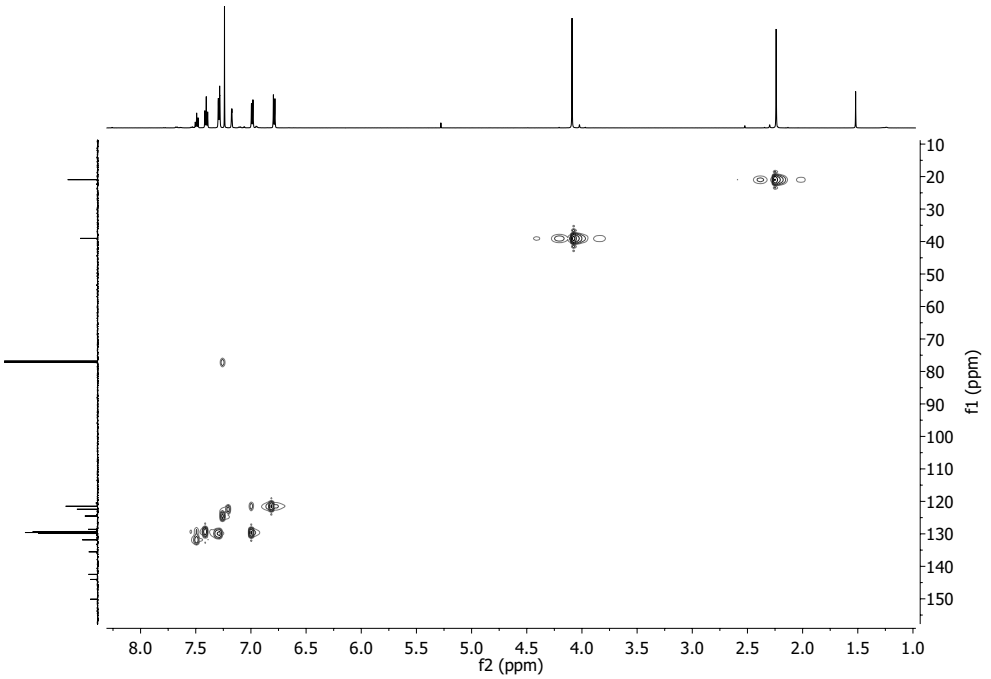

Figure 7.65: HSQC NMR ($CDCl_3$, 600 MHz) of compound **5a**

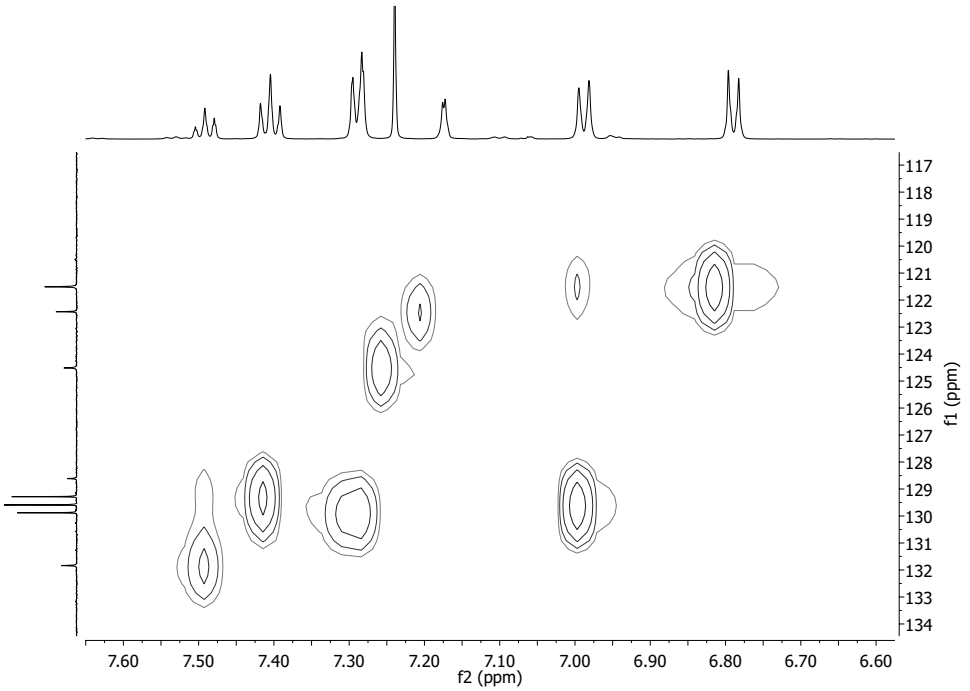

Figure 7.66: HSQC NMR ($CDCl_3$, 600 MHz) of compound **5a** (zoomed)

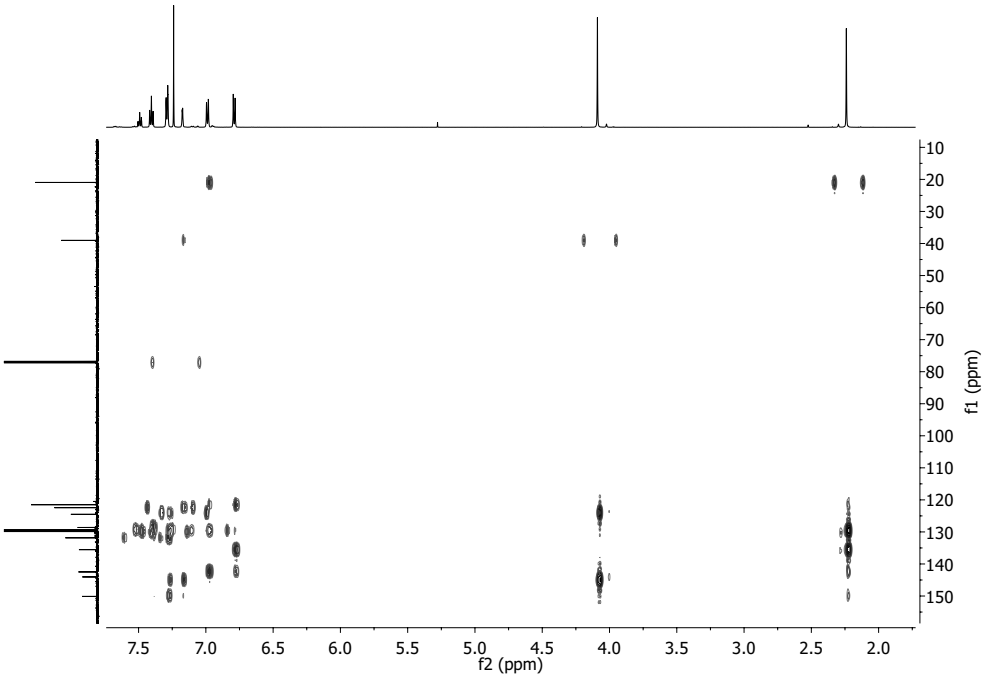

Figure 7.67: HMBC NMR ($CDCl_3$, 600 MHz) of compound **5a**

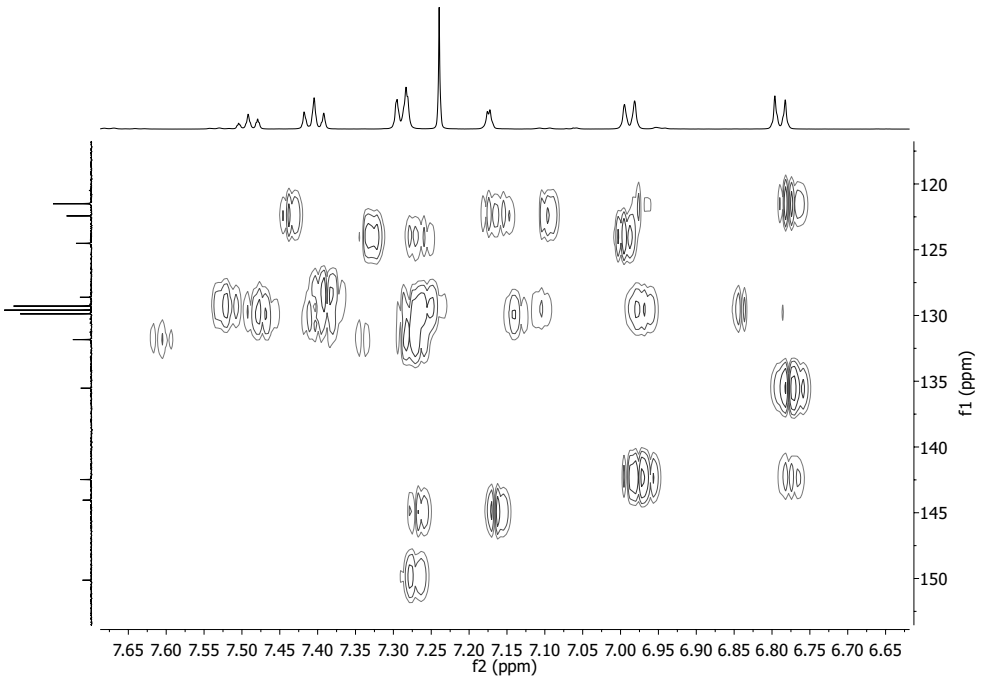

Figure 7.68: HMBC NMR ($CDCl_3$, 600 MHz) of compound **5a** (zoomed)

7.8 Compound 5b

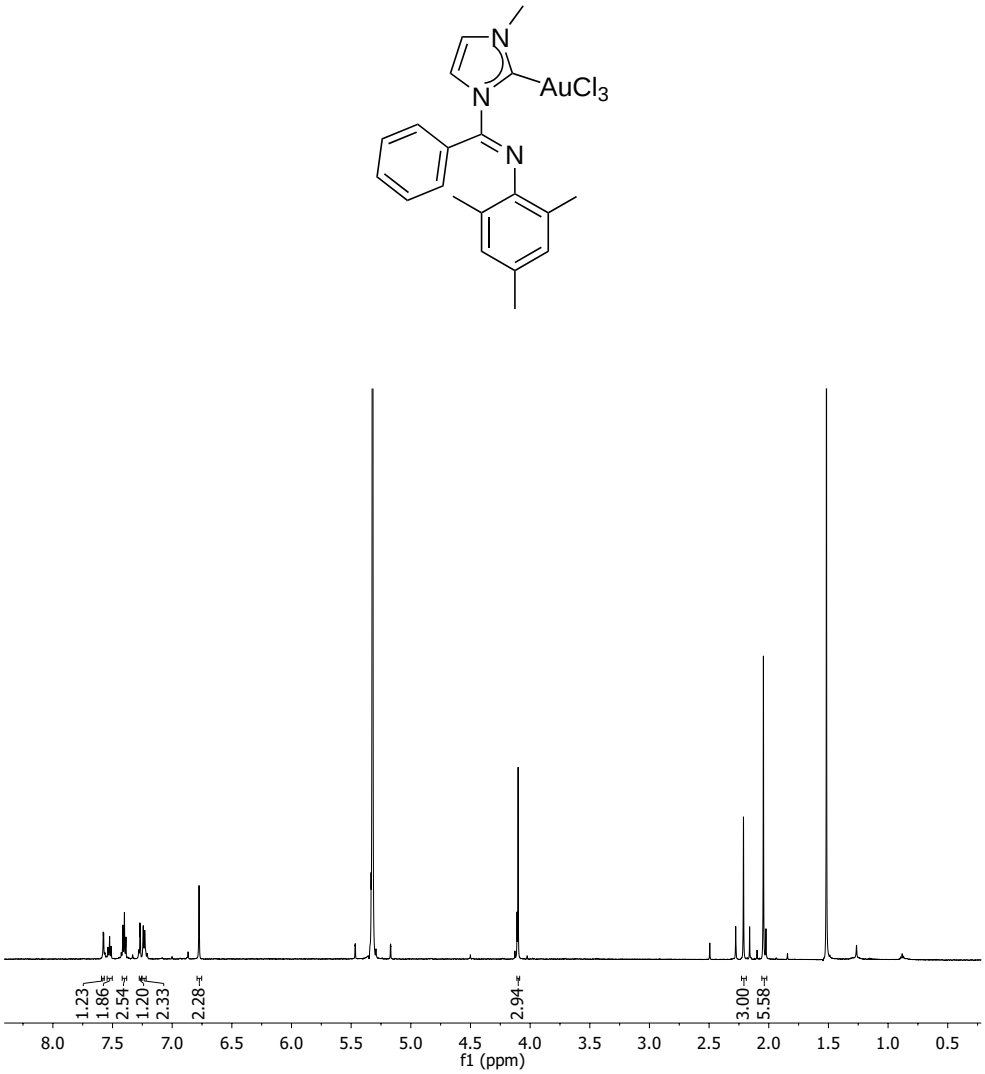

Figure 7.69: ^{1}H NMR (CD_2Cl_2, 600 MHz) of compound **5b**

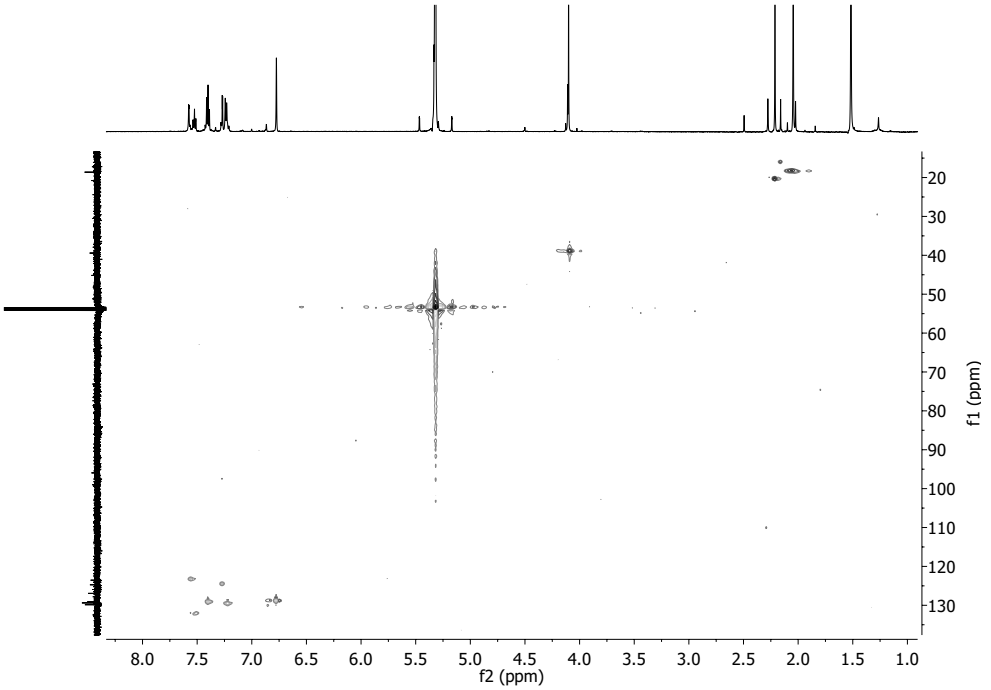

Figure 7.70: HSQC NMR (CD_2Cl_2, 600 MHz) of compound **5b**

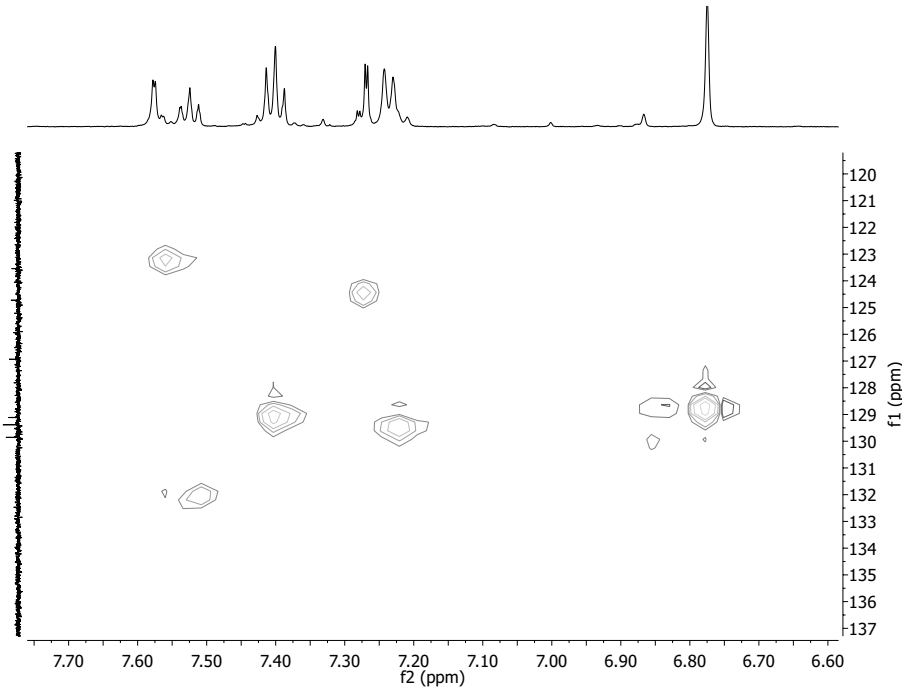

Figure 7.71: HSQC NMR (CD_2Cl_2, 600 MHz) of compound **5b** (zoomed)

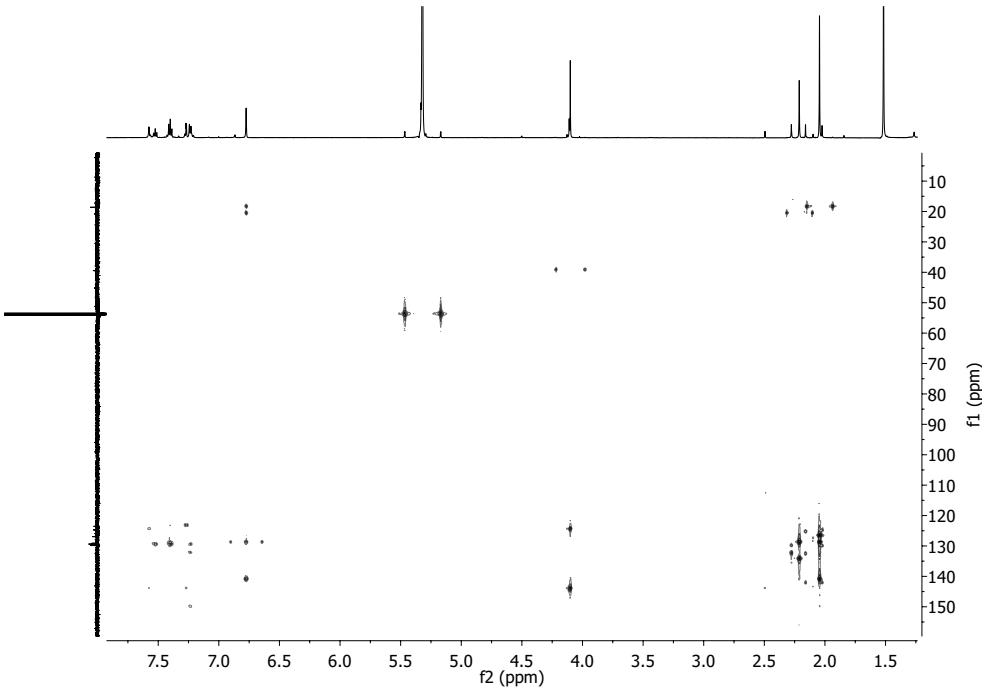

Figure 7.72: HMBC NMR (CD_2Cl_2, 600 MHz) of compound **5b**

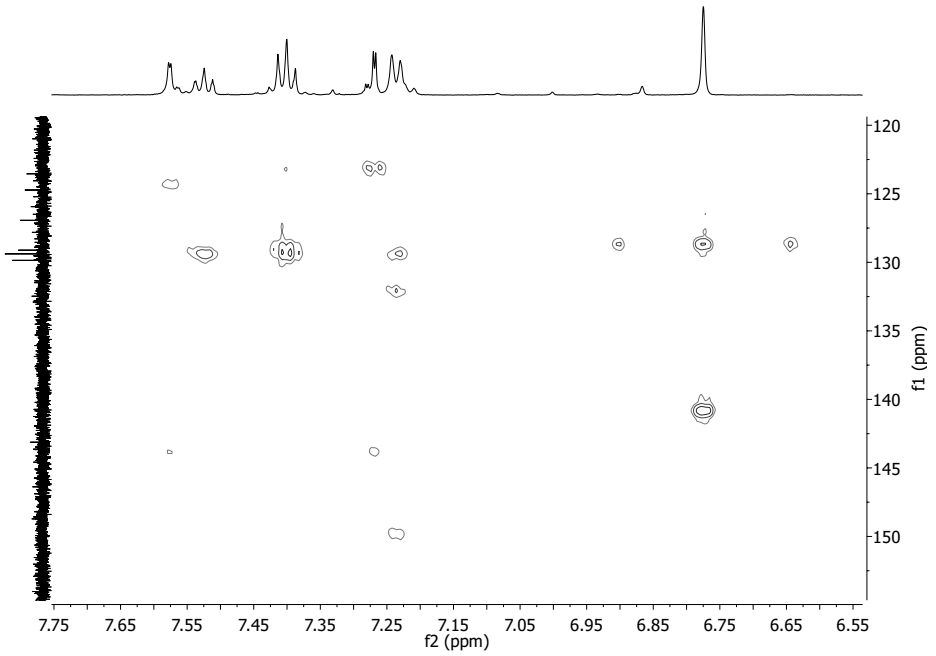

Figure 7.73: HMBC NMR (CD_2Cl_2, 600 MHz) of compound **5b** (zoomed)

Crystal data	
Name	KD0045
Formula	$C_{18}H_{17}N_3AuCl$
M_r	507.76
Crystal system, Space group	Monoclinic, $P2_1/n$
Crystal size	0.20 × 0.2 × 0.05 mm
Colour, shape	Plate, clear colourless
Cell length a	15.7937(6) Å
Cell length b	9.2769(3) Å
Cell length c	22.9183(8) Å
Cell angle β	94.5490(9)°
Cell volume, V	3346.3(2) $Å^3$
Formula units, Z	8
Sum of unit cell electrons, F(000)	1936
Radiation	Synchrotron,[60] λ= 0.7600 Å
Absorption coefficient (μ)	8.95 mm^{-1}
Temperature, T	100 K
Data collection	
Instrument	Bruker MD2
Beam line	Cassiopeia I911-3[60]
Measured reflections	25134
Independent reflections	8003
Reflextions with $I > 2\sigma(I)$	7764
R_{int}	0.089
Θ_{max}, Θ_{min}	28.3°, 1.5°
h	-21 → 20
k	-12 → 12
l	-30 → 30
Refinement	
Refinement on F^2	
$R[I^2>2\ \sigma(F^2)]$	0.048
$wR(F^2)$	0.123
S	1.07
Reflections	8003
Parameters	419
Restraints	0
$(\Delta/\sigma)_{max}$	0.001
$\Delta\rho_{max}$	2.15 e $Å^{-3}$
$\Delta\rho_{min}$	-2.28 e $Å^{-3}$
Hydrogen site location	Inferred from neighbouring sites. H-atom parameters constrained

Table 7.1: Crystallographic data for **3a**

Crystal data	
Name	KD0058
Formula	$C_{20}H_{21}AuClN_3$
M_r	535.81
Crystal system, Space group	Triclinic, $P_{\bar{1}}$
Crystal size	0.20 × 0.16 × 0.04 mm
Colour, shape	Prism, colourless
Cell length a	6.9464(3) Å
Cell length b	12.3411(6) Å
Cell length c	12.4525(6) Å
Cell angle α	67.3910(13)°
Cell angle β	78.4520(14)°
Cell angle γ	89.1350(14)°
Cell volume, V	963.26 $Å^3$
Formula units, Z	2
Sum of unit cell electrons, F(000)	516
Radiation	Mo Kα λ= 0.71073 Å
Absorption coefficient (μ)	7.78 mm^{-1}
Temperature, T	100 K
Data collection	
Instrument	Bruker D8 Discover
Measured reflections	18765
Independent reflections	4493
Reflextions with $I > 2\sigma(I)$	4046
R_{int}	0.037
Θ_{max}, Θ_{min}	27.3°, 3.0°
h	-9 → 9
k	-16 → 16
l	-16 → 15
Refinement	
Refinement on F^2	
$R[I^2>2\ \sigma(F^2)]$	0.026
$wR(F^2)$	0.047
S	1.14
Reflections	4493
Parameters	262
Restraints	0
$(\Delta/\sigma)_{max}$	0.001
$\Delta\rho_{max}$	1.18 e $Å^{-3}$
$\Delta\rho_{min}$	-0.84 e $Å^{-3}$
H atoms treated by a mixture of independent and constrained refinement	

Table 7.2: Crystallographic data for **3b**

Crystal data	
Name	KD0097
Formula	$C_{18}H_{18}N_3AuCl_2$
M_r	544.22
Crystal system, Space group	Orthorhombic, Pbca
Crystal size	0.20 × 0.13 × 0.03 mm
Colour, shape	Plate, Colourless
Cell length a	10.8438(5) Å
Cell length b	11.9065(5) Å
Cell length c	28.8163(13) Å
Cell volume, V	3720.5(3) $Å^3$
Formula units, Z	8
Sum of unit cell electrons, F(000)	2080
Radiation	Mo Kα λ= 0.71073 Å
Absorption coefficient (μ)	8.20 mm^{-1}
Temperature, T	108 K
Data collection	
Diffractometer	Bruker D8 Discover
Measured reflections	50189
Independent reflections	3668
Reflextions with $I > 2\sigma(I)$	3216
R_{int}	0.031
Θ_{max}, Θ_{min}	26.0°, 2.4°
h	-13 → 13
k	-14 → 14
l	-35 → 35
Refinement	
Refinement on F^2	
$R[I^2 > 2\ \sigma(F^2)]$	0.020
$wR(F^2)$	0.041
S	1.11
Reflections	3668
Parameters	219
Restraints	0
$(\Delta/\sigma)_{max}$	0.002
Δ/ρ_{max}	0.93 e $Å^{-3}$
Δ/ρ_{min}	-0.39 e $Å^{-3}$
Hydrogen site location	Inferred from neighbouring sites. H-atom parameters constrained

Table 7.3: Crystallographic data for **4**

Crystal data	
Name	KD0085
Formula	$C_{18}H_{17}AuCl_3N_3$
M_r	578.66
Crystal system, Space group	Monoclinic, $2P_1/c$
Crystal size	0.50 × 0.19 × 0.04 mm
Cell length a	14.8679(12) Å
Cell length b	18.4806(16) Å
Cell length c	14.4966(13) Å
Cell angle β	103.109(2)°
Cell volume, V	3879.4 $Å^3$
Formula units, Z	8
Sum of unit cell electrons, F(000)	2208
Radiation	Mo Kα λ= 0.71073 Å
Absorption coefficient (μ)	8.00 mm^{-1}
Temperature, T	100 K
Data collection	
Instrument	Bruker D8 Discover
Measured reflections	81126
Independent reflections	11840
Reflextions with $I > 2\sigma(I)$	9631
R_{int}	0.050
Θ_{max}, Θ_{min}	30.5°, 2.2°
h	-21 → 21
k	-26 → 26
l	-20 → 20
Refinement	
Refinement on F^2	
$R[I^2>2\ \sigma(F^2)]$	0.030
$wR(F^2)$	0.052
S	1.02
Reflections	11840
Parameters	455
Restraints	0
$(\Delta/\sigma)_{max}$	0.001
$\Delta\rho_{max}$	1.77 e $Å^{-3}$
$\Delta\rho_{min}$	-1.11 e $Å^{-3}$
Hydrogen site location	Inferred from neighbouring sites H-atom parameters constrained

Table 7.4: Crystallographic data for **5a**

Crystal data	
Name	KD0099
Formula	$8(C_{20}H_{21}AuCl_3N_3)$
M_r	4853.71
Crystal system, Space group	Orthorhombic, Pbcn
Crystal size	0.20 × 0.20 × 0.05 mm
Colour, shape	Clear, yellow plate
Cell length a	41.992(2) Å
Cell length b	11.2017(5) Å
Cell length c	17.8680(8) Å
Cell volume, V	8404.8(7) $Å^3$
Formula units, Z	2
Sum of unit cell electrons, F(000)	4672
Radiation	Mo Kα λ= 0.71073 Å
Absorption coefficient (μ)	7.393 mm^{-1}
Temperature, T	100 K
Data collection	
Instrument	Bruker D8 Discover
Measured reflections	75472
Independent reflections	8598
Reflextions with $I > 2\sigma(I)$	8171
R_{int}	0.028
Θ_{max}, Θ_{min}	26.4°, 2.2°
h	-52 → 52
k	-14 → 13
l	-22 → 22
Refinement	
Refinement on F^2	
$R[I^2>2\ \sigma(F^2)]$	0.029
$wR(F^2)$	0.070
S	1.12
Reflections	8598
Parameters	495
Restraints	0
$(\Delta/\sigma)_{max}$	0.002
$\Delta\rho_{max}$	2.99 e $Å^{-3}$
$\Delta\rho_{min}$	-1.38 e $Å^{-3}$
Hydrogen site location	Inferred from neighbouring sites H-atom parameters constrained

Table 7.5: Crystallographic data for **5b**

Crystal data	
Name	KD0105
Formula	$2(C_{11}H_{10}AuCl_3N_2O)$
M_r	979.05
Crystal system, Space group	Triclinic, $P\bar{1}$
Cell length a	8.3815(3) Å
Cell length b	8.8361(3) Å
Cell length c	11.2028(4) Å
Cell angle α	92.6010(12)°
Cell angle β	107.7710(11)°
Cell angle γ	114.6020(11)°
Cell volume, V	703.97(4) Å^3
Formula units, Z	1
Sum of unit cell electrons, F(000)	456
Radiation	Mo Kα λ= 0.71073 Å
Absorption coefficient (μ)	11.01 mm^{-1}
Temperature, T	100 K
Data collection	
Instrument	Bruker D8 Discover
Measured reflections	20838
Independent reflections	3113
Reflextions with $I > 2\sigma(I)$	3017
R_{int}	0.020
Θ_{max}, Θ_{min}	27.1°, 2.6°
h	-10 → 10
k	-11 → 11
l	-14 → 14
Refinement	
Refinement on F^2	
R[I^2>2 σ(F^2)]	0.012
wR(F^2)	0.028
S	1.07
Reflections	3113
Parameters	203
Restraints	0
$(\Delta/\sigma)_{max}$	0.001
$\Delta\rho_{max}$	0.86 e Å^{-3}
$\Delta\rho_{min}$	-0.32 e Å^{-3}
Hydrogen site location	Difference Fourier map All H-atom parameters refined

Table 7.6: Crystallographic data for **6**

Bibliography

(1) Frøseth, M.; Dhindsa, A.; Roise, H.; Tilset, M. *Dalton Trans.* **2003**, 4516–4524.

(2) Frøseth, M.; Netland, K. A.; Törnroos, K. W.; Dhindsa, A.; Tilset, M. *Dalton Trans.* **2005**, 1664–1674.

(3) Netland, K. A.; Krivokapic, A.; Schröder, M.; Boldt, K.; Lundvall, F.; Tilset, M. *J. Organomet. Chem* **2008**, *693*, 3703–3710.

(4) Netland, K. A.; Krivokapic, A.; Tilset, M. *J. Coord. Chem.* **2010**, *63*, 2909–2927.

(5) Rosenberg, M. L.; Krivokapic, A.; Tilset, M. *Org. Lett.* **2009**, *11*, 547–550.

(6) Rosenberg, M. L.; Krapp, A.; Tilset, M. *Organometallics* **2011**, *30*, 6562–6571.

(7) Holmsen, M. S., *Master Thesis: Synthesis, structure and dynamics of new metal N-heterocyclic carbene complexes*; University of Oslo: **2013**.

(8) Rosenberg, M. L.; Langseth, E.; Krivokapic, A.; Gupta, N. S.; Tilset, M. *New J. Chem.* **2011**, *35*, 2306–2313.

(9) Shaw, A. P.; Tilset, M.; Heyn, R. H. *J. Coord. Chem.* **2011**, *64*, 38–47.

(10) Langseth, E.; Görbitz, C. H; Heyn, R. H.; Tilset, M. *Organometallics* **2012**, *31*, 6567–6571.

(11) Langseth, E.; Scheuermann, M. L.; Balcells, D.; Kaminsky, W.; Goldberg, K. I.; Eisenstein, O.; Heyn, R. H.; Tilset, M. *Angew. Chem. Int. Ed.* **2013**, *52*, 1660–1663.

(12) Hashmi, A. S. K. *Chem. Rev.* **2007**, *107*, 3180–3211.

(13) Hashmi, A. S. K.; Hutchings, G. J. *Angew. Chem. Int. Ed.* **2006**, *45*, 7896–7936.

(14) Arduengo, A. J.; Harlow, R. L.; Kline, M. *J. Am. Chem. Soc.* **1991**, *113*, 361–363.

(15) César, V.; Bellemin-Laponnaz, S.; Gade, L. H. *Organometallics* **2002**, *21*, 5204–5208.

(16) Steiner, G.; Krajete, A.; Kopacka, H.; Ongania, K. H.; Wurst, K.; Preishuber-Pflügl, P.; Bildstein, B. *Eur. J. Inorg. Chem* **2004**, 2827–2836.

(17) Jacobsen, H.; Correa, A.; Costabile, C.; Cavallo, L. *J. Organomet. Chem.* **2006**, *691*, 4350–4358.

(18) Scott, N. M.; Dorta, R.; Stevens, E. D.; Correa, A.; Cavallo, L.; Nolan, S. P. *J. Am. Chem. Soc.* **2005**, *127*, 3516–3526.

(19) Dorta, R.; Stevens, E. D.; Scott, N. M.; Costabile, C.; Cavallo, L.; Hoff, C. D.; Nolan, S. P. *J.Am. Chem. Soc.* **2005**, *127*, 2485–2495.
(20) Normand, A. T.; Cavell, K. J. *Eur. J. Inorg. Chem.* **2008**, 2781–2800.
(21) César, V.; Bellemin-Laponnaz, S.; Gade, L. H. *Chem. Soc. Rev.* **2004**, *33*, 619–636.
(22) Samojlowicz, C.; Bieniek, M.; Grela, K. *Chem. Rev.* **2009**, *109*, PMID: 19534492, 3708–3742.
(23) Scholl, M.; Ding, S.; Lee, C. W.; Grubbs, R. H. *Org. Lett.* **1999**, *1*, PMID: 10823227, 953–956.
(24) Kantchev, E. A. B.; O'Brien, C. J.; Organ, M. G. *Angew. Chem. Int. Ed.* **2007**, *46*, 2768–2813.
(25) Nolan, S. P. *Acc. Chem. Res.* **2011**, *44*, 91–100.
(26) Gaillard, S.; Cazin, C. S. J.; Nolan, S. P. *Acc. Chem. Res.* **2012**, *45*, 778–787.
(27) Wang, H. M. J.; Lin, I. J. B. *Organometallics* **1998**, *17*, 972–975.
(28) Furst, M. R. L.; Cazin, C. S. J. *Chem. Commun.* **2010**, *46*, 6924–6925.
(29) Garrison, J. C.; Youngs, W. J. *Chem. Rev.* **2005**, *105*, 3978–4008.
(30) Lin, I. J. B.; Vasam, C. S. *Coord. Chem. Rev.* **2007**, *251*, 642–670.
(31) Collado, A.; Gomez-Suarez, A.; Martin, A. R.; Slawin, A. M. Z.; Nolan, S. P. *Chem. Commun.* **2013**, *49*, 5541–5543.
(32) Visbal, R.; Laguna, A.; Gimeno, M. C. *Chem. Commun.* **2013**, *49*, 5642–5644.
(33) Raubenheimer, H. G.; Olivier, P. J.; Lindeque, L.; Desmet, M.; Hrušak, J.; Kruger, G. J. *J. Organomet. Chem.* **1997**, *544*, 91–100.
(34) Gaillard, S.; Slawin, A. M. Z.; Bonura, A. T.; Stevens, E. D.; Nolan, S. P. *Organometallics* **2010**, *29*, 394–402.
(35) Huynh, H. V.; Guo, S.; Wu, W. *Organometallics* **2013**, *32*, 4591–4600.
(36) Samantaray, M. K.; Pang, K.; Shaikh, M. M.; Ghosh, P.
(37) Bhargava, S. K.; Mohr, F.; Bennett, M. A.; Welling, L. L.; Willis, A. C. *Organometallics* **2000**, *19*, 5628–5635.
(38) Topf, C.; Hirtenlehner, C.; Fleck, M.; List, M.; Monkowius, U. *Z. Anorg. Allg. Chem.* **2011**, *637*, 2129–2134.
(39) Tomás-Mendivil, E.; Toullec, P. Y.; Díez, J.; Conejero, S.; Michelet, V.; Cadierno, V. *Org. Lett.* **2012**, *14*, 2520–2523.
(40) Muuronen, M.; Perea-Buceta, J. E.; Nieger, M.; Patzschke, M.; Helaja, J. *Organometallics* **2012**, *31*, 4320–4330.
(41) Pažický, M.; Loos, A.; Ferreira, M. J.; Serra, D.; Vinokurov, N.; Rominger, F.; Jäkel, C.; Hashmi, A. S. K.; Limbach, M *Organometallics* **2010**, *29*, 4448–4458.
(42) Topf, C.; Hirtenlehner, C.; Zabel, M.; List, M.; Fleck, M.; Monkowius, U. *Organometallics* **2011**, *30*, 2755–2764.
(43) Topf, C.; Hirtenlehner, C.; Monkowius, U. *J. Organomet. Chem.* **2011**, *696*, 3274–3278.
(44) Wimberg, J.; Meyer, S.; Dechert, S.; Meyer, F. *Organometallics* **2012**, *31*, 5025–5033.

(45) Jacques, B.; Hueber, D.; Hameury, S.; Braunstein, P.; Pale, P.; Blanc, A.; de Frémont, P. *Organometallics* **2014**, *33*, 2326–2335.
(46) Kriechbaum, M.; List, M.; Berger, R. J.; Patzschke, M.; Monkowius, U. *Chem. Eur. J. 18*.
(47) Shaw, A. P.; Ghosh, M. K.; Törnroos, K. W.; Wragg, D. S.; Tilset, M.; Swang, O.; Heyn, R. H.; Jakobsen, S. *Organometallics* **2012**, *31*, 7093–7100.
(48) Bruno, I. J.; Cole, J. C.; Edgington, P. R.; Kessler, M.; Macrae, C. F.; McCabe, P.; Pearson, J.; Taylor, R. *Acta Crystallogr., Sect. B: Struct. Sci* **2002**, *58*, 389–397.
(49) Bondi, A. *The Journal of Physical Chemistry* **1964**, *68*, 441–451.
(50) Rowland, R. S.; Taylor, R. *J. Phys. Chem.* **1996**, *100*, 7384–7391.
(51) Espinosa, E.; Souhassou, M.; Lachekar, H.; Lecomte, C. *Acta Crystallogr., Sect. B* **1999**, *55*, 563–572.
(52) Grabowski, S. J. *J. of Phys. Chem. A* **2001**, *105*, 10739–10746.
(53) Johnson, E. R.; Keinan, S.; Mori-Sánchez, P.; Contreras-García, J.; Cohen, A. J.; Yang, W. *J. Am. Chem. Soc.* **2010**, 6498–6506.
(54) Hohenberg, P.; Kohn, W. *Phys. Rev.* **1964**, 864–871.
(55) Zupan, A.; Burke, K.; Ernzerhof, M.; Perdew, J. P. *J. Chem. Phys.* **1997**, *106*, 10184–10193.
(56) Contreras-García, J.; Johnson, E. R.; Keinan, S.; Chaudret, R.; Piquemal, J. P.; Beratan, D. N.; Yang, W. *J. Chem. Theory Comput.* **2011**, *7*, 625–632.
(57) Baker, M. V.; Barnard, P. J.; Brayshaw, S. K.; Hickey, J. L.; Skelton, B. W.; White, A. H. *Dalton Trans.* **2005**, 37–43.
(58) De Frémont, P.; Singh, R.; Stevens, E. D.; Petersen, J. L.; Nolan, S. P. *Organometallics* **2007**, *26*, 1376–1385.
(59) Herrmann, W. A.; Runte, O.; Artus, G. *J. Organomet. Chem.* **1995**, *501*, C1–C4.
(60) Ursby, T.; Unge, J.; Appio, R.; Logan, D. T.; Fredslund, F.; Svensson, C.; Larsson, K.; Labrador, A.; Thunnissen, M. M. G. M. *J. Synchrotron Radiat.* **2013**, *20*, 648–653.
(61) Putz, H.; Brandenburg, K., *Diamond—Crystal and Molecular Structure Visualization Crystal Impact*, http://www.crystalimpact.com/diamond, Accessed: 2014-05-15.
(62) De Frémont, P.; Scott, N. M.; Stevens, E. D.; Nolan, S. P. *Organometallics* **2005**, *24*, 2411–2418.
(63) Braunstein, P.; Müller, A.; Bögge, H. *Inorg. Chem.* **1986**, *25*, 2104–2106.
(64) *Gaussian 09 Revision D .01, Gaussian Inc. Wallingford CT* **2009**, Frisch, M. J.; Trucks, G. W.; Schlegel, H. B.; Scuseria, G. E.; Robb, M. A.; Cheeseman, J. R.; Scalmani, G.; Barone, V.; Mennucci, B.; Petersson, G. A.; Nakatsuji, H.; Caricato, M.; Li, X.; Hratchian, H. P.; Izmaylov, A. F.; Bloino, J.; Zheng, G.; Sonnenberg, J. L.; Hada, M.; Ehara, M.; Toyota, K.; Fukuda, R.; Hasegawa, J.; Ishida, M.; Nakajima, T.; Honda, Y.; Kitao, O.; Nakai, H.; Vreven, T.; Montgomery, J. A., Jr.; Peralta, J. E.; Ogliaro, F.; Bearpark, M.; Heyd, J. J.; Brothers, E.; Kudin, K. N.; Staroverov, V. N.; Kobayashi, R.; Normand, J.; Raghavachari, K.; Rendell, A.; Burant, J. C.; Iyengar, S. S.;

Tomasi, J.; Cossi, M.; Rega, N.; Millam, N. J.; Klene, M.; Knox, J. E.; Cross, J. B.; Bakken, V.; Adamo, C.; Jaramillo, J.; Gomperts, R.; Stratmann, R. E.; Yazyev, O.; Austin, A. J.; Cammi, R.; Pomelli, C.; Ochterski, J. W.; Martin, R. L.; Morokuma, K.; Zakrzewski, V. G.; Voth, G. A.; Salvador, P.; Dannenberg, J. J.; Dapprich, S.; Daniels, A. D.; Farkas, Ö.; Foresman, J. B.; Ortiz, J. V.; Cioslowski, J.; Fox, D. J.

(65) This work was performed on the Abel Cluster, owned by the University of Oslo and the Norwegian metacenter for High Performance Computing (NOTUR), and operated by the Department for Research Computing at USIT, the University of Oslo IT-department.

(66) McLean, A. D.; Chandler, G. S. *J. Chem. Phys.* **1980**, *72*, 5639–5648.

(67) Krishnan, R.; Binkley, J. S.; Seeger, R.; Pople, J. A. *J. Chem. Phys.* **1980**, *72*, 650–654.

(68) Figgen, D.; Rauhut, G.; Dolg, M.; Stoll, H. *Chem. Phys.* **2005**, *311*, 227–244.

(69) Marenich, A. V.; Cramer, C. J.; Truhlar, D. G. *J. Phys. Chem. B* **2009**, *113*, 6378–6396.

(70) Hariharan, P.; Pople, J. English *Theoretica Chim. Acta* **1973**, *28*, 213–222.

(71) Weigend, F. *Phys. Chem. Chem. Phys.* **2006**, *8*, 1057–1065.

(72) Humphrey, W.; Dalke, A.; Schulten, K. *J. Mol. Graphics* **1996**, *14*, 33–38.

(73) Perdew, J. P. *Phys. Rev. B* **1986**, *33*, 8822–8824.

(74) Becke, A. D. *J. Chem. Phys.* **1993**, *98*, 5648–5652.

(75) Grimme, J. *J. Comput. Chem.* **2006**, *27*, 2306–2313.

(76) Zhao, Y.; D. G. Truhlar, D. G. *Theor. Chem. Acc.* **2008**, *120*, 215–241.

(77) Perdew, J. P.; Burke, K.; Ernzerhof, M. *Phys. Rev. Lett.* **1996**, *77*, 3865–3868.

(78) Adamo, C.; Barone, V. *J. Chem. Phys.* **1999**, *110*, 6158–6170.

(79) Wang, D.; Cai, R.; Sharma, S.; Jirak, J.; Thummanapelli, S. K.; Akhmedov, N. G.; Zhang, H.; Liu, X.; Petersen, J. L.; Shi, X. *J. Am. Chem. Soc.* **2012**, *134*, 9012–9019.

(80) Hashmi, A. S. K.; Frost, T. M.; Bats, J. W. *J. Am. Chem. Soc.* **2000**, *122*, 11553–11554.

(81) Hashmi, A. S. K.; Weyrauch, J. P.; Rudolph, M.; Kurpejović, E *Angew. Chem. Int. Ed.* **2004**, *43*, 6545–6547.

(82) Gabillet, S.; Lecerclé, D.; Loreau, O.; Dézard, S.; Gomis, J. M; Taran, F. *Synthesis* **2007**, 7384–7391.

(83) Van den Nieuwendijk, A. M. C. H.; Pietra, D.; Heitman, L.; Göblyös, A.; IJzerman, A. P. *J. Med. Chem.* **2004**, *47*, 663–672.